Doctoral Thesis Reviewed
by Ritsumeikan University

Fabrication and Analysis of Magnet Based Soft Tactile Sensor and Its Application to Robotic Manipulation and Texture Classification

（磁石を用いた柔軟な触覚センサの開発ならびに解析とそのロボットマニピュレーションとテクスチャー識別への応用）

September 2016
2016 年 09 月

Doctoral Program in Advanced Mechanical Engineering and Robotics
Graduate School of Science and Engineering
Ritsumeikan University
立命館大学大学院理工学研究科
機械システム専攻博士課程後期課程

KATUDAMPE VITHANAGE Damith Suresh Chathuranga
カトウダンペ ヴイタナゲ ダミス スレス チャトランガ

Supervisor: Professor HIRAI Shinichi
研究指導教員：平井　慎一教授

Dedicated to my parents.

Abstract

This thesis presents the design and development of a novel soft 3 axis force sensor. It was developed to be used in soft tactile fingertips. Additionally, we present applications of the sensor in texture classification and object manipulation. The sensor was constructed after identifying the design requirements of the tactile system needed for a robot to perform both dexterous object manipulations and environment perception. The human tactile system was taken as the basis for the analysis. Finite Element (FE) models of biological fingers, experimental artificial fingertips and information obtained from previous literature were used to identify the requirements. The analysis pointed out that the force and vibration modalities were vital for tactile sensing while the placement of the sensors between the soft layers, the sensitivity of the sensors, and the sensor density were important factors to be considered.

Literature survey about tactile fingertips pointed to a void in tactile sensors that sufficiently satisfied all the above requirements. Thus, a novel soft three axis force sensor was developed. The sensor had a cylindrical cantilever beam made of silicone rubber that compressed and bent when normal and tangential forces were applied. The displacement of the beam's end was calculated by measuring the change of the magnetic field emitted by a permanent magnet embedded in the soft beam at fixed points in space. Spring theory and bending theory were used to calculate the normal and tangential force components. The sensor was capable of measuring forces as well as detecting vibrations in the frequency range of 1 - 500Hz. It could be fixed under the soft layers of the fingertip without wires obstructing the measurements. The design, development and characterization of the sensor were reported.

Next, this force sensor was used for developing a robot gripper to manipulate objects dexterously. The sensor system provided information about applied force and vibrations happening at the fingertip object contact surface that could be used in controlling the grip force.

Finally, the force sensor was used in texture classification experiments to illustrate that the proposed sensor and the tactile system was capable of performing environment perception tasks. A robust classification algorithm that utilized support vector machine was presented.

Acknowledgements

I take this opportunity to thank my mentors, family and friends, who helped and supported me through this long yet productive journey of graduate studies.

First, I would like to thank my supervisors Prof Shinichi Hirai who helped me at every step of the way. The depth of his knowledge, patients, supportiveness and companionate nature encouraged, and motivated me to pursue my dreams. Conducting research under his tutelage was an honor and I have no wards to thank him. I am much grateful for him when he helped me in my financial difficulties. I will be eternally indebt for his kindness.

I would like to express my gratitude to the students at my laboratory who were always ready to assist me with the research equipment and material purchases. Ms. Hatanaka, the secretary of Professor Hirai needs to be mentioned with gratitude as she helped immensely with equipment purchases, document handling and conversing in Japanese to improve my Japanese ability. I also want to thank the past and the current group members of the Hand Group for their assistance.

Thanks and gratitude should go to my mentors Dr. Thrishantha Nanayakkara of King's College London, Dr. Wang Zongkui of Ritsumeikan University, Dr. Van Ahn Ho of Ryukoku University, Dr. Akio Noda of Mitsubishi Advanced Technical Research Center, Dr. Atsuchi Mitani of Sapporo University and Prof. Susumu Sugiyama of Ritsumeikan University, who encouraged, guided and inspired me to realize my dreams. Their inspiring personalities and motivating talks always helped me to ride through the worst tides of my PhD.

I would also like to thank my parents, who encouraged me to pursue my dreams with passion and dedication. During this journey, they have sacrificed much more that no words ever can fathom. I find their words a

driving force to find the light at darker times. My brother and sister, the help and support of my life need to be mentioned with utmost gratitude. You have all inspired me and helped me to remain focused and finish my studies. Next, my loving wife and the in laws who encouraged motivated me to do my very best.

I would like to thank my good friends Mr. Masashi Hirose, Mr. La Nat Tam, Mr. Han Yechen, Mr. Kitaro Quy, and the people from Kusatsu International Friendship Association whom gave me a home away from home.

Lastly, I would like to thank Ritsumeikan University and the staff, Japanese government and Monbukagasho scholarship which supported my PhD.

- Damith Suresh Chathuranga

September 2016

Contents

Chapter 3

List of figures

List of tables

Chapter 1

Introduction

In recent years, research into robots with human like features has gained momentum and we can assume that it will continue for the next decade and beyond. This shift from traditional robotics research that consisted of industrial automation and industrial robots to robots that mimic human behavior and motion is because of our intention to incorporate robots into our day to day activities to work alongside humans. Limitation of human labor, aging populations in developed countries, and high demand in goods and services which needs to be customer specific, further pushed the humanoid robot research into overdrive. This resulted in an increase in investments to develop intelligent robot systems to address issues in healthcare, and highly configurable robot systems that can work alongside humans in human friendly environments. Currently many companies and institutes develop number of robot systems that target health care [**1**] [**2**] [**3**], robots for personal assistance [**4**] [**5**] [**6**], and highly configurable manufacturing robot systems for industry [**7**]. Apart from these systems, prosthetics [**8**] [**9**] and brain machine interfaces [**10**] for disabled are also trending. These robot systems employ vision, and audition sensing extensively as sensors for navigation, planning and follow commands. However, when it comes to physically interacting with the environment, tactile sensing plays a vital role which vision sensing even with much complex algorithms cannot substitute.

1.1 Tactile sensing for robot systems

One of the most important physical interactions by a robot is the grasping and manipulation of objects. A typical industrial robot will have a predefined set of objects with known dimensions, tolerances, weight to grasp and manipulate, making it easy to develop a gripper suitable to execute those specific tasks. However, if a robot to interact in a house hold, and manipulate verity of objects and manipulations which the objects are originally intended to be used by the humans, traditional two or three finger grippers which were ideal for industry will not be suitable. Therefore with the advances in robots developed for human interaction, hands that can grip and manipulate everyday objects have been a requirement. However, the lack of robotic hands that are capable of robust grasping, manipulating objects dexterously, and exploring is limiting the advances in such robot systems. The main reasons for lacking in hands design are difficulty in fabricating grippers/hands with multiple degrees of freedom in a compact structure with necessary rigidity and ability to apply required grip force, and the inability to incorporate necessary number of sensors and; process that sensor information as tactile data to derive control ques for manipulation and exploration tasks. In this thesis, we wish to address the second obstacle.

The tactile sensor system of the robot hand should have the ability to gather tactile data which is needed for contact detection, object classification, material classification and dexterous object manipulation. Because the human has the highest dexterity and can manipulate objects better than animal paws [**11**], and if the robot to interact in an environment occupied by humans and operate machinery and equipment made for human operators, human hands and its tactile system can be taken as a baseline for developing robotic tactile systems. From the human hand, the fingertips, which have the maximum sensor density [**12**] plays a crucial role when it comes to grasping and manipulation. The grasping and dexterous manipulation of objects and

perception of the environment is mainly by the fingertips and when designing robot hands/grippers, special consideration has to be given to fingertips. Therefore, this thesis mainly focuses on the fingertip design guidelines suitable for robot applications, design of tactile fingertips, tactile signals obtained by such systems, use of these tactile data to manipulate objects and explore environments.

Human fingers have two primary functions [**13**] :

- grasping and manipulating objects, and
- perceiving the environment

In most of the robotics research, these two functions are addressed separately. This is due to the differences in the characteristics of the tactile sensors and methods needed for performing each functions. Grasping and manipulating tasks requires the sensing of bulk properties (hardness, viscoelasticity etc…), mass distributions, textures, forces, localization of the force, gravitational and inertial effects, and detection of localized vibrations which happen at the onset of slip [**14**] [**15**] [**16**]. This requires a distributed tactile sensor (an array) that could sense pressure distribution and vibrations. Additionally, to derive tactile information, amalgamation of two types of modalities: pressure and vibration, is needed [**17**]. Environment perception utilizes mostly the frequency domain or vibrations signals if the features detected are small [**18**], and if the features are considerably large, pressure distribution data is used [**19**]. To measure vibrations sensors such as accelerometer [**20**] or a sensor that reacts to fast stress changes such as PVDF [**21**] can be used. The main requirement of such sensor would be to have high sampling rates.

When designing fingertips, the softness or the hardness of the finger embodiment matters much when conducting exploration or grasping

operations. Generally, soft fingertips create stable and encompassing grasps because they deform during grasp and apply a large frictional force and torque due to the large contact area than that of rigid fingertips which apply point loads and no counteracting torque [**22**]. However development of soft fingertips with necessary tactile sensing ability has its own challenges. The soft materials make the finger prone to wear, the elastic nonlinear material properties such as stiffness make the force calculations difficult, the damping of the soft materials make it difficult to sense small vibrations happening far away from the sensor and the forces applied to the fingertip is disbursed making it hard to localize.

Aforementioned requirements and the limitations of such systems have hindered the development of human like robots systems that work alongside humans. Thus it has become evident, new technologies and methods needed to be invented. This thesis is a result of the work that was conducted to fulfilling that goal.

1.2 Aim of the present work

The aim of this research was to develop a tactile fingertip useful for robots in exploration and dexterous object manipulation. In order to achieve this goal, below mentioned objectives had to be fulfilled.

The first objective of this research was to understand the necessary requirements of a tactile sensing system needed for a robot fingertip. Previous literature, Finite Element Analysis (FEA) of a human fingertip and experiments conducted using an anthropomorphic tactile fingertip yielded the understanding and requirements of a tactile fingertip. As this research pointed out a necessity of a soft force sensor that can measure forces dynamically, such sensor system was developed.

Second objective was to develop tactile fingertip using the force sensor developed and evaluate its ability to perform tasks similar to that of a human fingertip.

Third objective was to identify the information that a soft tactile sensing fingertip could give and use this information to develop control methods to control robot hands when manipulating objects dexterously. In order to demonstrate the ability to explore environments, a task to discriminate textures and materials were conducted.

1.3 Dissertation organization

This thesis is based on the development of a tactile fingertip system for robots. To fulfil this objective, a soft force sensor was developed. The first chapter gives a brief introduction into the thesis topic.

The second chapter explains the human tactile system. Then, moves on to explaining the requirements of a robot tactile system and finally explains the information that could be obtained from an anthropomorphic tactile fingertip using a previously developed tactile fingertip. The sensor's ability to detect

incipient slip, control gripped objects in manipulation is reported with experiments.

Third chapter presents design, construction, modeling and the calibration of the proposed soft force sensor. It includes detailed design parameters and the experiments carried out for the calibration and the validation of the sensor. This chapter furthermore includes the construction of the tactile fingertip using the above mentioned force sensor.

Fourth chapter is dedicated to explaining the construction of the tactile fingertip gripper. Then the fingertip was used in object manipulation tasks and the sensor signals were analyzed.

Fifth chapter is presenting the proposed force sensor as a texture classification tool useful in humanoid robots. The features generated for the classification algorithm Support Vector Machine (SVM) is presented and evaluated for its robustness to be used in robotic systems. The experiment results are presented as well.

Chapter six concludes the thesis with the closing remarks and future possibilities and research to pursue.

Chapter 2

Analysis of Human Tactile Systems, Requirements of Robotics Tactile System, and Information obtained by a Robotic Tactile System

Literature states that human has the highest dexterity considering manipulating objects [**11**]. Therefore, it is prudent to analyze the functions of human hand, particularly the tactile sensing system so that the robot tactile systems can be copied to have the same capabilities. This Chapter analyzes the human tactile systems exploring its utilization of sensors, and the information obtained from such sensors. Next, the chapter explains the requirement of a tactile system that could be used on a robot which will perform similar tasks as the human tactile system. These requirements are stated after analyzing a 3D fingertip model using FEA models, and conducting experiments using fingertips that could detect force and vibrations [**23**].

2.1 Introduction

Tactile sensation is an important sensory modality for the humans because tactile sensory data plays a major role in object manipulation and environment exploration tasks. In order to manipulate objects, the object has to be grasped by the hand with a suitable grip force. According to [**17**] factors that directly affect the applied grip force are: frictional conditions between the surface and the finger, weight of the object and the safety margin necessary for the object (which is determined by the human). Then detection of onset of slip is the key factor in tuning (secondary adjustment) the gripping force necessary for holding the object.

Apart from object manipulation, the second most important task of the tactile system is to perceive the environment. The information necessary for interacting with the environment are: detection of object contact, detection and discrimination of material and surface conditions such as rough/ soft surfaces, surface textures, metals/ wood/ concrete etc.

The objective of this chapter is to focus on the issues arising when designing human like fingertips that is capable of grasp, and manipulating objects and environment perception. We present analytical experiments, experimental validations and previous research to develop these requirements.

2.2 Human fingertip – A basis for robotic tactile fingertips

The human skin has four types of mechanoreceptors. These mechanoreceptors are sensitive to vibrations, pressure and skin stretch [**12**]. Tactile sensing data collected from these mechanoreceptors help humans to complete grasping and environment perception tasks. The non-linear, hysteresis signals generated by the mechanoreceptors due to mechanical stimuli [**24**], [**25**] coupled with previous experiences allow humans to evaluate surfaces

for texture differences, similarities, roughness, stiffness etc. and manipulate objects with precision. This is possible because of the high spatial sensor density in the fingertips. A fingertip consist about 17000 mechanoreceptors in the hand. In a single fingertip there is about 250 mechanoreceptors in a square centimeter area give enough spatial and temporal tactile information so that the brain could extract information and then execute complex manipulation tasks. Although mimicking such a system for the robot is beneficial; fabricating that system with same resolution and sensing capabilities using available sensors and methods is still a challenge.

Further exploring this aspect, researchers have found that mechanoreceptors in the hands can be divided into for type depending on the sensitivity to different types of modalities and frequencies of vibrations. The four types of mechanoreceptors are Fast-Adapting type 1 (FA-1, Meissner endings), Slow-Adapting type (SA-1, Merkel endings), Fast-Adapting type 2(FA-2, Pacini ending), and Slow-Adapting type 2(SA-2, Ruffini-like endings). From these, FA1 and SA1 respond to the micro vibrations happening at the instance of slip. The location, properties and the sensations of these sensors are presented in the **Table 2-1**.

Table 2-1: Characteristics of skin mechanoreceptors [**26**] [**27**]

Name	Location	Function	Frequency Hz	Receptive field mm^2	Receptors per cm^3	Adaptation
Meissner endings (FA1)	Dermis of the skin	Responds to motion and vibrations	10-200	1-100	140	Moderate adaptation
Pacini ending (FA2)	Deep layers of the skin	Responds to vibrations	40-800	10-1000	21	Rapid adaptation
Merkel endings (SA1)	Epidermis of the skin	Responds to pressure of the skin and texture	0.4-100	2-100	70	Slow adaptation
Ruffini-like endings (SA 2)	Dermis of the skin	Responds to pressure and skin stretch	7	10-500	49	Slow adaptation

The tactile information obtained by mechanoreceptors help humans to grasp and manipulate objects with their fingertips. When a human grasps and manipulates an object, he or she would reach for the object and grip the object

with their fingertips. Then a force is applied to the object by predicting the weight, and texture using previously retained knowledge of similar objects. Next, the fingers lift the object. At that instance, if there are localized vibrations at the contact surface of the object and the fingertip; the finger increases the gripping force slightly. If no vibrations are detected, the grip is loosened until localized vibrations are detected. This control of grip force triggered by the occurrence of localized vibrations is called incipient slip based grip control. This control scheme keeps the grip force slightly above the minimum gripping force needed to keep the object at the onset of slip. The force control scheme allows the hand to grip the object with minimum deformation to the object and minimum energy usage.

Applying enough force to hold an object securely and manipulating that object without dropping is achieved through the detection of incipient slip at the contact surface of the object and the fingertip. Researchers have understood that humans detect incipient slip of the objects through detecting the localized vibrations that happen at the contact surface of the object and the skin [24]. These vibrations are caused because the points on the finger at contact surface start to slide relative to one another. This relative motion causes the skin to stretch and contract. This relative displacement induces stresses in the direction of the motion of the finger. A FEA simulation was carried out to analyze this phenomenon further.

2.2.1 FEA simulation of a biological fingertip holding an object

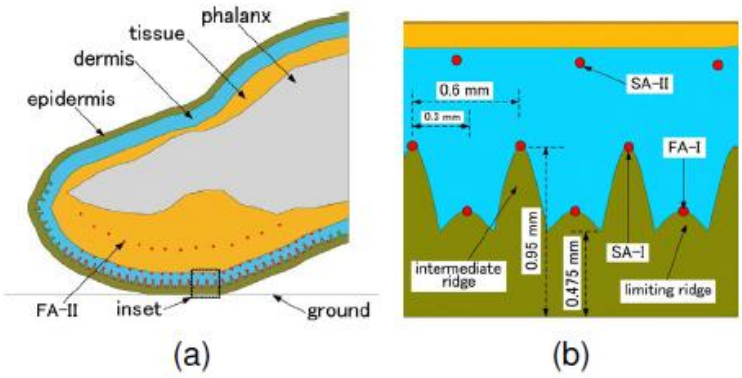

Figure 2-1: 2D FEA model of a human fingertip (a) the two dimensional fingertip with different layers and mechanoreceptors (b) the microstructures in the dermis and epidermis layer [**28**]

Two dimensional model of a human fingertip with micro structures was developed (see **Figure 2-1**). Microstructures were created between the epidermis and dermis of the fingertip (see **Figure 2-1(b)**). The four types of mechanoreceptors were positioned as stated in the literature at different depths of the skin (refer **Table 2-1**). For the simulation, the fingertip was pressed against a flat surface (ground) and dragged on the surface until gross slip occurred which was similar to finger gripping an object and trying to lift the object but slid from the fingertip due to its weight. Results from the simulation presented the following conclusions:

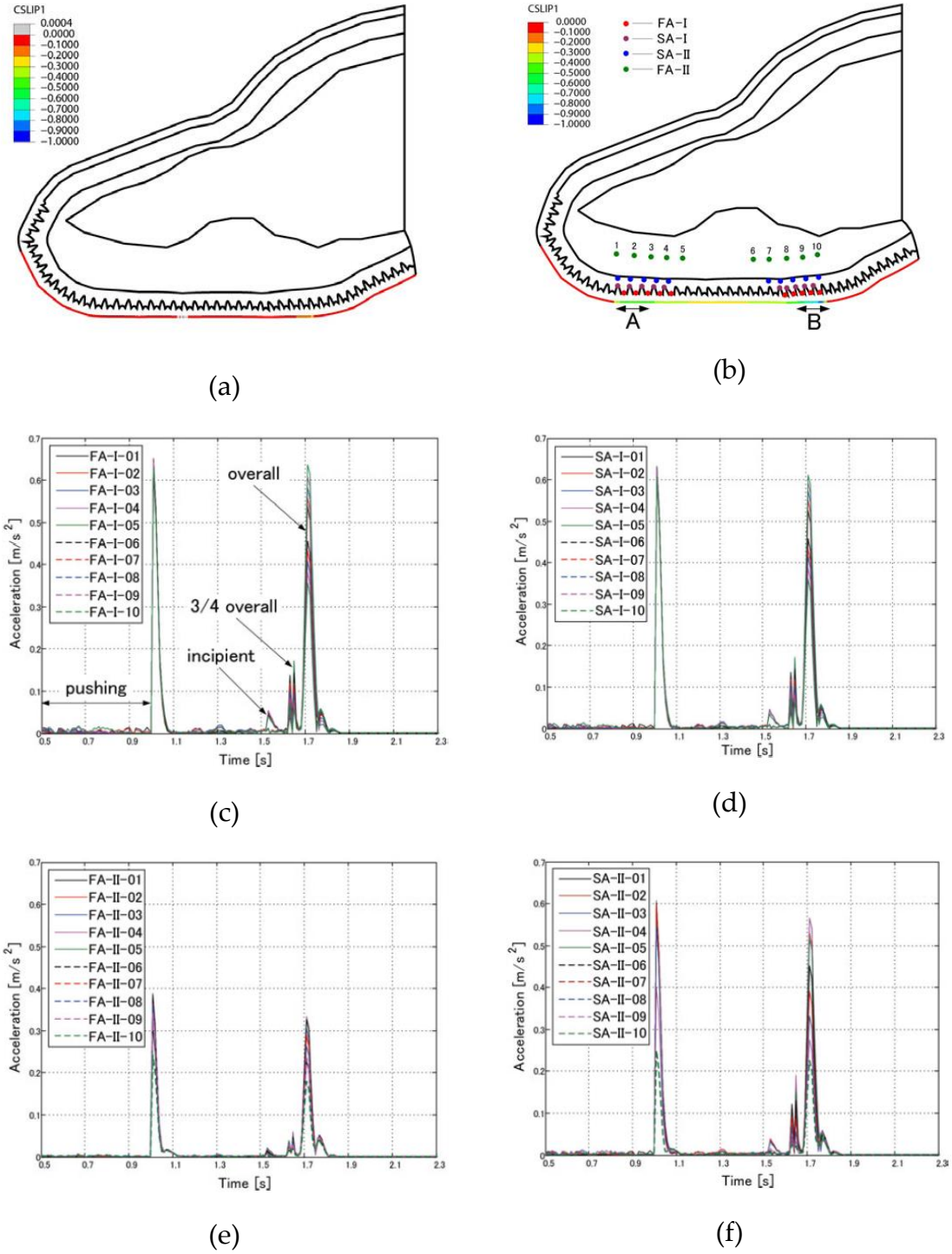

Figure 2-2: Simulated results. Slip occurring (a) when the fingertip was pressed on to the surface, (b) when the fingertip slides on the surface. Acceleration response at different mechanoreceptors (c) FA-I (d) SA-I (e) FA-II (f) SA-II [**28**]

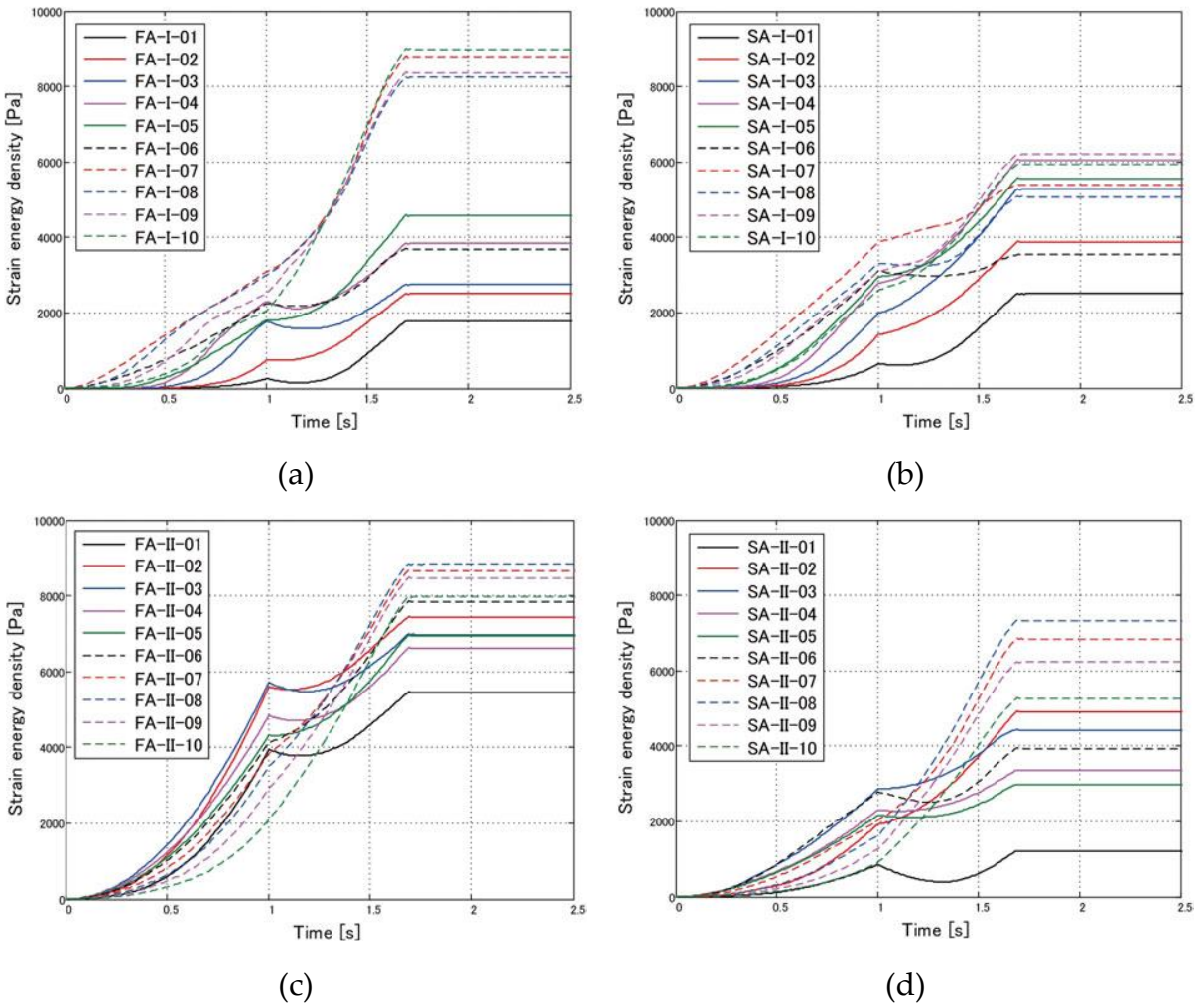

Figure 2-3: Simulated Strain Energy Density (SED) as a function of time at different locations of the mechanoreceptors: (a) FA-I, (b) SA-I, (c) FA-II (d) SA-II [**28**]

1. **Figure 2-2(a)** and **(b)** shows the simulation results on the skin surface. Color red indicates no slip while blue indicates slip of 1mm. It could be noticed that incipient slippage appeared firstly in the peripheral contact (A, B on the **Figure 2-2(b)**) area and propagated towards the center of the contact area and gross slippage appeared when the center nods started to slip. In order to detect this incipient slippage, the sensors should be close to the contact surface and should be at the peripheral of the contact area.

2. Ten reference locations around the peripheral area which is shown in **Figure 2-2(b)** were selected for the analysis. **Figure 2-2 (c)-(f)** shows the acceleration responses of each mechanoreceptor type at the above selected sensor nodes. The first peak on the signal was at the moment of transitioning from pushing to sliding. While sliding, distinct peaks with increasing magnitudes could be observed. These can be considered as the start of incipient slip, the instance where approximately 3/4 of the contact area had slipped, and instance where gross slip had occurred. The mechanoreceptors FA1 and SA1 which are at the boundary of the epidermis and dermis layer were able to sense vibrations due to slip than the sensors that were in the dermis layer. This provided the deduction that if to detect vibration signals, the sensors should be embedded between the skin and tissue layer of the fingertip and there should be a layered construction with multiple layers of thickness and stiffness.
3. Simulation also showed that a time latency of more than 100ms (from 1.53 s to 1.63 s or 1.65 s) is present from detection of incipient slip to gross slip which that time could be used for the compensation adjustments when griping objects.
4. Previous research has stated that Strain Energy Density (SED) is the best mechanical measurement for analogy of the neural signal during edge enhancement indentation [**29**]. **Figure 2-3(a)-(d)** represents the SED plot with time for the reference sensors. During pushing, the SED was increased rapidly, and during sliding, the SED was increased and then remained constant after overall slippage. In most of the receptors (FA-I, FA-II, and SA-II), the SED in area B (indicated by dotted lines) was clearly larger than the SED in area A (indicated by solid lines). This suggested that the SED might be able to capture the phase changes such as phase changes from pushing to

sliding and from incipient to overall slippage. However, this could only be performed after the phase changed. Thus, we cannot utilize the mechanical measurement of the SED as a sensing function to detect the incipient slippage and may not be able to be used to prevent slipping.

After these findings, a 3D fingertip model was used to analyze the phenomenon further. Magnetic resonance (MR) images of an index finger were taken [**30**]. Using image processing, the boundaries of finger, and bone were selected (see **Figure 2-4(a)**). Next, 3D geometries of bone; tissue and skin (see **Figure 2-4(b)**) were reconstructed by connecting the boundary nodes. The internal skin boundary was generated by scaling down the boundary of the finger surface by 1mm. Accordingly; the fingertip was separated into three regions denoted by skin, subcutaneous tissue, and bone. The geometries of these regions were then imported into FE package ABAQUS™ for further processing.

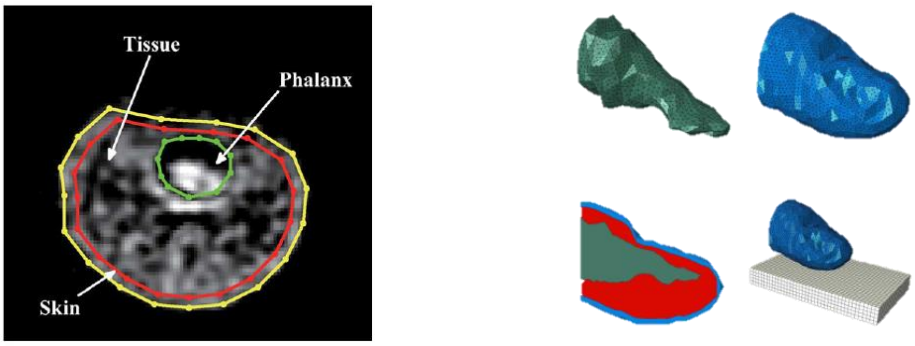

(a) (b)

Figure 2-4: 3D fingertip model generation (a) Using image processing selecting layers from MR images, (b) modeling bone, tissue and skin of fingertip

Similar to the 2D fingertip model, the 3D fingertip was pushed onto a surface and slid along the surface to simulate an object grasping and slipping experiment. **Figure 2-5** shows the simulation results of the skin surface. The

slippage was defined as the relative displacement of the skin to the flat surface. Similar to the results of the 2D simulations the 3D simulations yielded that the incipient slip propagated from the peripheral of the fingertip to the center of the finger. From the simulations we realized that there was about 200ms time delay between incipient and gross slip, which we can utilize to increase gripping force or change gripping strategy to avoid slipping.

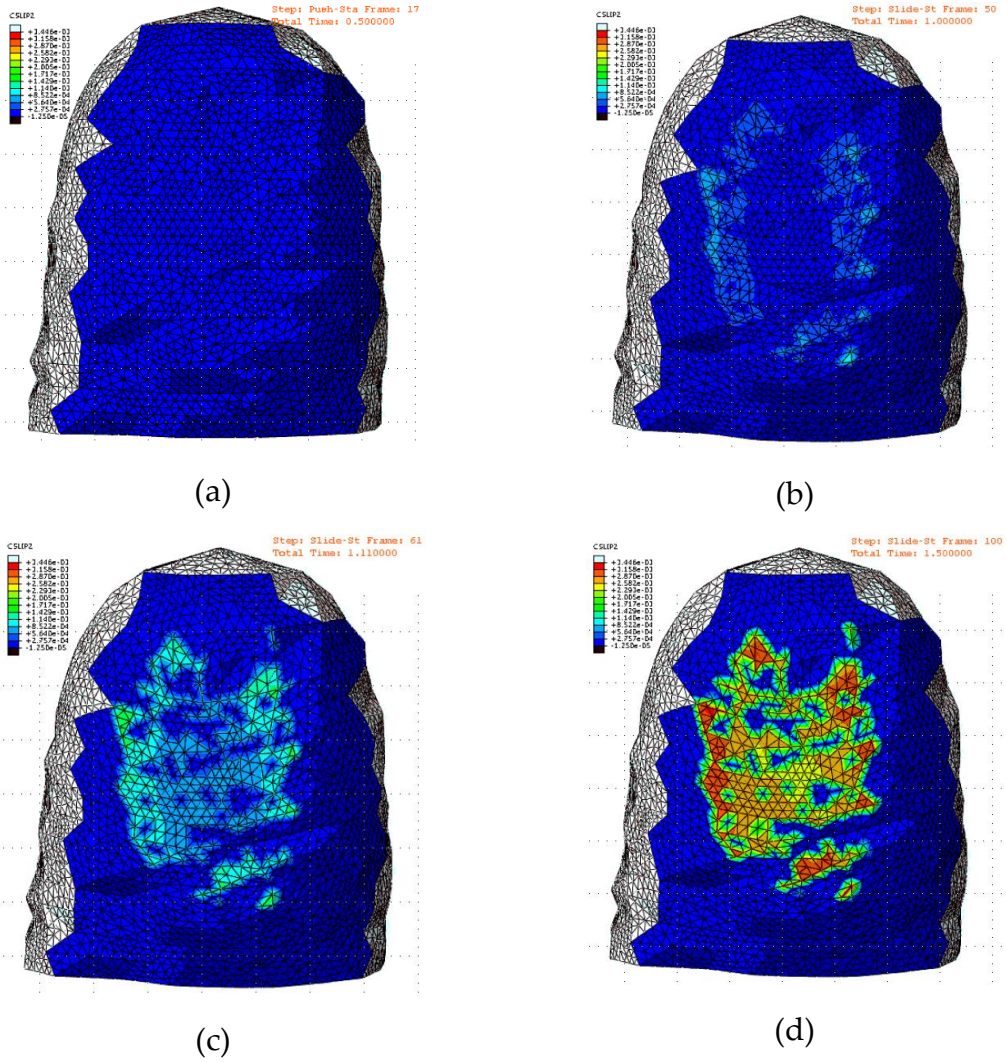

Figure 2-5: Simulation results of slippage in sliding direction at (a) start (b) incipient slip start (c) Slip propagate (d) gross slip. The colors represent the relative motion of the skin to the flat surface.

Some reference nodes on the skin and in the tissue were selected to analyze the mechanical behaviors further. Nodes were selected in both horizontal (h1 through h7) and vertical (v1 through v7) directions (see **Figure 2-6**).

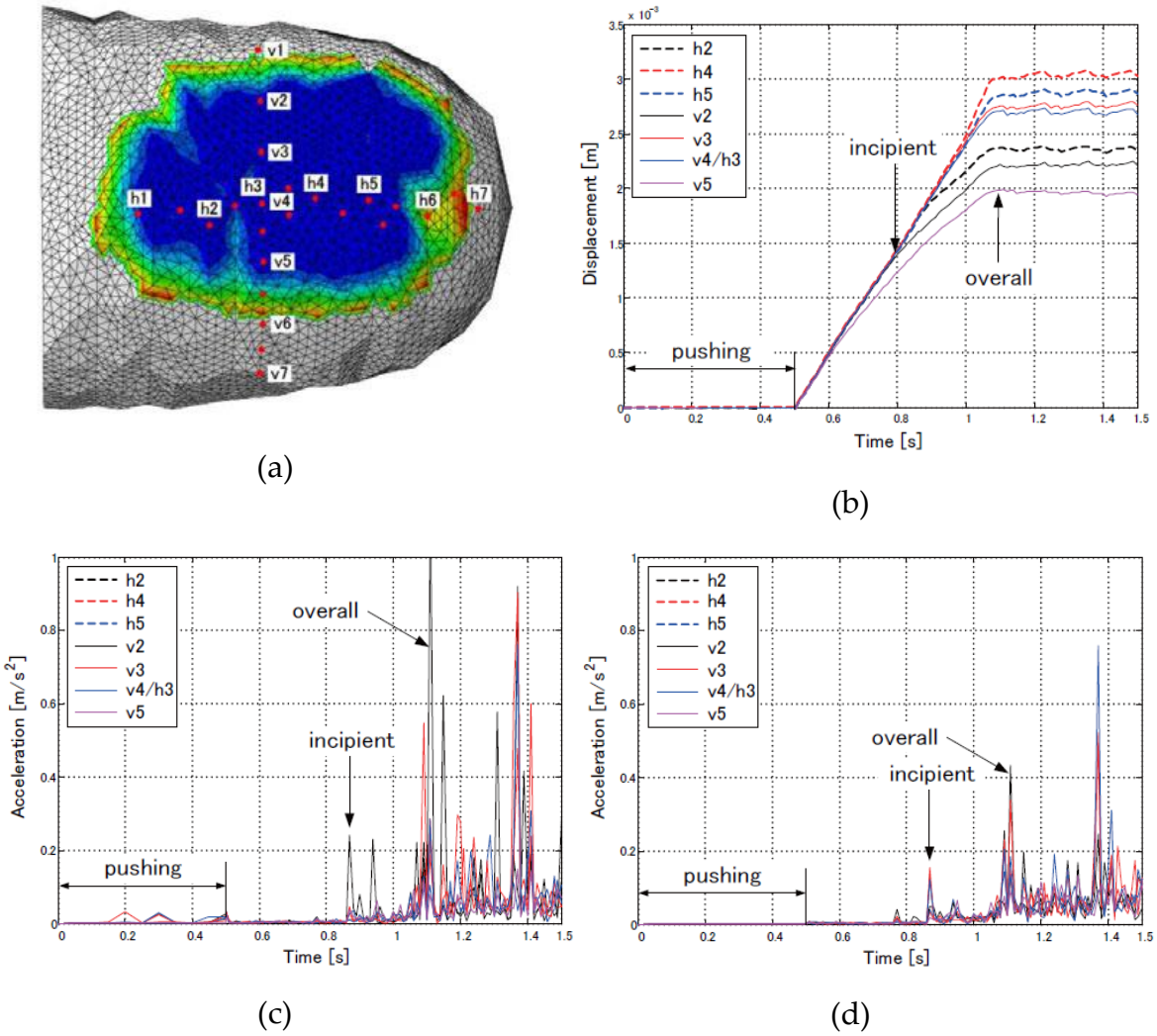

Figure 2-6: 3D model simulation results of nodal displacement and acceleration: (a) Selected vertical and horizontal nodes, (b) displacement of the nodes in sliding direction on the skin surface, (c) acceleration amplitudes of the nodes in the skin, (d) acceleration amplitudes of the nodes in the tissue surface

From **Figure 2-6(a)** we can see that nodes h2 through h5 and v2 through v5 were contact with the flat surface. At first the nodes stick to the flat surface and moved together which represented with the same velocity (see **Figure 2-6(b)**). After certain time, few nodes gave away and moved apart from the slop. This moment was considered as the start of the incipient slip. After certain time all the contacted nodes gave away showing start of gross slip.

Based on **Figure 2-6(b)**, the incipient slippage started around 0.8s (indicated by the arrow), and the gross slippage started around 1.1s. Thus, there was a time delay of 300ms between incipient slip and gross slip. This suggests measuring movements of the nodes on contact area is a straightforward and effective way to detect incipient slippage; however, it is a challenging task since it requires real-time motion capture and image processing with high resolution to detect relative motions of the nodes.

Figure 2-6(c) and **(d)** shows the acceleration responses of the nodes on the skin and the tissue layers. The figures show large peaks which corresponds to gross slip. Before this moment, two relatively large peaks can be observed and these are believed to be caused by the incipient slip. There, it shows a time delay of 240ms between the incipient slip and gross slip. Based on these figures it can be concluded that both incipient and gross slip can be identified in the acceleration signals of nodes on both skin and tissue layers.

2.3 State of the art survey of tactile sensors and tactile fingers and shortcomings of such technologies

It is prudent to investigate the tactile sensors and techniques that have been constructed for robotics applications particularly detecting tactile sensation by hands.

Similar to that of a human skin, the sensitivity of the artificial tactile system should vary in the different portions of skin in order to minimize the wiring and the processing needed. Therefore, in a humanoid robot, the hands should be the most sensitive area and the rest of the body should have enough sensitivity to detect contact situations and localize those contacts. Thus, these artificial skins should have sensors distributed according to the sensitivity required. Mittendorefer [**31**] developed a hexagonal multimodal sensor module that could be assembled into a skin. It had multiple sensors in each module and sensor signals were processed within the module and transmitted to a central computer. These sensor modules could be connected with each other to expand the sensing area. The system showed promise though still the modules were large and rigid where it was difficult to wrap the module in a non-flat surface making the applications of such a system limited. Furthermore, use of microprocessors for individual modules have resulted a higher cost for a square sensing area. The sensor was rather large making it difficult to be used in robot fingers. A similar modular based sensing skin was introduced by Schmitz [**32**] where capacitive technology based distributed pressure sensors were used to detect tactile signals. Compared to Mittendorefer [**31**] this sensor skin was flexible to be fixed into curved surfaces though only pressure could be measured. This pressure sensor based skin would be used to detect contact events of the robot body but use it in the hands for object manipulative tasks is quite questionable as it lacked the ability to detect incipient slip. An electromagnetic induction based compliant three axis tactile sensor which had the ability to measure force and detect slip was reported by Takenawa [**33**]. This sensor operated on the basis of detecting the displacement of the magnets and it yielded promising results to be used in artificial skins. Ohmura [**34**] developed an optical technology based sensor with modular capability. This sensor too had the similar traits of Mittendorefer [**31**] capacitive sensor where only force

was measured, thus having the similar downside of not being able to detect slip even though the sensor was a contender for large area tactile sensing. The state of the art survey of Yousef [**35**] gave a detailed look at sensors and technologies that could have been used for tactile sensing by robots.

The above publications gave sensors and technologies that could have been used in general for tactile perception. Special care has to be taken to developing tactile sensors that can be used in the hands, particularly the fingertips; where it plays a key role in dexterous object manipulation. These fingertips should have the ability to detect force and vibrations modalities in order to be useful in dexterous manipulation. Reading the literature of tactile feedback fingertips, most of the fingers were developed for a certain task, either material or texture recognition or object manipulation. Liu [**36**] developed an intelligent finger that can identify contact location, normal and tangential forces and vibrations generated in contact. The fingertip was used in material recognition experiments. Though this fingertip was successful in material identification, the use of this fingertip in object manipulation was not presented. Additionally, the fingertip was rigid making it a limitation for object manipulation.

Micro Electro Mechanical Systems (MEMS) technologies are widely used to develop sensors. Tactile fingertips too are developed using MEMS force/moment sensors. Oddo [**37**], Muhammad [**38**], Kim [**39**], Ho [**40**] and Boissieu [**41**] developed MEMS based fingertips (capacitive and resistive based sensing mechanisms) and used those for texture recognition. Nonetheless these fingertips were still in research stages and far from robotics applications. They had limited sensing modalities and limited area of sensing. Additionally, these were used in specific applications such as texture recognition or slip detection. Jamali [**42**] conducted material discrimination experiments using a fingertip

made from polyvinylidene fluoride (PVDF) and strain gauges randomly distributed in silicon rubber layers. This approach yielded good results though the reproducibility of the fingertip system in mass scale is difficult because of the random distribution of sensors. Readers are advised to read work of Schmidt [**43**], Ding [**44**], Tanaka [**45**], Liu [**46**], and Tanaka [**47**] to understand more about different type of tactile sensors and technologies.

Above section presents the current state of the art in tactile sensor technology. Although many sensors and technologies have been discovered, very fewer researches were conducted in order to assimilate the different sensors and technologies to develop a biomimetic fingertip that can detect multiple modalities and would be commercially available for robotics applications.

Research team of professor Hosoda [**48**] developed an anthropomorphic finger that has randomly embedded strain gauges and PVDM film in a polyurethane material. This fingertip had the ability to sense temperature as well. The team developed technique to use this fingertip in material discrimination, slip detection [**49**] and object manipulation [**50**].

BioTac is a fingertip made by the research team in University of Southern California [**51**]. It has thermal, force and vibration sensing ability and has been commercialized for the use in robotic applications. It has the ability to detect the force and the position of the applied force [**52**], vibrations occurring due to object interactions [**53**] and discrimination of textures by analyzing those vibration signals. This fingertip and the system by far have come up using in robotics applications and paved the way for object manipulation research. The downside of this sensor is its construction where the vibrations are sensed by a hydrophone inside the fingertip. Because the fingertip has a liquid layer, it is

susceptible to leakage. Furthermore it is difficult to be used in environments where the temperatures change quickly.

By analyzing acoustic emission signals generated during the relative motion of two contacting surfaces Dornfeld [**54**] identified onset of slip and further stated that roughness and material affects the amplitude and presence of the slip signal. Similarly Tremblay [**55**] used an accelerometer sensor signal to detect the vibrations generated by the onset of slip and by measuring normal and tangential forces at that moment, estimate the frictional coefficient accurately. They also utilized this for grasp force control. Similarly, Son [**56**] developed a stress rate sensor that could provide localized information such as detection of contact event, detect local skin curvature for understanding contact shape and area, and incipient slip. Melchiorri [**14**] also proposed a system of controlling objects through detection of slip. He considered the linear Coulomb friction effect and rotational movement of the objects when in manipulation and proposed a controller with force/torque and tactile sensors signals as inputs. Gajin [**57**] also used tactile sensor based slip detection to control a robot hand to regulate grasping force. They used the force output of center of pressure tactile sensor.

Holweg [**58**] proposed two methods to detect slip. One method was frequency analysis of the position of the center of force distribution. In this method, by applying Fast Fourier Transform **(FFT)** to the center of distribution, they identify the micro movements of the objects due to the elasticity of the rubber. The next method was to measure the FFT signal of normal force before and while the object is in slip. It was noted that while the object was in slip, the normal force fluctuated in a certain frequency due to the "catch and snap back" effect. These researches had limited applications because the sensors which were used in these analyses were not developed enough to be used in robotic

hands. Furthermore these researches had been discontinued afterwards and many questions are still not being answered.

By reading these findings it can be understood that still, the sensing of incipient slip is a problem for the robotic tactile systems. Even with advances in sensor technologies, no significant headway was seen in slip based grasp controlling methods.

2.4 Information obtained from an artificial tactile system

Artificial tactile system of a robot can give number of information. This information can be utilized in robot motion planning, task planning and environment perception. This section presents the information that can be obtained by such tactile system. The experiments were conducted using an anthropomorphic tactile sensing fingertip.

2.4.1 Application of a anthropomorphic tactile sensor to manipulate objects dexterously

2.4.1.1 Anthropomorphic Tactile Sensor Design and fabrication

The anthropomorphic tactile fingertip (ATF) mimicked the human distal phalanx in shape and functionality. A human finger has mechanoreceptors distributed throughout the skin that can detect forces and vibrations. Similarly, the ATF could detect vibrations and sense pressure using accelerometers and force sensors. Detailed design aspects of the fingertip sensor were presented in [**59**].

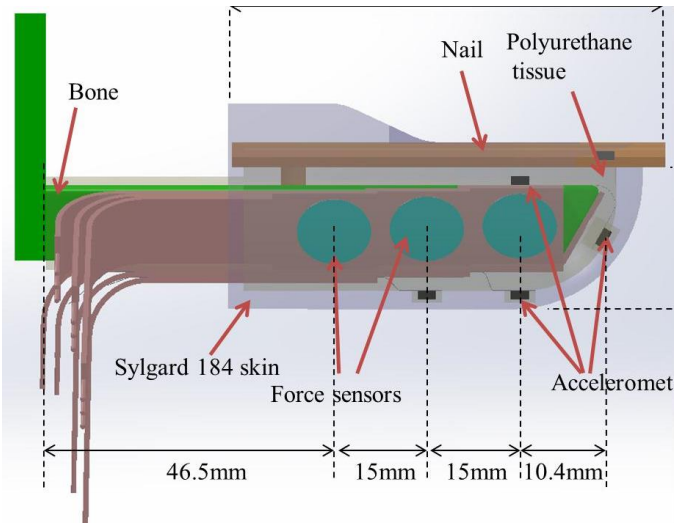

Figure 2-7: Anthropomorphic tactile fingertip (ATF) [**23**]

The ATF had a rigid core made from ABS plastic similar to the bones of a human finger (**Figure 2-7**). Forces were measured with commercially available `FlexiForce™ A201' sensors. Seven force sensors were attached to the surfaces of the bone. The vibrations were detected by MEMS accelerometers. These sensors were responsive up to a frequency of about 500Hz, similar to a human fingertip [**60**]. The fingertip had five three-axis accelerometers (Analogue Devices™ ADXL327BCPZ). Three accelerometers were suspended between skin and tissue and located 1mm away from the outer boundary. One was on the top surface of the fingertip bone and the last one was on the bottom surface of the fingernail. The fingertip was fabricated with two layers of soft material having different stiffness, similar to the epidermis and dermis of skin. Ridges on the skin surface were also created to make the fingertip more sensitive to textures and surfaces.

2.4.1.2 Sensing abilities and digital signal processing

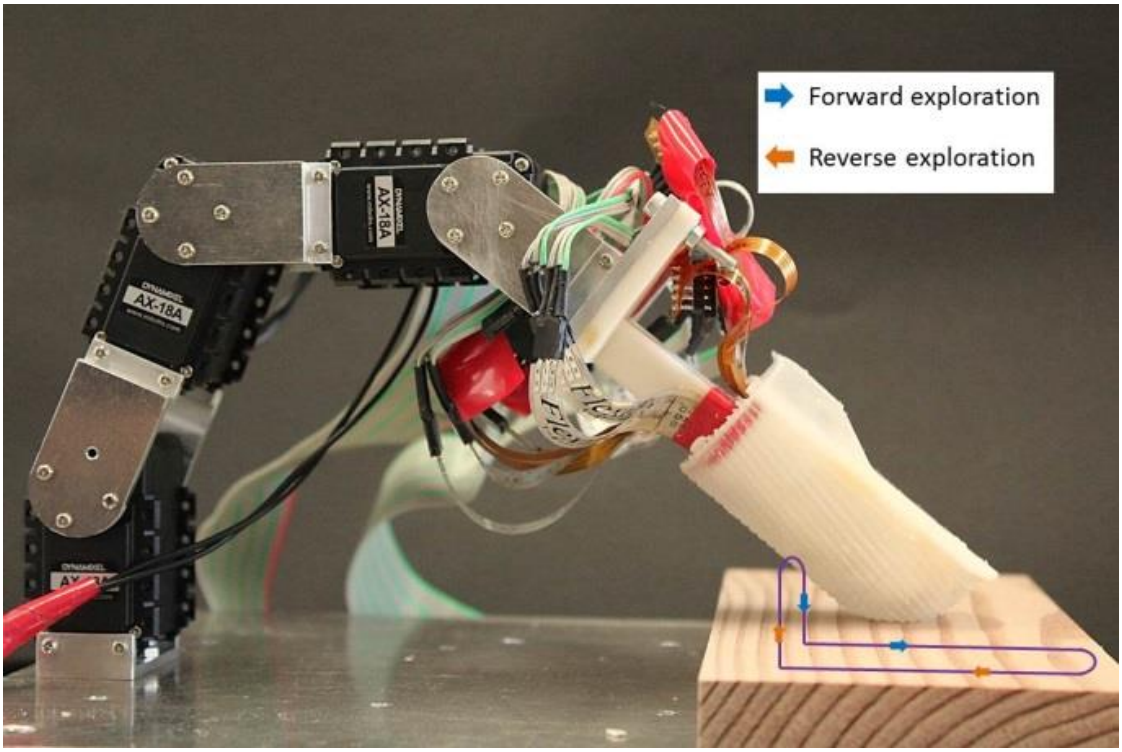

Figure 2-8: Active exploration: motion of the fingertip while exploring (arrowed lines) [**61**]

The ATF was fixed to three servo motors (Dinamixel™ 18A) with torque and position feedback. The tests mostly used active touch motion (see **Figure 2-8**). When ATF was slid on surfaces vibrations were generated. These vibrations propagated along the skin by deforming the soft layers (**Figure 2-9**). It caused the accelerometers to move in x, y, and z directions. The signals were sampled at a rate of 1.2kHz for each input. A 500Hz central frequency low pass filter was used to filter noise from the sensor signals. The filter and the sampling rate were adequate, as the human dynamic sensor field is susceptible only to micro vibrations of frequencies ranging from 50-500Hz [**60**].

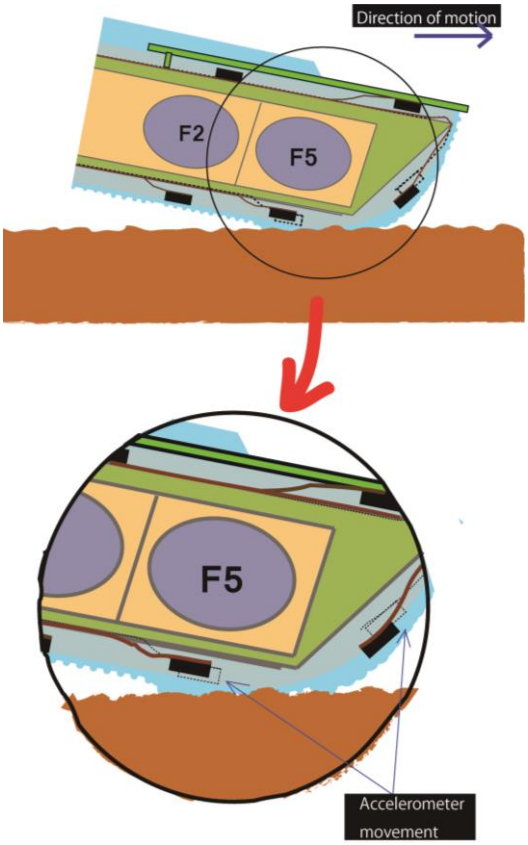

Figure 2-9: Movement of the fingertip along a rough surface result in the deformation of the skin and tissue. The vertical force f_i is measured by the i-th force sensors F_i. The acceleration components x, y and z are detected by accelerometer A_i [**59**]

2.4.1.3 Evaluation of ATF for grasping and manipulation

Johansson [**12**], reported that the stability of a grip depends on the object's size, shape, mass, and the friction coefficient between the fingertip and the object surface. Cutaneous and kinesthetic tactile data are used to calculate these properties of an object and the occurrence of slippage. We therefore proposed methods and performed experiments to show that ATF can provide tactile cues to successfully perform manipulation tasks. The steps required for object manipulation include [**12**]:

1. detection of the making and breaking of contact between the finger and the object;
2. localizing the contact point;
3. evaluating the properties of the object, including its size, shape, frictional characteristics, stiffness and predicted weight;
4. measuring the grip force while gripping the object;
5. detecting incipient slip when adjusting the grip force;
6. detecting external vibrations, such as a tool contacting a second object.

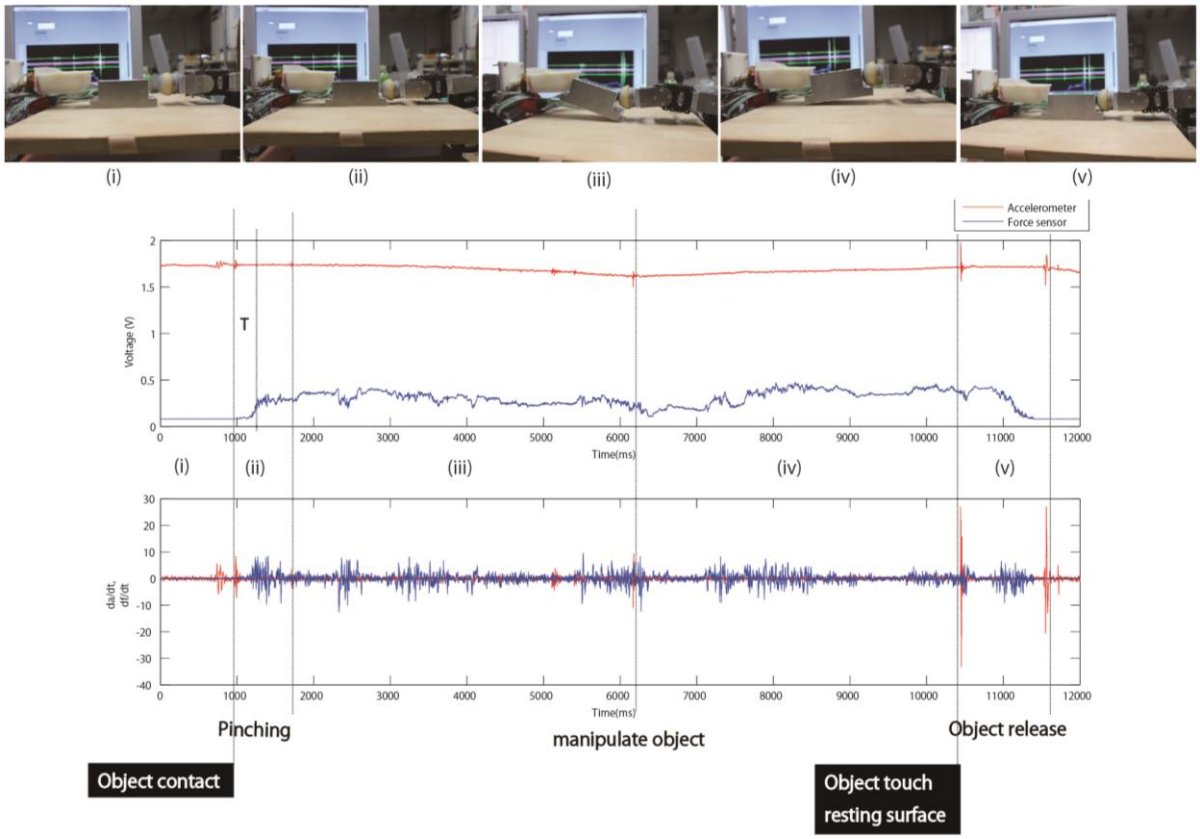

Figure 2-10: Accelerometer and force sensor data obtained while gripping, manipulating and releasing an object. The accelerometer and force sensors closest to the contact were selected and data from those sensors were recorded. The object was placed on a surface and the two fingers were moved closer until the fingertips touched the object. The object was pinched by the two fingers and lifted. The object was rotated clockwise and counter-clockwise for a few degrees

each and rotated back to its initial position. The object was subsequently lowered until it touched the horizontal surface and was finally released by the fingers [**59**]

Figure 2-10 shows a typical accelerometer and force sensor signal and its derivative for grasping and manipulation of an object. Following information could be deduced from analyzing the above signal.

2.4.1.4 Detection of the making and breaking of contact

While controlling the robot hand during object manipulation, it is necessary for the fingertip to contact with the object. This transient event is a cue for the hand to shift from position control to force control. By analyzing the force sensor and accelerometer signal together, it was possible to identify the instant of contact.

The derivatives of the force and accelerometer signals were calculated (**Figure 2-10**). If, within a given period of time T (250ms), the derivatives of the accelerometer and force sensor signals increased above a threshold, it was assumed that the fingertip had made contact with an object. After contact was detected, the system moved to the grip phase, in which a predefined force was applied to the fingertip to pinch the object (phase (ii) of **Figure 2-10**). In **Figure 2-10**, the portion (ii) was considered T. At the moment contact was broken; the force sensor value was gradually reduced to zero while the accelerometer signal showed a large deviation.

2.4.1.5 Predicting the point of contact

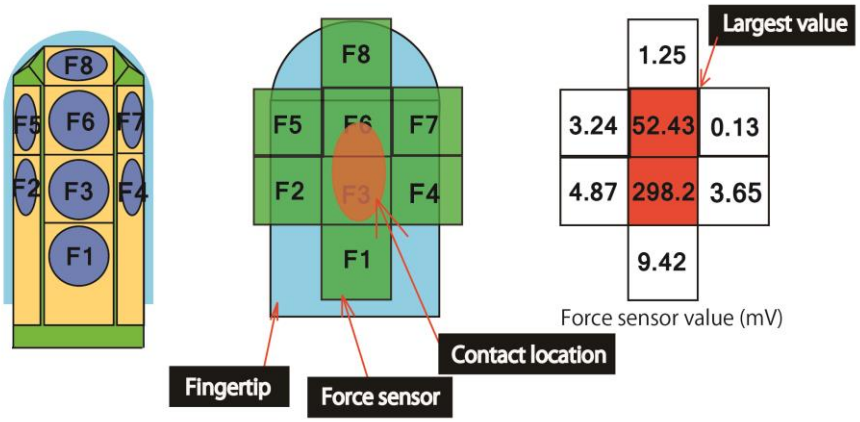

Figure 2-11: Predicting the point of contact. The contact locations would be areas F3 and F6, with F3 being more affected and having a greater area of contact [**59**]

Knowledge of the contact position can result in the selection of correct accelerometers for calculations. **Figure 2-11** shows a typical value array obtained for a certain instance of contact. The program identified the positions that had the largest value. The next largest value, which was adjacent to the largest value, was selected. The two values were compared and a position between these two sensor positions that would distribute the load proportionally was determined to be the contact position.

2.4.1.6 Surface stiffness classification

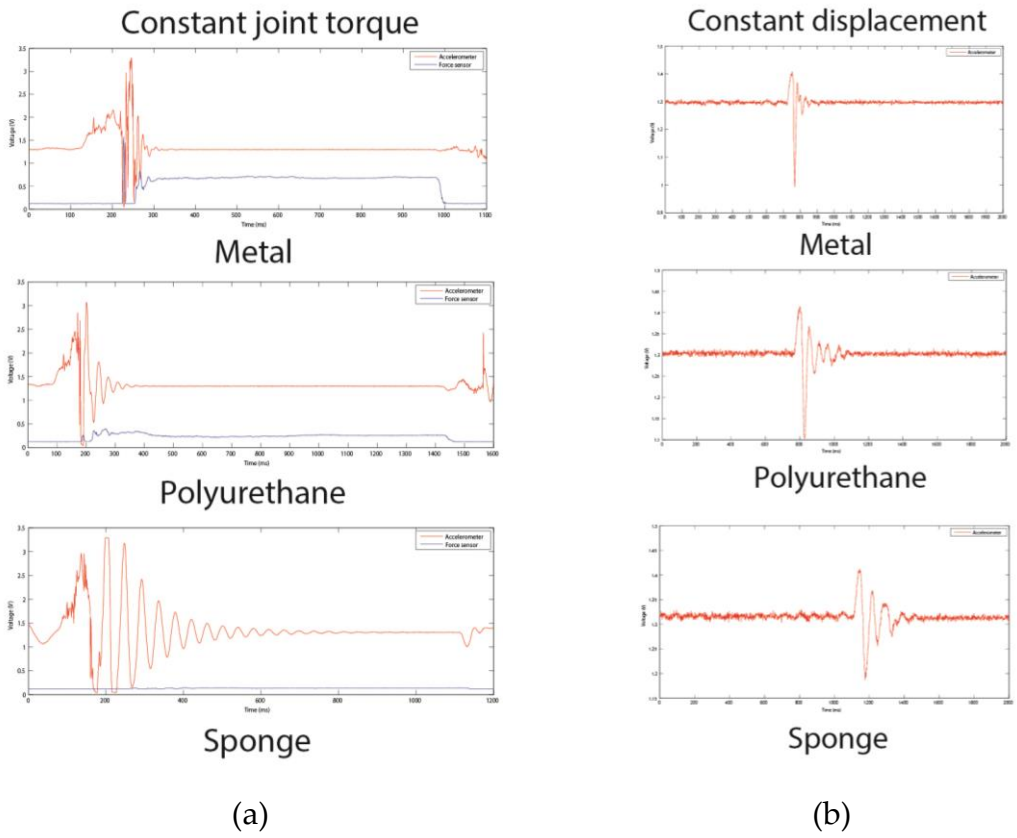

Figure 2-12: Accelerometer and force sensor signals of hard and soft materials at (a) constant joint torque and (b) constant contact depth [**59**]

The ATF was used to classify objects qualitatively according to stiffness, as ”high”, “medium” or “low”. The fingertip was tapped against the object and data from the accelerometer and force sensor were analyzed. Two types of tapping were considered. In one, the joint torques were kept constant while the contact depths were varied, and in the other, the contact depth was held constant. **Figure 2-12** shows the accelerometer and force signals when tapping on aluminum (high stiffness), polyurethane rubber (medium stiffness) and sponge (low stiffness).

For the constant torque tapping, the force sensor values were an indication of the stiffness of the material, with the harder material yielding a higher force due to a smaller contact area than softer materials such as polyurethane and sponge, where the contact area was larger due to material deformation. For tapping at constant contact depth, the energy of the accelerometer signal **Figure 2-12** was inversely proportional to the stiffness of the material. Softer material had a higher energy signal than stiffer material due to the high energy loss of the vibrations in the stiffer material.

2.3.1.7 Contour identification and surface identification

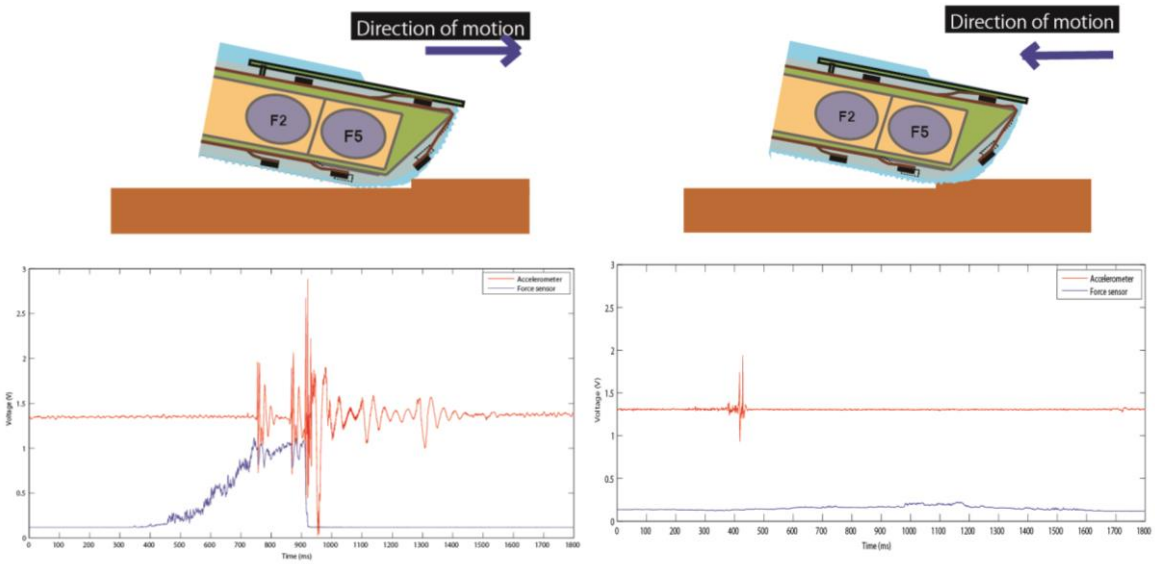

(a) (b)

Figure 2-13: Accelerometer and force sensor signals when a fingertip encounters a (a) step-up edge (b) step-down edge [**59**]

Even without visual data, humans are able to determine the shapes of objects from cutaneous and kinesthetic data. Humans follow contours on an object to determine its size and shape. Edges and corners constitute the boundaries of an object. Thus, by identifying edges, a robot should be able to estimate the size of an object.

The ATS could be slid over (an exploratory motion similar to that of a human fingertip) the object to find the edge. Upon encountering a step-up edge (**Figure 2-13**), the force on the fingertip increased because the edge resisted the motion of the fingertip. To overcome the edge, the fingertip must be deformed, such that the area of the fingertip in contact with the edge decreases. A larger vibration could be detected at this point. Thus, by comparing the force sensor values before and after the large vibration, the edge could be detected. Upon encountering a step-down edge, the force signal of the fingertip did not increase suddenly. Rather, only the accelerometer experienced a sudden change.

2.3.1.8 Detection of incipient slippage

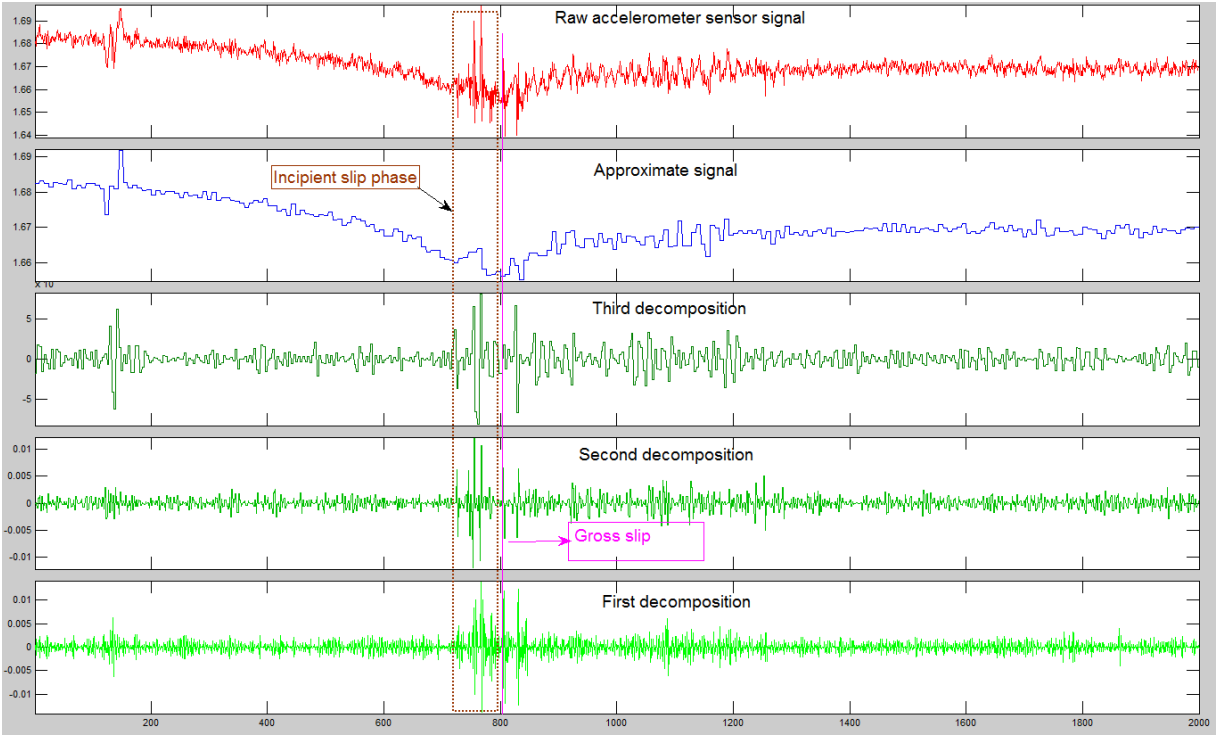

Figure 2-14: DWT signal of accelerometers at incipient and gross slippage [**59**]

Initially, Tremblay [**62**] proposed using accelerometers to detect incipient slippage and control grip forces. It was difficult to identify incipient slippage by analyzing raw accelerometer signals from ATF. This was likely due to the combined damping of the soft tissue layers and skin layers, making these

sensors less sensitive to vibrations. This drawback was overcome by using the Discrete Wavelet Transform (DWT) to separate the high frequency components of the accelerometer signal. Careful examination of **Figure 2-14** showed that, just prior to gross slippage, the first decomposition signal changed markedly. By introducing a threshold value, the states of slippage and non-slippage were determined. These two states were used to control the pinch grip force when manipulating the object (phases (iii) and (iv) of **Figure 2-10**). If slippage was detected, the controller shifted from position control back to force control. The force was increased by 5% of its initial value and position control reinstituted. Similarly, the fingertip controller changed from position control to force control and back to position control. These changes among control algorithms were not smooth, although they were ignored in this study. Applying higher-level control strategies (e.g. fuzzy controllers or neural controllers) may make the transitions from position to force control smoother.

2.5 Discussion

The conducted experiments and the literature review have suggested the following considerations when developing tactile sensors for robot hands.

2.5.1 Design considerations for a robot fingertip

Table 2-2: Design guidelines for tactile sensing system of a fingertip

Materials for the sensing surface	Compliant and durable
Sensing modalities	Force modality and vibration modality
Measurement for force	Pressure, stress, strain
Measurements for vibrations	Displacement, acceleration, frequency
Sensitivity needed for force modality	1g [**63**]
Frequency response for force modality	100Hz [**63**]
Frequency response for vibrations modality	1-500Hz [**60**]
Spatial resolution between sensing points for force modality	1-2mm [**63**]
Special resolution between sensing points for vibration modality	Less than 1mm
Sensor depth for vibration modality	Highest vibration sensed at the boundary of the tissue and skin layer
Maximum vibration sensed for incipient slip detection	At the perimeter of the contact surface

It has been evident that to have an effective tactile system, the fingertips should have the ability to sense force and vibrations signals relating to object manipulation and environmental perception tasks.

Apart from these guidelines, the papillary ridges of the fingertip have an important role to amplify the environment perception tasks. Therefore, an artificial fingertip would also benefit largely with components that mimic the functionality of the papillary ridges. The nail too acts as an additional sensing surface for the fingertip.

Above design guidelines are for tactile fingertips that are capable of both dexterous manipulations as well as environment explorations. In the past few fingertips which tried to mimic these guidelines appeared in the literature. Basically, only few fingertips with the shape of the actual fingertip have been seen. As the shape of the fingertip is cylindrical with a hemispherical end, the construction and the calculations of the deformations is complex. Therefore many researchers tried to simplify the design by making the fingertips hemispherical instead of the cylindrical. This allowed the calculations of the contact surface and deformations much straight forward. Furthermore, the hemispherical shape helps the grasping control of the fingertip as the direction of the grip force will always go through the center of the hemisphere making the object stability equations simple. Additionally, in a human fingertip, the front most hemispherical portion is used in pinch grip and which has the most sensor density and the mostly used portion of the fingertip for manipulation and environment explorations.

Another important aspect of fingertip design is the sensor density. As it is suggested in **Table 2-2**; in order to detect the incipient slip occurrence, the vibration sensor should be at the perimeter of the contact surface. Furthermore, the sensor should be placed at the skin, tissue boundary to detect the maximum

amplitude of vibration. After the sensor detects the vibration relevant to incipient slip, the system has about 100-300ms to react and control the grip force before gross slip happens. Thus, the tactile sensing system should have a high sensor density while being able to read and process multiple number of sensor inputs within few hundred micro seconds.

The tactile sensors and tactile systems presented till recently did not address all the requirements presented above. The main reason for limiting ability of the tactile sensor is the difficulty of developing a soft tactile sensor capable of measuring forces and sensing vibrations in the 100-500Hz range. Another reason was that a soft sensor was prone to wear. A fingertip will be used often making the soft embodiment susceptible to wear and tear. This will affect the force measurement greatly. Therefore, the soft embodiment may be needed to be replaced regularly. This meant that the sensor system had to be cheap. Thus, in order to have an advance in tactile sensing system development, a new soft force senor needed to be developed.

The next chapter introduces a new soft force sensor developed for tactile application.

Chapter 3

Design, Development and Characterization of the Soft Force Sensor

Force is a fundamental component of classical mechanics and measurement of this component is a necessary task in most of the static and dynamic systems. When it comes to robotic applications, the force measurement is paramount for a force feedback control strategies and safe operation. Traditionally, force sensors were made rigid. The reason is that these sensors used the stress or strain as the sensing mechanism and these properties were linear in metals. Thus, strain gauges bonded to metal structures (columns and cantilever beams) is still the widely used sensor type for strain/force measurement. By properly designing the sensor structure, the force (required measurement) applied on to the sensor will be proportional to the strain (measured physical property) of the structure. However recent development in many robot applications, medical technologies have requested the force sensors to be soft and deformable. This chapter explains a force sensor that can measure force in 3 axes. It was originally designed for robot tactile fingertips.

3.1 Introduction

In this chapter, we propose a soft force sensor (see **Figure 3-1**) that could be utilized in number of applications ranging from humanoid robots, biomedical applications to industrial quality assurance tasks. This chapter explains the sensor's design, fabrication and characterization. The presented sensor is a force sensor capable of detecting forces in three axes.

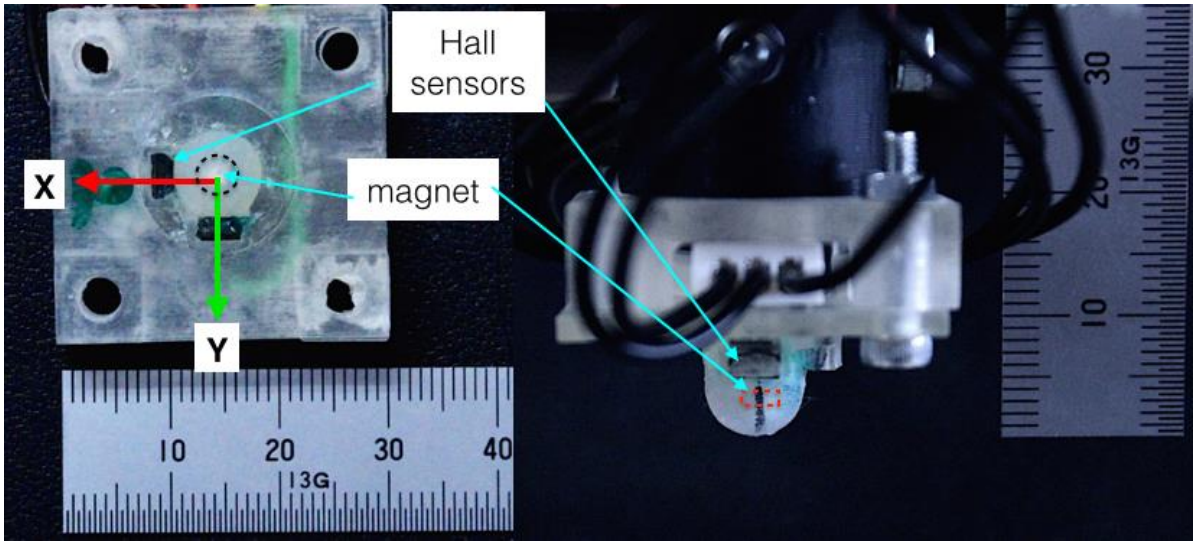

Figure 3-1: Developed soft 3 axis soft force sensor

Many commercial force and tactile sensors utilize beams and columns structures for sensing force. The structure gets deformed from the measured force, and this deformation is measured through the change in the physical properties: stress, strain, displacement or pressure using different types of transducers such as strain gauges, conductive ink, piezoelectric crystals, pressure gauges, light intensity, and magneto-elastic devices. The difference between above mentioned sensors and soft sensors is that, even though soft sensor use the same transduction principles, the structures or the transduction components are made of soft materials such as plastic [**64**], silicone [**65**], yarn and fabrics [**66**].

Table 3-1 contains a summary of soft sensors that measure force and stresses made from soft materials and utilize different transduction principles. The advantages of these sensors are that they are small, inexpensive and withstand impulse loads and loads that are much larger than the rated values. The downsides of these sensors are the none-linear behavior of measurements, higher hysteresis values, and inconsistency of the readings. These problems can be reduced significantly by correctly modeling the sensor output. If the behavior of the soft embodiment is correctly predicted, the relationship between the measured value and the sensor output can be derived and used as the characteristic curves for the soft sensor. This information can be used to decide the sensor parameters, operational range, signal filters and methods to linearize the measured values.

Therefore, in order to correctly construct and utilize a soft sensor, the steps of designing, fabricating, modeling and validating, and characterizing the sensor are important. This chapter introduces the design, modeling and the construction of a three dimensional force sensor. The sensor comprise of a soft cylindrical beam element that compresses and bends when a force is applied to the free end. A neodymium permanent magnet is embedded in the soft element. The free end of the beam displaces due to the force applied and this displacement is calculated by triangulating the location of the magnet by measuring the change in the magnetic field emitted (using Hall sensors) by the magnet at fixed locations.

Table 3-1: Soft tactile sensors employing different transduction principles to sense force, strain, and stress [**67**]

Sensing modality	Transduction principle	Examples	Ability to detect dynamic forces (vibrations)
Force	Resistivity	strain gauges [**68**]	N/A
		fabric [**69**]	100 Hz
		organic semiconductor [**70**]	N/A
		piezoresistance/MEMS [**71**], [**41**]	100 Hz
		Quantum Tunneling Composites (QTC) [**72**]	N/A
		Microfluidic channels [**73**]	100 Hz
		Electromagnetic induction [**33**]	1kHz
	Light intensity	Fiber optic sensor [**74**]	N/A
Shear force	Capacitance	differential capacitance [**75**]	N/A
	Piezoelectric	polyvinylidene fluoride (PVDF) films [**49**]	detects vibrations
	Resistivity	Quantum Tunneling	Can sense

		Composites (QTC) [**76**]	dynamic loads
	Light intensity	Photodiode [**77**]	30 Hz
strain	Resistivity	microchannel filled with conductive liquids [**78**]	N/A
	Magnetics	Magnetic field measurement using Hall sensors [**79**]	N/A
stress	Ultrasonic	electric impedance of a piezoelectric resonator [**80**]	N/A
	Light intensity	Photodiode [**70**]	N/A

Clark [**81**] and Nowlin [**82**] first mentioned the use of Hall sensors to measure magnetic field when developing tactile sensors. Torres-Jara [**83**], Jamone [**84**] [**85**], Ledermann [**79**], and Youssefian [**86**] too presented similar tactile sensors that use the principle though the design and characterization of the sensors were different to that of ours. The above mentioned sensors differ in construction mainly by having a hollow cavity that causes problems when larger loads (above the rated load) are applied. The other difference is the placement of the Hall sensors which is parallel to the permanent magnet. The proposed sensor in this thesis has solid embodiment without any cavities and the Hall sensors are placed orthogonal to each other. This construction helped to triangulate the location of the magnet in the 3D space, while the previous research focused only on the displacement in one direction except for [**79**]. Furthermore, the proposed sensors use a mathematical model that accurately analyzes the relationship between applied normal and tangential forces, the soft

material deformation, change in the magnetic field at fixed points in space due to movement of the magnet, and the induced voltage of Hall sensors.
Much literature can be found stating that the soft sensors were modeled using finite element analysis (FEA) [**87**] [**88**]. This is due to the complexity in the sensors physical effects (deformation of materials) [**89**], non-linear behavior in properties of the sensor [**90**] and the complex geometric shapes utilized in the sensors [**91**]. There were only few examples of mathematical representations of soft sensors. Even then, geometry of the sensors was simplified to a simple geometric shape. Van [**40**] represented a force sensor that had a hemispherical embodiment to a bundle of beams that compressed and bent due to normal and tangential forces. Zhang [**92**] used a cantilever beam based modeling approach to model a slip sensor. We propose a mathematical model for the proposed sensor making the calculations faster than FEA simulation. In the current study, the sensor's mathematical modelling and its characterization was done by representing the sensor as a single cantilever beam compressed and bent under normal and tangential forces.

The chapter is organized such that in the first and second section the operating principle and fabrication of the sensor is described. Next sections explain the mathematical modelling of the sensor. Then discusses the results of the simulation and following section states the experimental results obtained. Next section explains about the use of this concept in developing a hemispherical tactile fingertip. The simulation of the sensor and the calibration is reported. Final section concludes with a discussion of the variables influencing the sensor performance.

3.2 Sensor principle

The proposed sensor uses the concept of triangulating a displaced point of a bent cantilever beam so that the total bending of the cantilever can be calculated by interpolating the known point. This displacement of the points in

the sensing element is measured by triangulating its location by analyzing the change in the magnetic field generated by a magnet placed at the location of the stated point. The proposed sensor uses three Hall sensors that are orthogonally placed near a cylindrical soft beam made of silicone rubber. The free end of the beam was made as a hemisphere. A neodymium permanent magnet was embedded in the silicone. When a force was applied to the free end of the cylinder, it was compressed and bent, displacing the magnet (see **Figure 3-2**). This displacement caused changes in the magnetic field near the Hall sensors. By detecting these magnetic field changes, the position of the magnet was calculated. Next, trigonometry was used to calculate the displacement of the free end of the soft beam element. This deformation was analogues to a soft cantilever beam under compressive and bending force. Finally, using spring theory and bending theory, the normal and tangential force components were calculated.

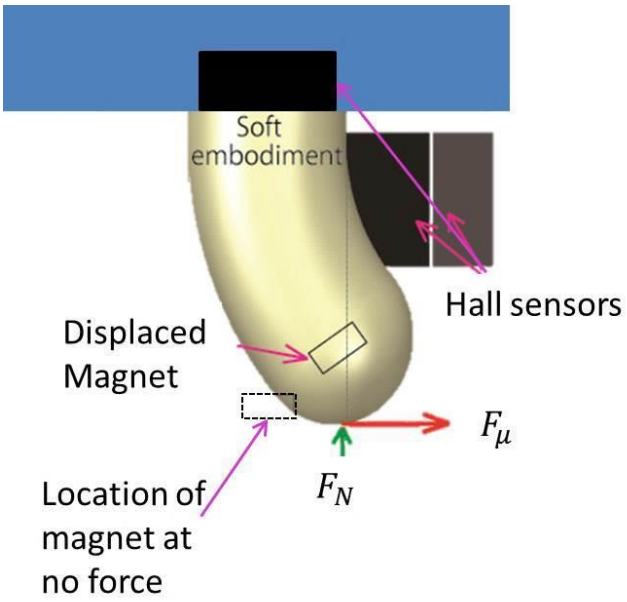

Figure 3-2: Sensor's sensing concept

3.3 Fabrication

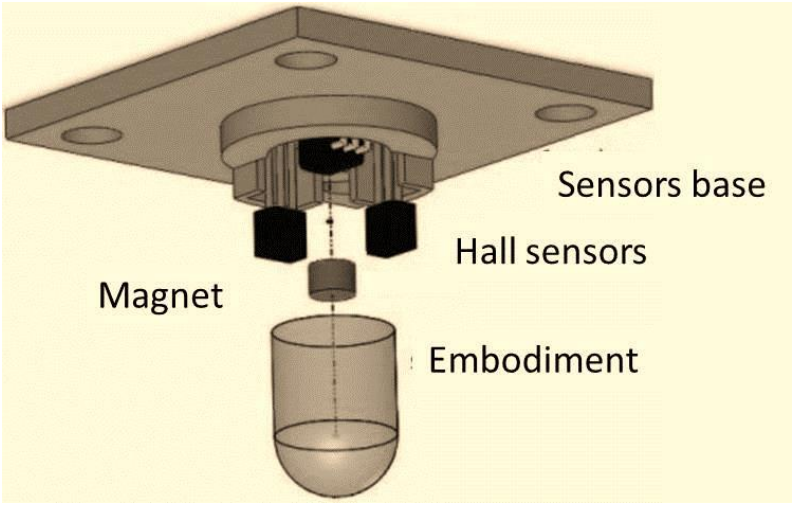

Figure 3-3: Force sensor components

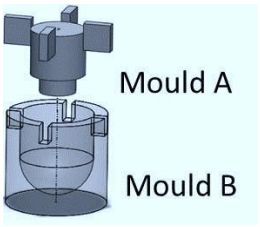

Figure 3-4: The mold assembly used for the fabrication of the soft element

The sensor was constructed with a soft sensing element fixed to a base (see **Figure 3-3**). The base was made of ABS plastic using a 3D printer. Three Honeywell™ SS495A Hall sensors were fixed to the base orthogonally. The Hall sensors have directional sensitivity to the magnetic field. Therefore, the sensors were facing the center of the construction to ensure that a positive voltage change represented a positive change in the magnet displacement and a negative voltage change represented a negative displacement of the magnet in x, y or z direction.

The sensing element was made of a soft material (Smooth-on Dragon Skin™ 30) embedding a Niobium cylindrical magnet of diameter 4mm. The outer layer of the sensing element was made using molds A and B (see **Figure 3-4**). Mold A was inserted into mold B. Then, soft material mixture was poured

in to the mold. Then, the mold was placed in a vacuum chamber (vacuum pressure 0.1MPa) to remove the air bubbles. Next, the mold was held at a temperature of 80˚C, for one hour in an oven to cure. Then, the part was removed from the oven, and mold A was removed. The magnet was inserted into the part, keeping the magnetic North down. The magnet was glued to the soft embodiment so that the soft body and magnet move together. Next, silicone rubber was used to cover the magnet and the cavity. The mold was placed again in the vacuum chamber and then, the oven. After the layers were formed, the molds were removed. Finally, the sensor base and the sensing element were fixed together using adhesive. It should be noted that the total price for the components of the sensor were not more than $20 making this construction inexpensive.

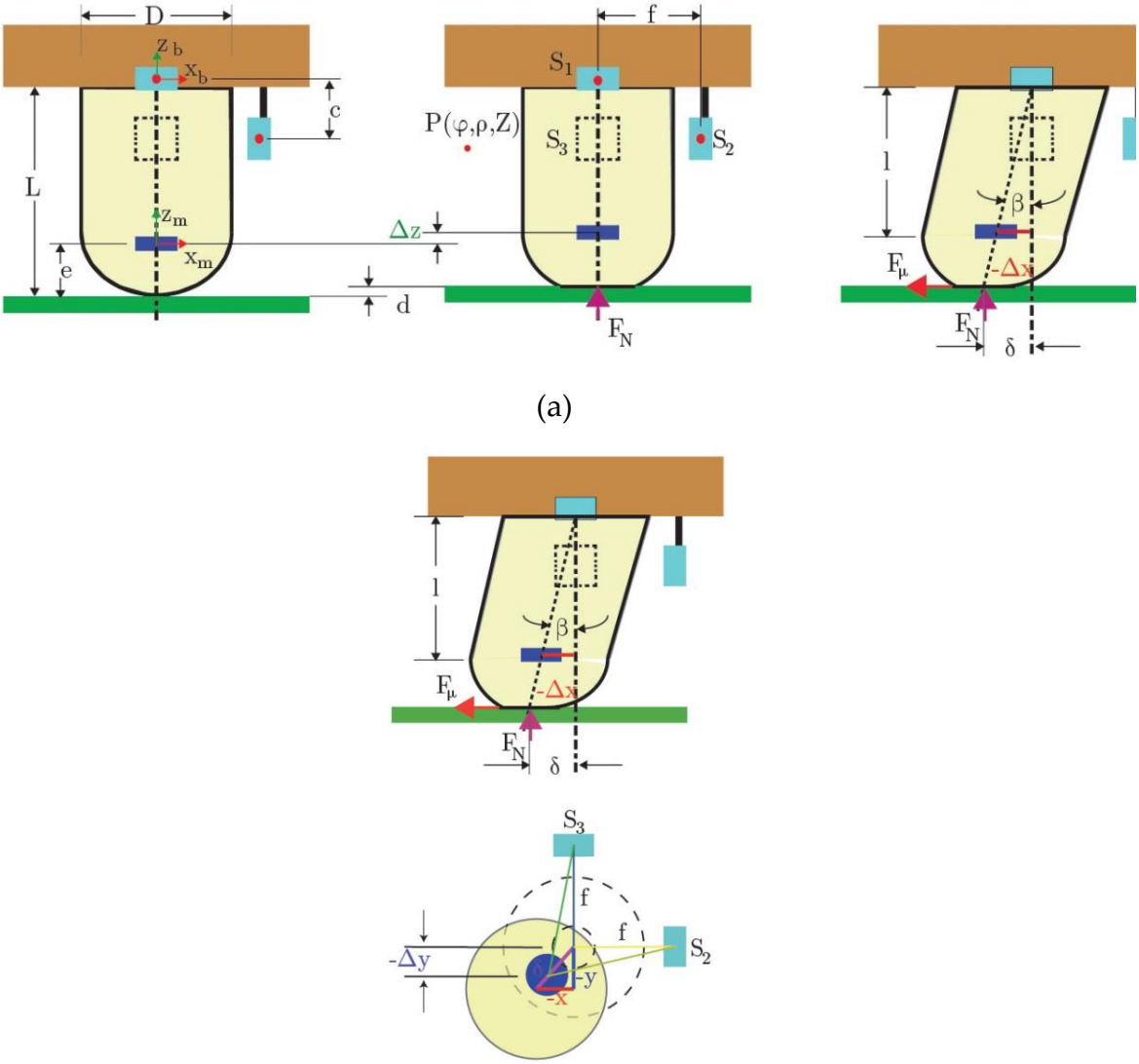

Figure 3-5: (a) Coordinate system used for the calculation of the change in magnetic field near the Hall sensors. The Hall sensors were orthogonal to each other (x, y, z). X_b , Y_b , and Z_b are base coordinates, and X_m, Y_m , and Z_m are magnet coordinates. The sensor element is assumed to be a cylindrical cantilever beam element influenced by a horizontal and vertical load F_μ, F_N. (b) The end of the cylinder has a displacement of d, δ while magnet has a displacement of $\Delta x, \Delta y$ and Δz.

The soft sensing element was a cylindrical cantilever with a diameter of D that has a hemispherical end (see **Figure 3-5a)**). The length of the total element was L. The magnet was placed at the center of the hemisphere. The hemispherical end allows for the use of the assumption that an applied force on the surface will go through the center of the cylinder, where the magnet was placed, every time. Outside this soft element, the Hall sensors on the x, y directions were placed at a distance of f from the axis of the cantilever. When an external force was applied to the soft silicone hemisphere, the material deformed, displacing the magnet $\Delta x, \Delta y, \Delta z$. This caused the magnetic field to change near the Hall sensors.

3.4 Sensor modeling – magnetic field modeling

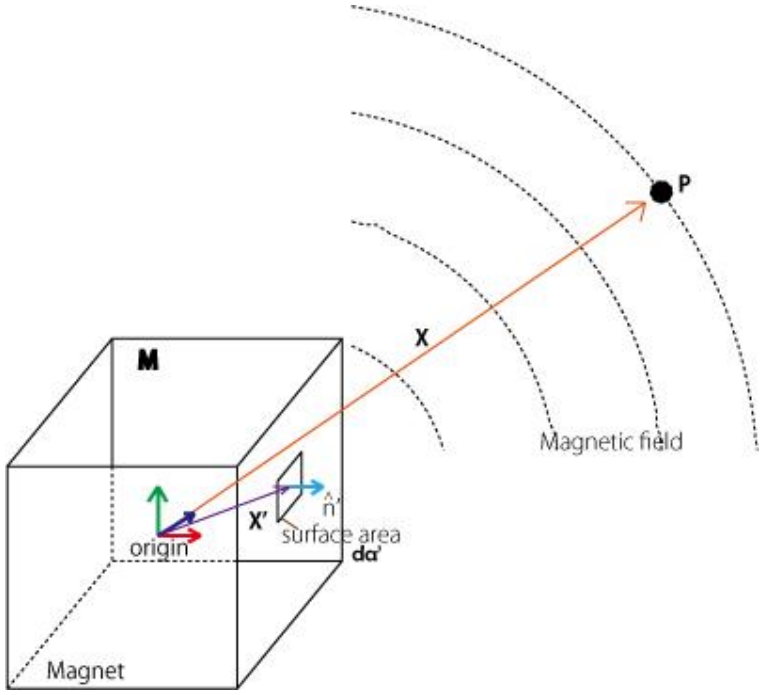

Figure 3-6: Magnetic field calculation of a magnet

The magnetic field of a permanent magnet can be calculated from the vector potential: $\boldsymbol{B} = \nabla \times \boldsymbol{\Phi}$, where $\boldsymbol{\Phi}$ is the magnetic vector potential. Let $\boldsymbol{M}$ be the volume magnetization of the magnet, $\widehat{n'}$ be the unit vector normal to the surface area da' on the magnet at a location represented by position vector$\boldsymbol{X'}$,

and μ_0 be the permeability of air (it is assumed that silicone rubber has the same permeability of air/vacuum). As shown in **Figure 3-6**Error! Reference source not found., the magnetic field at arbitrary point P which is presented by position vector X is given by the following surface integral **[93]**

$$\mathbf{B} = \frac{\mu_0}{4\pi} \oint \frac{M(\boldsymbol{X}') \times \widehat{n'}}{|\boldsymbol{X} - \boldsymbol{X}'|} da' \qquad (1)$$

Equation (1) is the general expression for calculating the magnetic field of any permanent magnet. For calculating the magnetic field of a cylindrical magnet, we utilize the following method.

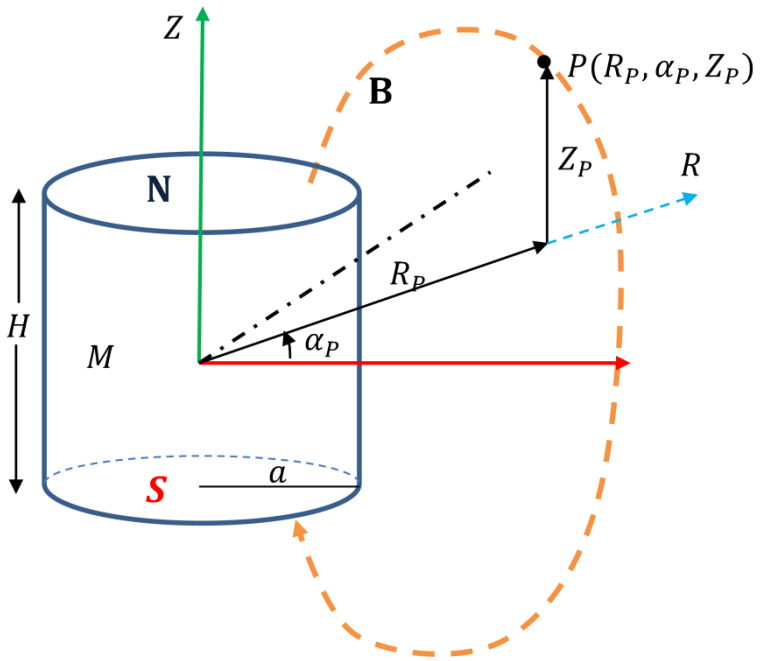

Figure 3-7: Magnetic field calculation of a cylindrical magnet

According to **Figure 3-7**, $[R, \alpha, Z]$ is the cylindrical coordinates fixed to the magnet. Volume magnetization is represented by M. The magnetic field $\boldsymbol{B}$ of a magnet can be expressed as the negative gradient of the magnetic scalar potential **[94]**, **[93]**. The magnetic scalar potential at a point $P(R_P, \alpha_P, Z_P)$ is given

as follows. If point P is in $\alpha_P = 0$ plane, the magnetic scalar potential Φ at point $P(R_P, 0, Z_P)$ can be written as

$$\Phi(\mathrm{R_P}, 0, \mathrm{Z_P}) = \frac{\mu_0}{4\pi} M \iiint \frac{(Z_P - Z) R \, d\alpha \, dR \, dZ}{[R_P^2 - 2RR_P \cos\alpha + R^2 + (Z_P - Z)^2]^{3/2}} \qquad (2)$$

This was derived from equation (1). Because the magnet is symmetric along Z axis, the magnetic field is invariant along directional angle α. Therefore α values are ignored in later calculations. The magnetic field components in R and Z directions $(\mathrm{B_R}, \mathrm{B_Z})$ at the point P can be derived from the negative gradient of the magnetic scalar potential Φ. Thus, following partial differential equations gives the magnetic field components at point P.

$$\mathrm{B_R}(R_p, 0, Z_p) = \frac{\partial \Phi(R_P, 0, Z_P)}{\partial R} \qquad (3)$$

$$\mathrm{B_Z}(R_p, 0, Z_p) = \frac{\partial \Phi(R_P, 0, Z_P)}{\partial Z} \qquad (4)$$

solving these equations gives the magnetic field components as

$$\mathrm{B_R}(R_P, 0, Z_P) = -\frac{\mu_0}{4\pi} M \int_0^{2\pi} \int_0^{a} -\frac{R(2R_P - 2R\cos\alpha)}{2\left[R^2 + \left(\frac{H}{2} - Z_p\right)^2 + R_p^2 - 2RR_P\cos\alpha\right]^{\frac{3}{2}}} + \frac{R(2R_P - 2R\cos\alpha)}{2\left[R^2 + \left(\frac{H}{2} + Z_P\right)^2 + R_P^2 - 2RR_P\cos\alpha\right]^{\frac{3}{2}}} \, dR \, d\alpha \qquad (5)$$

$$\mathrm{B_Z}(R_P, 0, Z_P) = -\frac{\mu_0}{4\pi} M \int_0^{2\pi} \int_0^{a} -\frac{R\left(\frac{H}{2} - Z_P\right)}{\left[R^2 + \left(\frac{H}{2} - Z_p\right)^2 + R_p^2 - 2RR_P\cos\alpha\right]^{\frac{3}{2}}} + \frac{R\left(\frac{H}{2} + Z_P\right)}{\left[R^2 + \left(\frac{H}{2} + Z_P\right)^2 + R_P^2 - 2RR_P\cos\alpha\right]^{\frac{3}{2}}} \, dR \, d\alpha \qquad (6)$$

where a and H are the radius and height of the magnet respectively. The magnetic field components B_R and B_Z are given by the unit Tesla. Next, the magnitude summation B of the magnetic field components at point P can be calculated as

$$B(R_P, 0, Z_P) = \sqrt{B_R^2 + B_Z^2} \qquad (7)$$

The hall-effect sensor voltage was proportional to the magnitude of the magnetic field B.

3.5 Sensor modeling - force calculation

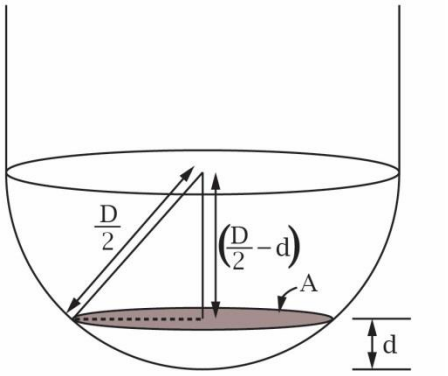

Figure 3-8: Contact area of the cantilever beam

We assume that two forces F_N, F_μ are applied at the end of the cylinder. These forces are perpendicular to each other. Due to the tangential force F_μ, the cylinder bends δ at the end. When there is a relative motion, this bending force can be assumed to be equal to the friction force between the soft cylinder and the contact surface. The force F_N, which is normal to the contact surface, is compressing the soft cylindrical beam to a depth of d. We assume that the soft cylinder behaves like a cantilever elastic beam (see **Figure 3-5(b)**). We then write the compression equations as

$$F_N = \frac{EA}{L} d \qquad (8)$$

The tangential force F_μ is calculated from the bending formula as

$$F_{\mu} = 3EI\frac{\delta}{l^3} \qquad (9)$$

where A, E, L, I are the cross sectional area of beam, the Young's modulus of the soft material, the natural length of beam and the moment of inertia of the cross section of the cantilever beam. The contact area (Error! Reference source not ound.) of the cantilever beam is calculated as

$$A = \pi\left[\left(\frac{D}{2}\right)^2 - \left(\frac{D}{2} - d\right)^2\right] \qquad (10)$$

where D is the diameter of the cantilever beam and d is the deformation of the contact point in the z direction.

3.6 Sensor modeling - displacement calculation

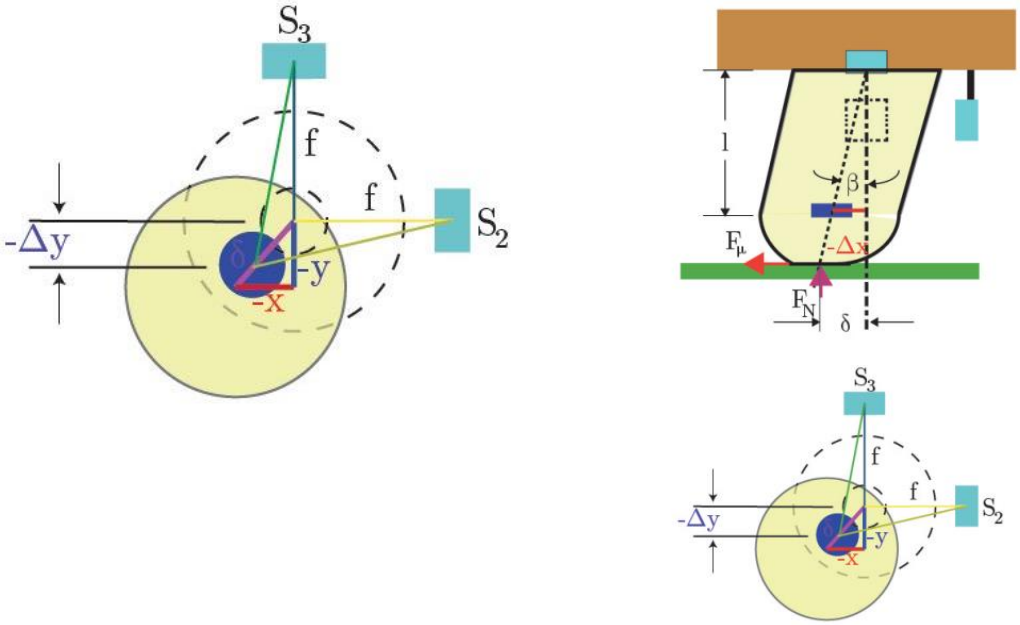

Figure 3-9: Displacement of the magnet due to the displacement of the beam

Due to the normal and tangential (frictional) force F_N, F_{μ}, the end of the soft cylinder moves x, y, d from the initial position, causing the magnet to move Δx, Δy, Δz. Then, from geometric relations we find

$$\Delta x = \left[\frac{(L-d)-(\Delta z+e+d)}{(L-d)}\right] x,$$

$$\Delta y = \left[\frac{(L-d)-(\Delta z+e+d)}{(L-d)}\right] y$$

$$\Delta z = l + d - e$$

where e is the unstressed distance from the end of the cantilever beam to the center of the magnet. The coordinates of the Hall sensors (S_1, S_2 and S_3) can be written from the magnet coordinate system (R, α, Z) for **Figure 3-9**Error! Reference source not found. as

$$S_1: \left(\sqrt{\Delta x^2 + \Delta y^2}, \phi_1, l\right)$$

$$S_2: \left(\sqrt{\Delta y^2 + (f + \Delta x)^2}, \phi_2, l - c\right)$$

$$S_3: \left(\sqrt{\Delta x^2 + (f + \Delta y)^2}, \phi_3, l - c\right)$$

As the magnet has a symmetry around its Z axis, the magnetic flux density around axis at a distance of (R_P, Z_P) is the same for a given ϕ. Therefore, ϕ_1, ϕ_2, ϕ_3 are ignored in these calculations.

3.7 Simulation results

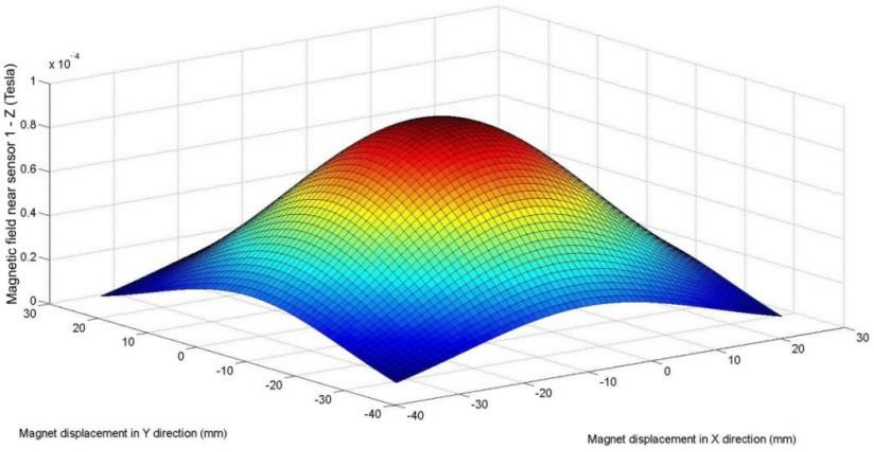

(a)

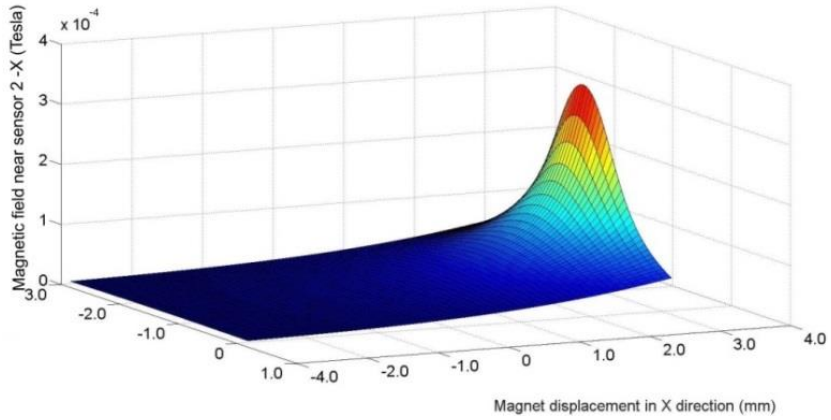

(b)

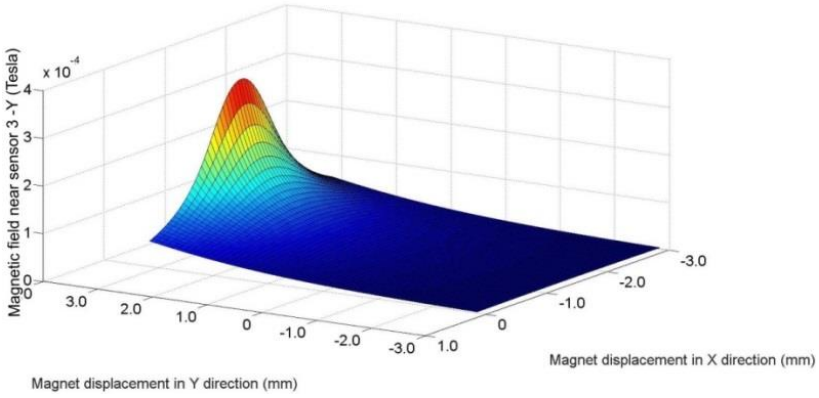

(c)

Figure 3-10: Magnetic field values near sensors which were obtained from the model (a) sensor 1 values for $x; y = -3 : 3$ mm, $z = 1$mm (b) sensor 2, and sensor 3 values for $x; y = -3 : 3$ mm, $z = 1$mm **[67]**

In order to develop the lookup table that contains magnetic field values induced near sensors 1, 2, and 3 for a given displacement of the magnet, a numerical simulation was carried out. Parameters for the Equations (5) and (6) are given in **Table 3-2**.

Table 3-2: Simulation parameters

Parameter	value
Diameter of cantilever beam (D)	8mm
Length of cantilever beam (L)	9mm
Distance of Hall sensors in directions $x; y$ from z (f)	5mm
Young's Modulus (E)	1MPa
Volume magnetization (M)	1 A/m
Permeability - of air/vacuum (μ_0)	$4\pi \times 10^{-7}$H/m

Figure 3-10 represents the value of the magnetic field near sensor 1 (Z direction), sensor 2 (X direction) and sensor 3 (Y direction) for the displacement in the horizontal directions and a contact depth $d = 1\,\text{mm}$ calculated by Equations (5), (6) and (7). Similarly, the magnetic field values for a contact depth d up to 3mm and horizontal displacements x, y between -3mm to 3mm were calculated and saved as a lookup table. The values were conducted in steps of 0.01mm.

From **Figure 3-10**, it is noticed that if the magnet displaced in a 3D space, the set of magnetic field values near three sensors, are unique to each location. Therefore, if magnetic field at the three locations is matched with the above developed lookup table, the displacement of the magnet, and then the displacement of the end of the cantilever beam can be calculated. Finally, the normal and tangential force is calculated using Equations (8) and (9).

3.8 Experimental validation

The simulation results were verified with experimental results.

3.8.1 Experimental setup

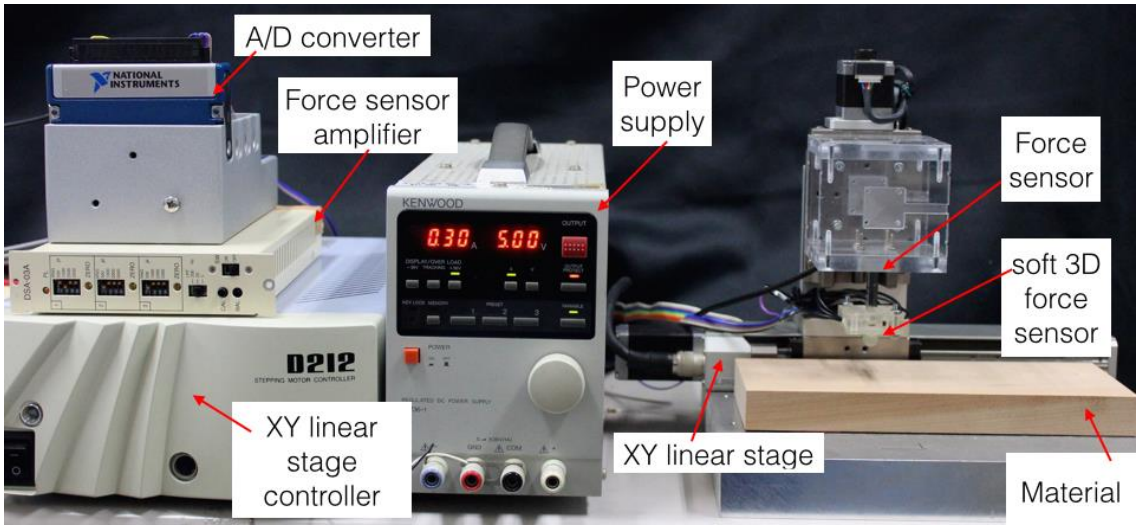

Figure 3-11: Experimental setup to validate sensor model

The experimental setup is shown in **Figure 3-11**. The system consists of a soft tactile sensor rigidly fixed to the vertical linear stage of the XY table (Suruga Seiki KXL06100-C2-F) using a Tech Gihan (USL 06-H5-50N-C) force sensor. The vertically moveable linear stage is fixed to a horizontal linear stage. Both stages allow the tactile sensor to move in x and z directions. The linear stages have a step size of 4μm. The force sensor is capable of measuring the forces in three dimensions. The force sensor has an amplifier of its own, and the processed signal is sent to a National Instruments NI9205 analog to digital converter.

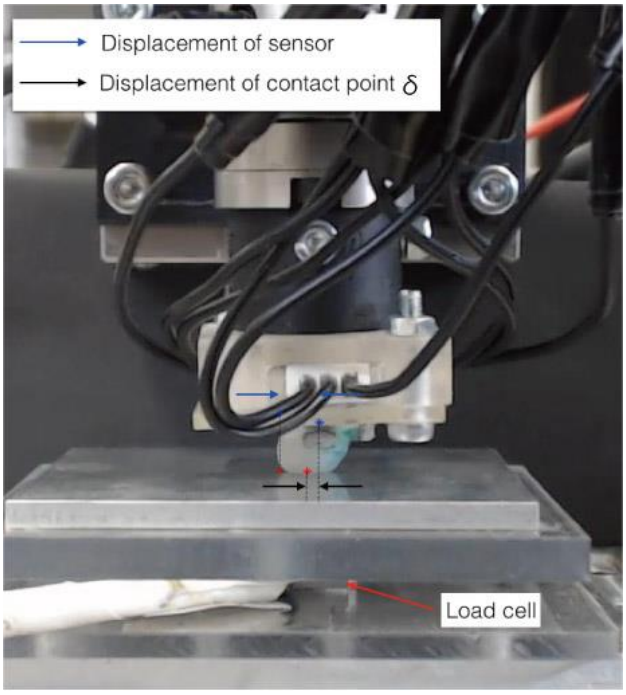

Figure 3-12: Setup used for the calculation of the displacement in the horizontal direction. Displacement in the x direction d is measured by processing the image and measuring the distance between the initial and final position of the feature point.

The linear stages and the AD converters are connected to a computer and controlled through LabView™ software. The data retrieval and the linear stage motion are synchronized by the software. The sampling rate of the AD converter is 1000Hz. For most of the tests, the output signal is filtered using a 500Hz cut off frequency low pass and an average filter (see **Figure 3-13**).

From calibration tests, we found that Hall sensor has a conversion factor of 31.3V/T (volts per Tesla). Therefore, by measuring the sensor's output voltage (offset compensated), we could measure the magnetic flux density induced by the magnet at the location of the sensor. The Hall sensor offset voltage was 2.87V for sensor 1 and was subtracted from the sensor output voltage value. This offset value is unique to each sensor and depends on the Hall sensor and the initial distance of the sensor from the permanent magnet.

3.8.2 Experiments and simulations

For the experiments, a normal force F_N was applied by pushing the soft tactile sensor onto a hard surface for a depth d. The sensor was stationary in the horizontal direction ($F_\mu = 0$). After waiting for 30s for the sensor value to settle, the force was measured using the force sensor. The displacement was measured using the encoders in the linear stage. The voltage output of the three Hall sensors $V_{S_x}, V_{S_y}, V_{S_z}$ was recorded for each step of the normal force F_N and the deformation d. The depth of the contact was changed with steps of 4μm. The average of the voltages for the increase in depth and decrease in depth were calculated and saved in a table. The voltage relevant for a given contact depth was calculated by averaging the voltage values from ten trials.

In order to validate the sensor behavior, numerical simulation values and experimental results were compared. **Figure 3-14** represents the measured normal force F_N and the calculated normal force from the Equation (8). The calculated values and the experimental values behaved similarly up to a contact depth of $d = 3$mm. The contact depth of 3mm was chosen as the limit. This was needed in order to limit the deformation of the soft material. The maximum error between the calculated and the actual force values was less than 5%. This suggests that for normal load calculations the assumption of an elastic beam under compression was valid.

Next, for a given normal force F_N, the displacement of the magnet in the z direction was calculated, and using Equation (5), (6), and (7), the magnetic field was calculated. Subsequently, this value was converted to sensor voltage by multiplying the magnetic field value by the Hall sensor conversion factor. The results of the normal force vs sensor voltage are presented in **Figure 3-15**. It can be noted that the calculated voltage and the actual voltage have similar trends yet the deviation is increases with the normal load yet error was under 5% of the maximum measurement.

Similar to normal force F_N, the tangential force F_μ was calculated using Equation (9). The actual horizontal force was measured using the force sensor that was fixed to the bottom contact surface (**Figure 3-12**). The measurement of the horizontal deformation δ posed a problem, as this was affected by the frictional coefficient of the bottom contact surface and the slippage between the palate and the tactile sensor. Therefore, in order to obtain a relatively accurate result, the deformation caused by the dynamic frictional force at the moment of slipping was used. The deformation was measured by visual odometry (**Figure 3-12**). Again, ten trials were conducted, and the average of the values was taken for the calculations.

Figure 3-16, shows the relationship between the horizontal displacement δ and the horizontal force F_μ. For a horizontal displacement of up to 3.1mm, the simulated value and the actual values have similar trends. The measured force had an error much larger than expected. The error was under 10% of the maximum value. We believe that this error is due to the soft material being stuck to the contact surface. As the normal deformation is small; the frictional force due to normal force (coulomb friction) is small compared to the frictional component due to the surfaces being sticking (adhesion). In the current model, only the frictional force F_μ due to the normal force (coulomb friction) is considered. In future we hope to include the frictional force due to stick in the sensor modelling.

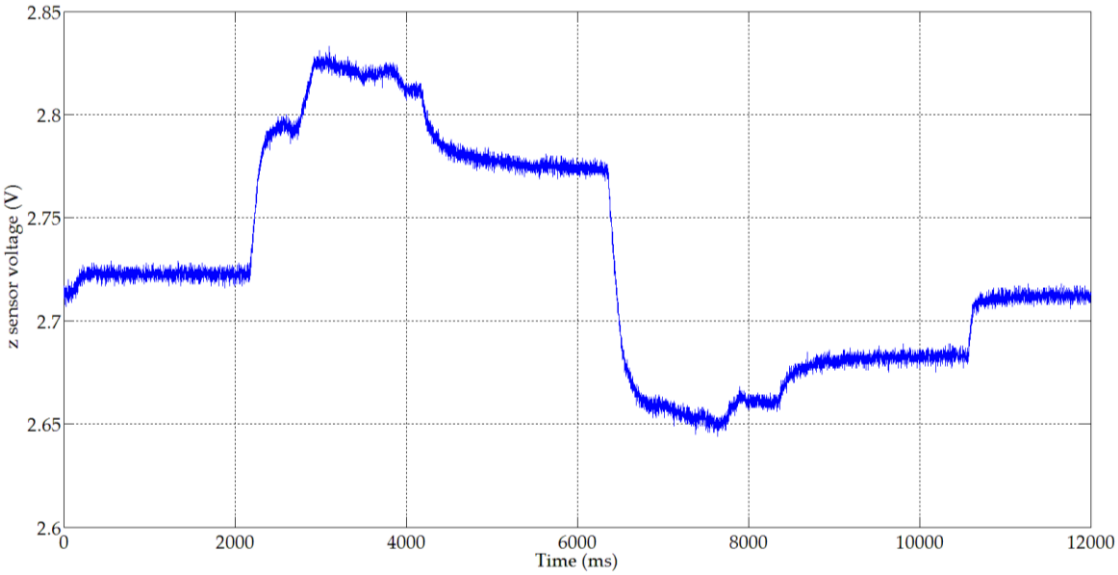

(a)

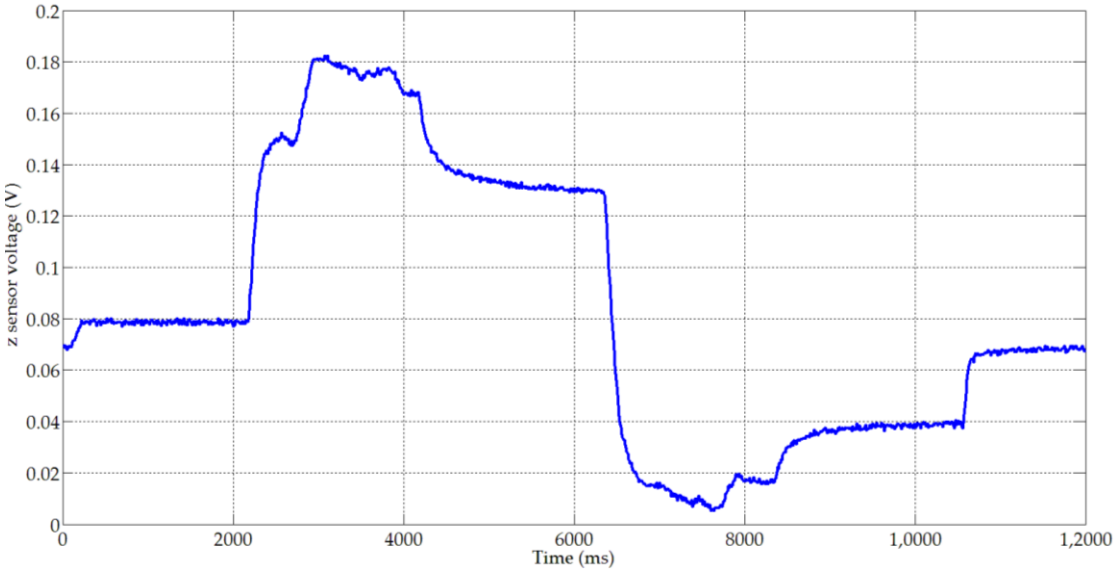

(b)

Figure 3-13: (a) raw sensor output from the z axis hall sensor. (b) Sensor output was processed by offset adjustment of 2.64V, 500Hz low pass filter and averaging with 10 values.

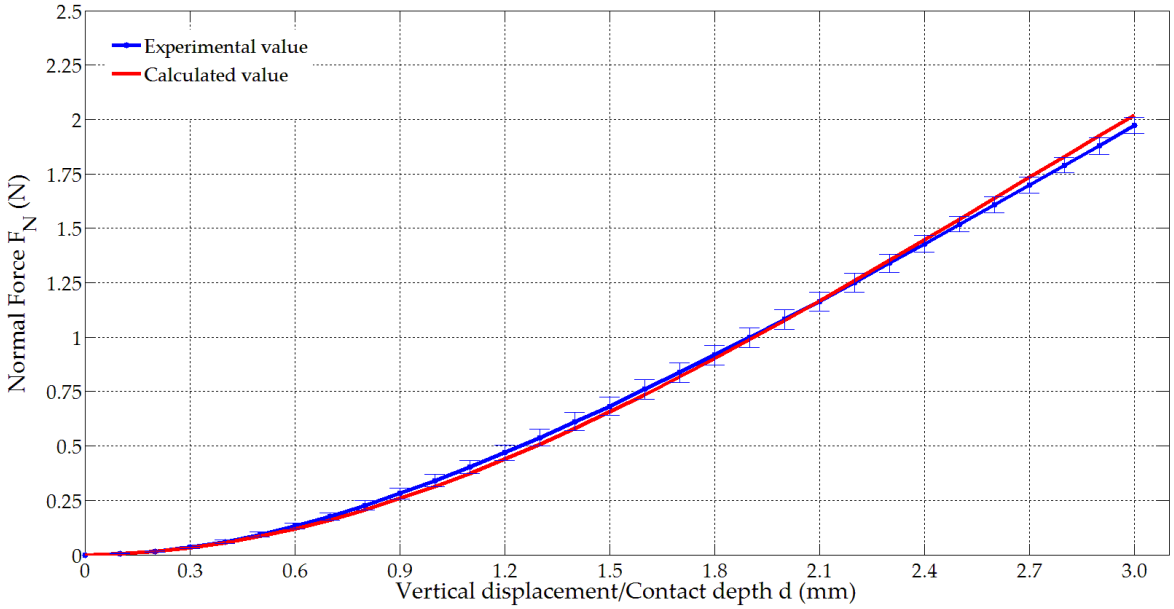

Figure 3-14: Normal force F_N vs. z directional displacement

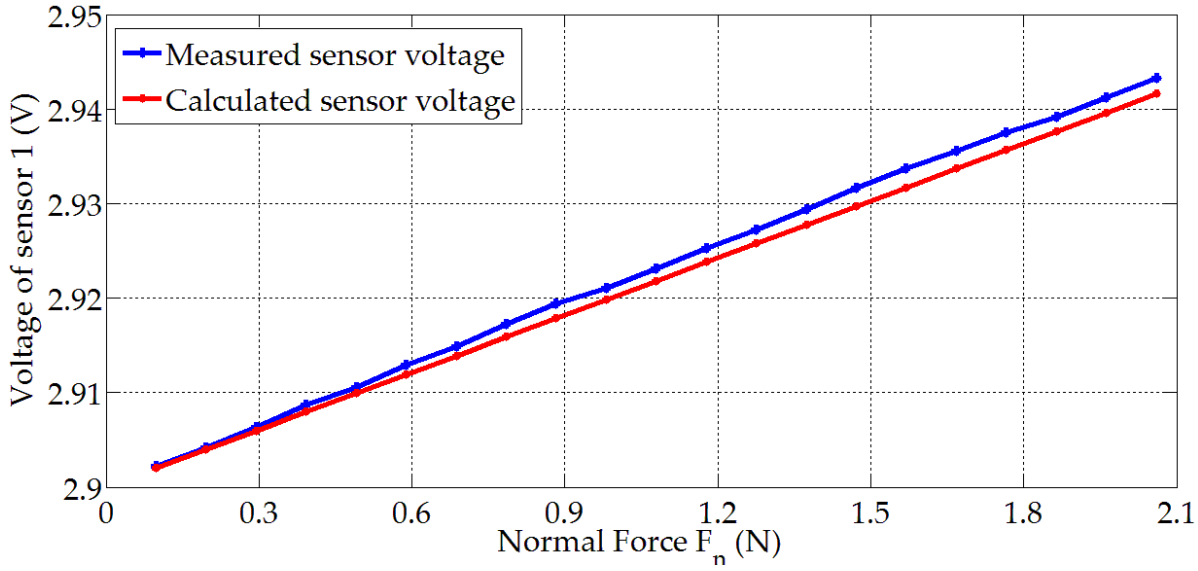

Figure 3-15: Normal force F_N vs. sensor 1 voltage

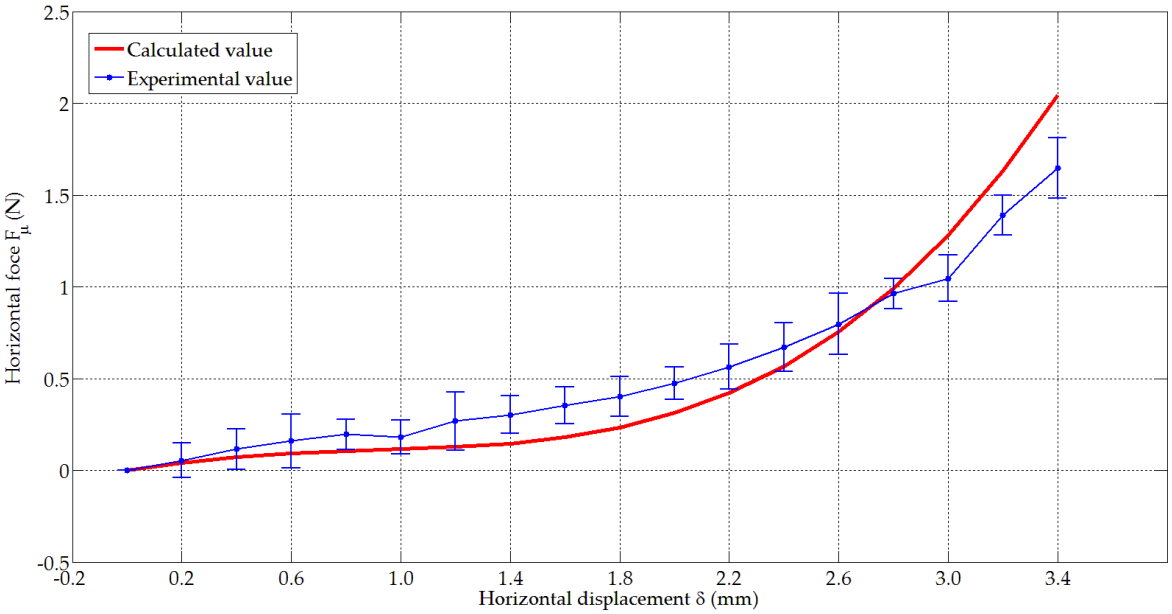

Figure 3-16: Horizontal force F_μ vs. x directional displacement

3.8.3 Frequency response

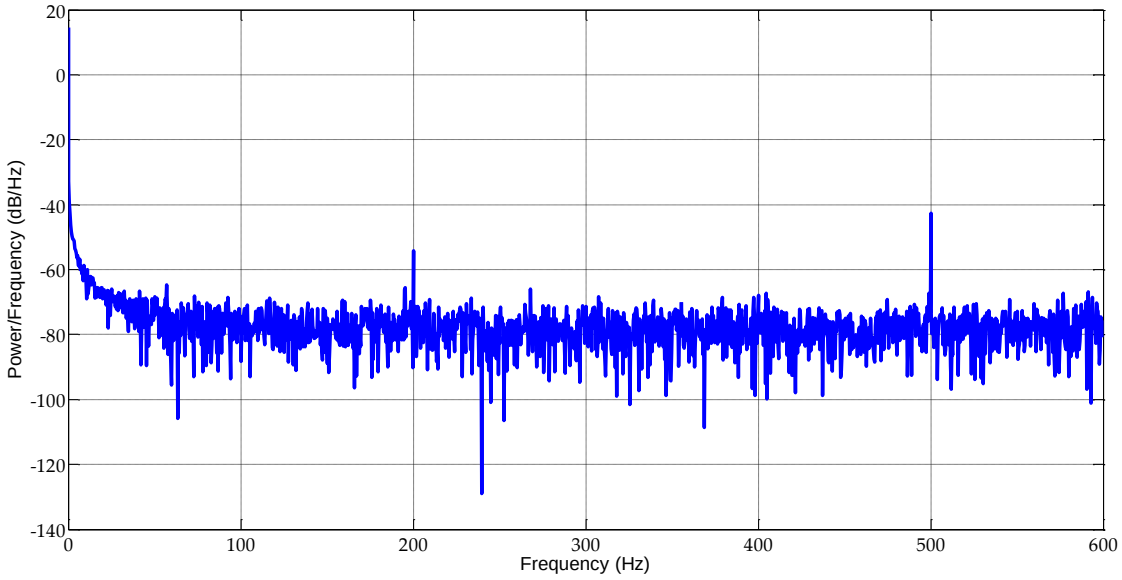

Figure 3-17: Frequency plot for a sensor signal obtained by the sensor after exposing to a vibration of 500Hz.

In order for this sensor to be used as a tactile sensor in robotic hands, the sensor should be able to measure vibrations up to 500 Hz [**60**]. Thus, the sensor was subjected to vibrations of up to 500 Hz using a vibration table. The signal

was converted to the frequency domain and shown in **Figure 3-17**. The peak at 500Hz shows that the sensor could detect vibrations of 500Hz and it implied that the sensor was sensitive enough to sense vibrations up to 500 Hz. Calculations that used the principle of undamped natural frequency of a mass-spring system indicated that natural frequency of the sensor was approximately 970Hz, which is above the sensor functioning region.

3.8.4 Influence of close by magnets to the measurements of the hall sensors

Hall sensor readings could be influenced by magnetic fields generated from sources other than the embedded magnet. Furthermore, to use these force sensors for gathering pressure distribution data, array of force sensors needs to be incorporated. This poses the problem of changing the magnetic field generated by a permanent magnet due to the influence of nearby magnets, which will in return influence the accuracy of the force measurement. Thus, influence of permanent magnet of adjacent sensor elements to the relevant hall sensors readings was analyzed with a sensor array made of four force sensor elements (see **Figure 3-18 (a)**).

A sensor array was constructed having four elements spaced 10mm apart which each element had three hall sensors and a permanent magnet embedded on soft material (see **Figure 3-18 (a)**). Next, vertical force (up to 10N) was applied to a single sensor. The voltage of the hall sensor which the force was applied and the hall sensor voltages of the adjacent sensor were recorded (see **Figure 3-18 (b)**).

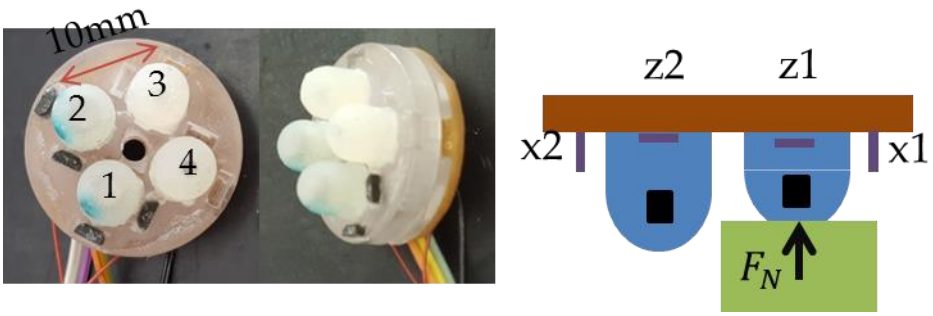

(a)

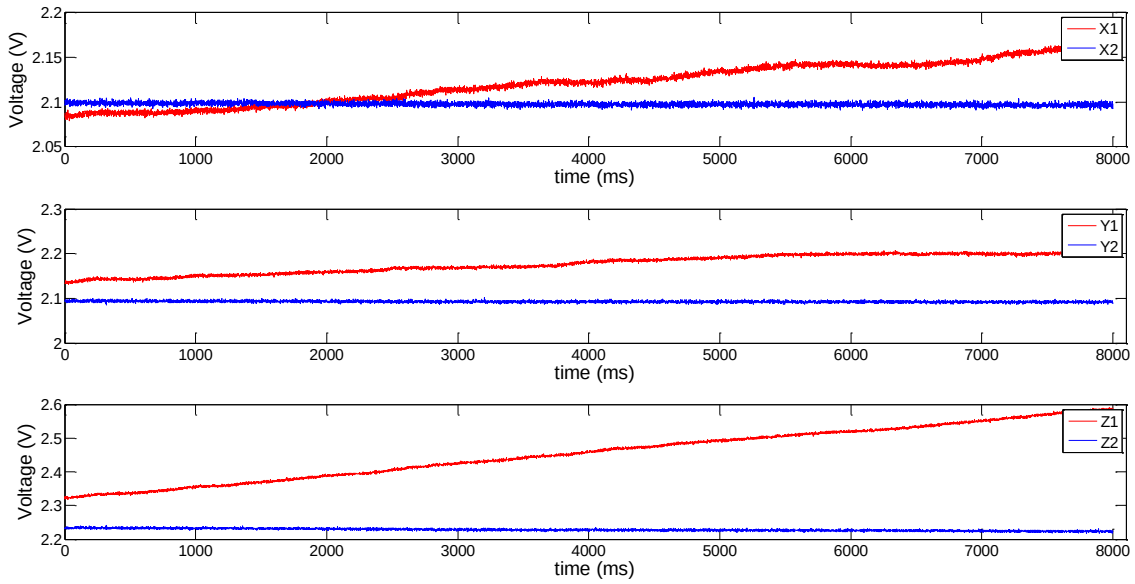

(b)

Figure 3-18: x, y and z directional hall sensor voltage of two adjacent (10mm apart) force sensors. (a) Sensor 1 was applied a vertical force F_N that gradually increased to 10N. (b) The sensor signals of x, y and z hall sensors in force sensor 1 and 2.

According to **Figure 3-18(b)**, the hall sensor voltages of adjacent sensor did not change considerably. Calculations showed that the x, y and z hall sensors of sensor 2 (see **Figure 3-18(a)**) had variations less than 0.1%, 0.1% and 0.5% change due to the change in the displacement of the adjacent magnet.

Therefore, it could be confirmed that if the two adjacent force sensors are 10mm apart, the influence of the permanent magnet to the adjacent hall sensors of the sensor array element could be neglected.

3.9 Soft force sensor used in a tactile fingertip

When designing fingertips, finger hardness plays a critical role. A soft fingertip creates stable and encompassing grasps than a rigid fingertip. The reason is, the fingertip deforms when grasping objects and applies a large frictional force and torque due to the large contact area while rigid fingertips do not deform and apply point loads and no counteracting torque [**22**]. However development of soft fingertips with necessary tactile sensing ability has its own challenges. The soft materials make the finger prone to wear, the elastic nonlinear material properties such as stiffness make the force calculations difficult, the damping of the soft materials make it difficult to sense small vibrations happening far away from the sensor and the forces applied to the fingertip is disbursed making it hard to localize forces. Consequently, developed soft sensors should be cheap if to replace when warn out, robust and reliable to be used in industrial applications, and have a simpler geometry to localize grip forces (by design, the grip forces can be made to go through a single location irrespective of the position where the force was applied). Thus, many researchers utilized the hemispherical shape to develop fingertips. These fingertips had advantage of simple design and construction due to the shape compared to the humanoid fingertips or cylindrical fingers. Having a hemispherical shape finger was easy for the contact area calculations (as the contact area is a circle for a flat surface) and direction of the force. This made the friction calculations easy for most of the soft fingers.

Tremblay [**55**] developed a soft fingertip using soft material and had accelerometer sensors on the side and contact surface of fingertips to detect tactile information. Ho [**40**] developed another hemispherical fingertip using a MEMS micro-force/moment sensors which was embodied by a polyurethane soft hemisphere. He kept the MEMS sensor at the center of the hemisphere and developed a model called the beam bundle model to derive the vertical and tangential forces that were applied at the contact surface of the sensor. Similar to Ho, Boissieu [**41**] developed a soft hemispherical fingertip composing a 3 axis MEMS force sensor made from peizoresistive films. Back [**95**] used the same concept and developed a hemispherical fingertip with a force moment sensor fixed at the center of the hemisphere. Yussof [**96**] and Winstone [**97**] developed a fingertip with columnar feelers attached to hemispherical surface. When this fingertip griped an object, these feelers bend and the area under the feelers change with the size and directions of the fingertip. The change in the feeler area was measured by visual odometry.

Keeping the above mentioned reasons in mind, a hemispherical soft tactile sensor was developed (see **Figure 3-19**). The fingertip sensor was constructed with a soft sensing element fixed to a base (**Figure 3-20 (d)**). The base was made of ABS plastic using a 3D printer. Three Honeywell™ SS495A Hall-effect sensors were fixed to the base orthogonally to each other and the pins of the sensor were connected to a PCB layer which was placed after the base. The Hall sensors had directional sensitivity to the magnetic field. Therefore, the sensors were facing the center of the construction to ensure that a positive voltage change represents a positive change in the magnet displacement and a negative voltage change represents a negative displacement of the magnet in the x, y, or z direction.

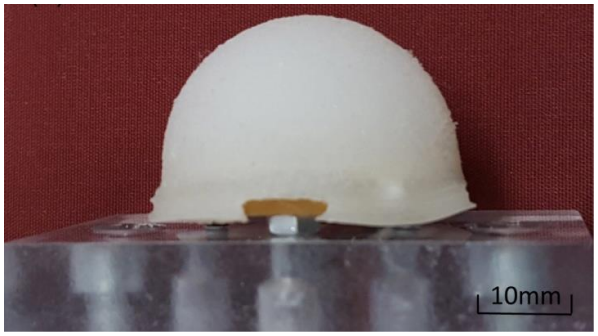

Figure 3-19: Hemispherical tactile fingertip

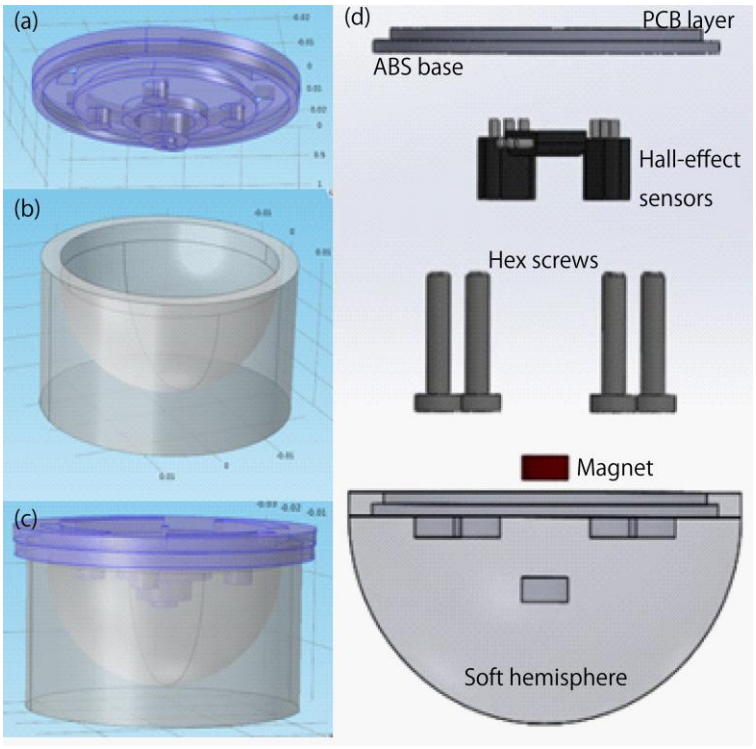

Figure 3-20: (a), (b) - upper and lower portions of the mold used to fabricate the soft hemisphere. (c) Mold assembly (d) Schematic representation of the components of the sensor.

The sensing element was made of a soft material (Smooth-on™ Dragon Skin 30) embedding a neodymium cylindrical magnet of diameter 4mm. The outer layer of the sensing element (soft layer) was made using molds A and B (**Figure 3-20 (a), (b)**). Mold A was inserted into mold B. Then, soft material mixture was poured in to the mold. Next, the mold was placed in a vacuum

chamber (vacuum pressure 0.1MPa) to remove the air bubbles. Next, the mold was held at a temperature of 80˚C, for one hour in an oven to cure. Next, the part was removed from the oven, and mold A was removed. The magnet was inserted into the part, keeping the magnetic North down. The magnet was glued to the soft embodiment so that the soft body and magnet move together. Next, silicone rubber was used to cover the magnet and the cavity. The mold was placed again in the vacuum chamber and then, the oven. After the layers were formed, the molds were removed. Finally, the sensor base and the soft overlay were fixed together using adhesive.

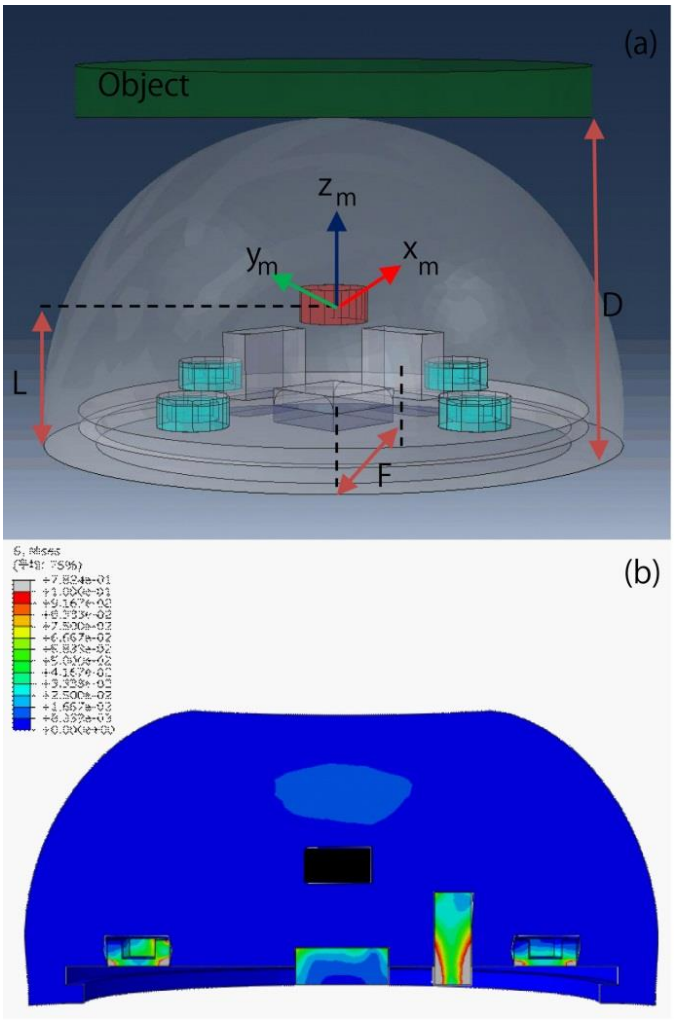

Figure 3-21: (a) Coordinate system used for the calculation of the change in magnetic field near the Hall sensors. The Hall sensors were orthogonal which is

represented by $x; y;\ z$. $X_b; Y_b;$ and Z_b were base coordinates, and $x_m; y_m;$ and z_m were magnet coordinates. The hemisphere was influenced by a vertical load F_N which was applied by the movement of the object. (b) The displacement of the magnet $d_x; d_y$ and d_z was calculated from the FEM simulation by moving the object towards $-z_m$ direction.

The soft sensing element was a hemisphere with a diameter of D (see **Figure 3-21(a)**). The magnet was placed at a length L from the centre of the hemisphere. The hemispherical shape allows for the use of the assumption that an applied force on the surface will go through the center of the hemisphere every time, making the calculation of the force closure much simple in grasp planning.

Due to the asymmetric shape of the soft embodiment, the displacement of the magnet could not be obtained using analytical methods such as the beam bundle model proposed by Ho [**40**] or the Kao proposed model [**89**]. Therefore, we used a finite element model (FEM) do calculate the displacement of the magnet when the sensor is exposed to a vertical load F_N with a deformation of d. ABAQUS™ software was used with the FEM simulation. The soft hemisphere was subjected to a vertical force by pushing the fingertip onto a flat surface with a velocity of 5mm/s up to a depth d of 3mm. The displacement of the magnet with the contact depth d was calculated and used in the calculation of the induced magnetic field at the hall-effect sensors. Next, the voltage output of the sensors was calculated by multiplying the magnetic field value and conversion factor of $6.463 \times 10^5 \mathrm{V/Wb}$ (volts per weber) of the hall-effect sensor.

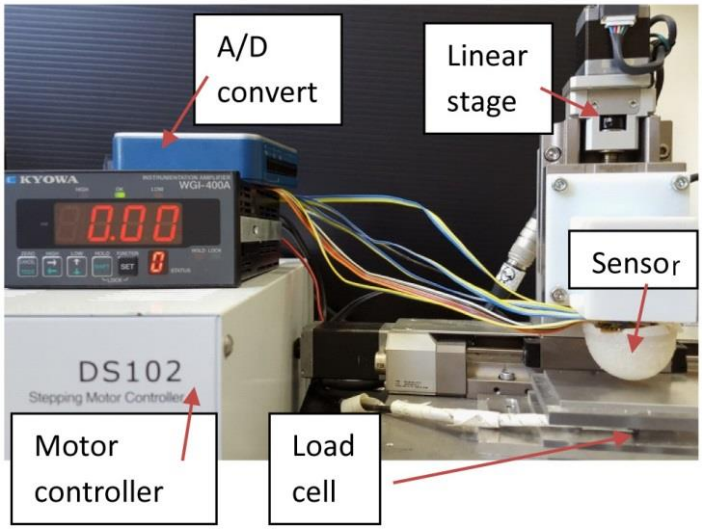

Figure 3-22: Experimental set up to calibrate the tactile fingertip sensor

The experimental set up is shown in **Figure 3-22**. The system consists of a soft force sensor rigidly fixed to the vertical linear stage. The applied normal force was measured by using a Tech Gihan™ (USL 06-H5-50N-C) force sensor. The force sensor was capable of measuring the forces in three dimensions. The vertically moveable linear stage was fixed to a horizontal linear stage. Both stages allow the soft force sensor to move in the x and z directions. The linear stages have a step size of 4μm. The force sensor signal was sent to a National Instruments USB6003 analog to digital converter.

The linear stages and the AD converters were connected to a computer and controlled through LabView™ software. The data retrieval and the linear stage motion were synchronized by the software. The sampling rate of the AD converter was 1000Hz. For most of the tests, the output signal was filtered using a 500Hz cut off frequency low pass and an average filter. The experimental data were collected and later stage processed using MatLab™ software. The computer used included an Intel Core I5-2400 3.10Ghz system with 4GB internal memory running Windows 7(64 bit).

From calibration tests, we found that Hall sensor had a conversion factor of $6.463 \times 10^5 \mathrm{V/Wb}$ (volts per weber). Therefore, by measuring the sensor's output voltage (offset compensated), we could measure the magnetic flux induced by the magnet at the location of the sensor. The Hall sensor offset voltage was 2.87V for sensor *Z* and was subtracted from the sensor output voltage value. This offset value was unique to each sensor and depended on the Hall sensor and the initial distance of the sensor from the permanent magnet.

The tactile sensor was moved vertically with a velocity of 5mm/s and pushed against the base. The contact depth of the soft sensor was controlled by the motion of the *z* directional linear stage. The data from the both force sensors were collected. In these experiments, 20 trials were recorded and the average values were taken for the plotting.

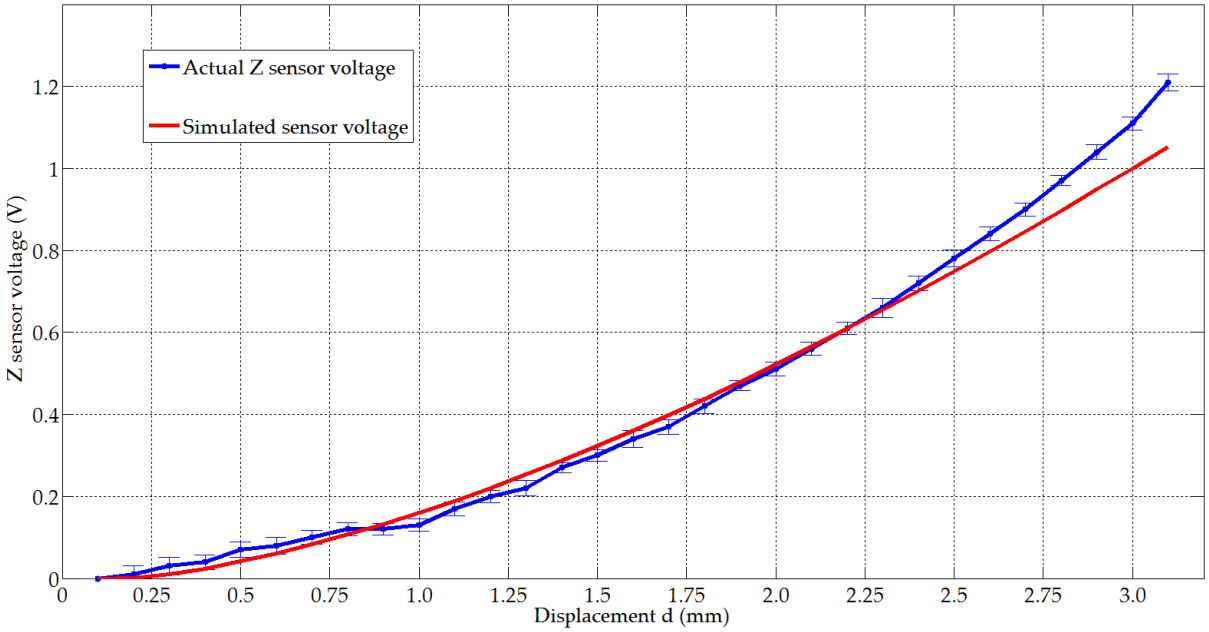

Figure 3-23: Displacement Vs Z sensor Voltage.

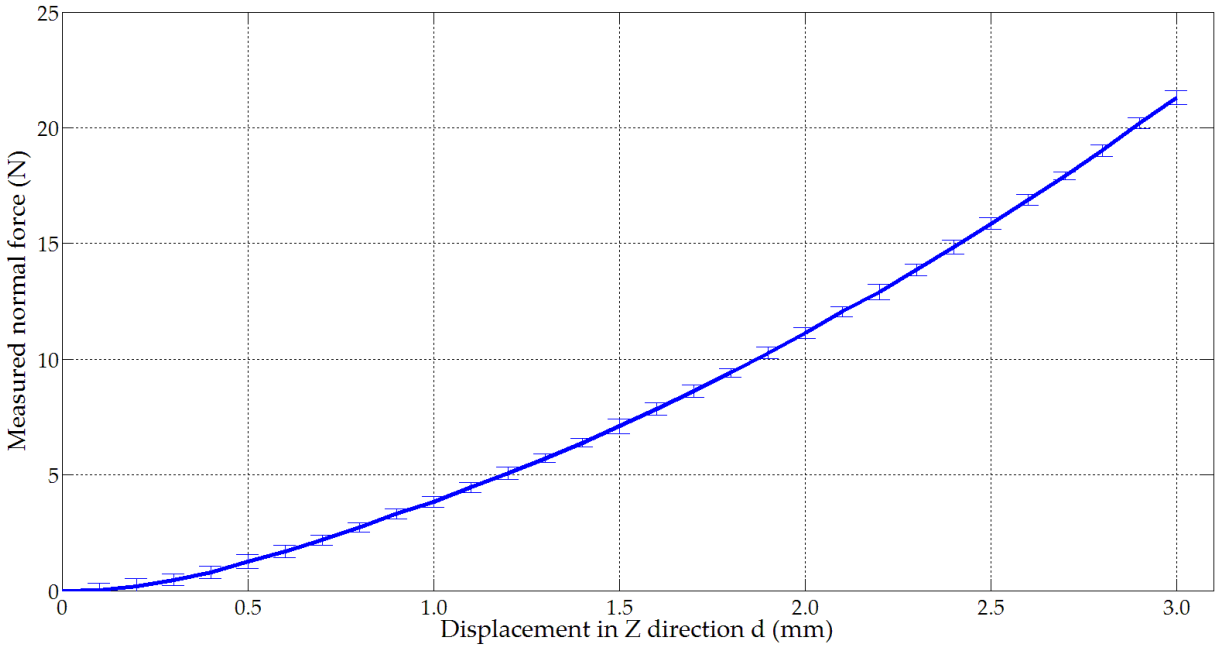

Figure 3-24: Displacement vs Normal Force.

The calculate voltage and the actual voltage was represented in **Figure 3-23**. It could be noted that the actual voltage of the Z directional sensor and the calculated voltage value was behaving similarly up to the contact depth of 2.4mm or 15N compared to the **Figure 3-24**. Furthermore this deviation is under 5% of the actual value making our simulation valid.

3.10 Discussion

This chapter introduces the initial prototype of a soft force sensor and its modelling in order to calculate normal (F_N) and tangential (F_μ) force components. The deformation of the sensor's soft embodiment due to the above forces is calculated indirectly by measuring the magnetic field variation of a permanent magnet embedded in the soft embodiment. The magnetic field around the space of the magnet is calculated numerically and stored in the system as a lookup table. The magnetic field of three fixed locations is measured using Hall sensors. When the magnet displaces from its initial location, the magnetic field values around the fixed locations change. The new magnetic field values are measured using the Hall sensors and the three value

set is matched with the numerically calculated value set (lookup table) and the location of the magnet relative to the three fixed locations are retrieved. Next, using trigonometry, the displacement of the free end of the cylindrical soft embodiment is calculated. As the cylindrical embodiment is assumed as a cantilever beam under compressive and bending forces, using spring theory and bending theory, the normal F_N, and tangential F_μ force is calculated. Initially these calculations were carried out post process. The results show that the normal force F_N and tangential force or friction force F_μ can be measured using this sensor accurately. The force sensor has the ability to measure dynamic loads, making it suitable for tactile sensing applications. The proposed mathematical model describes the sensor behavior well. Therefore, the simulated results can be used in constructing the lookup table for the sensor. This is an advantage compared to many other soft tactile sensors, where the mathematical representation of the sensor behaves differently than the actual sensor.

Major assumption of the above stated force calculations is that when normal and horizontal forces (F_N, F_μ) applied to the soft embodiment, the magnet will only displace in x, y and z directions without any rotation in pitch or roll (see **Figure 3-2** for the translation and rotation of the magnet due to the vertical and horizontal force). **Figure 3-25** shows the magnetic field change for a magnet rotation in the pitch axis (y axis). It could be noted that up to a pitch angle of 30 degrees, the voltage change is less than 6% which justify the above stated assumption.

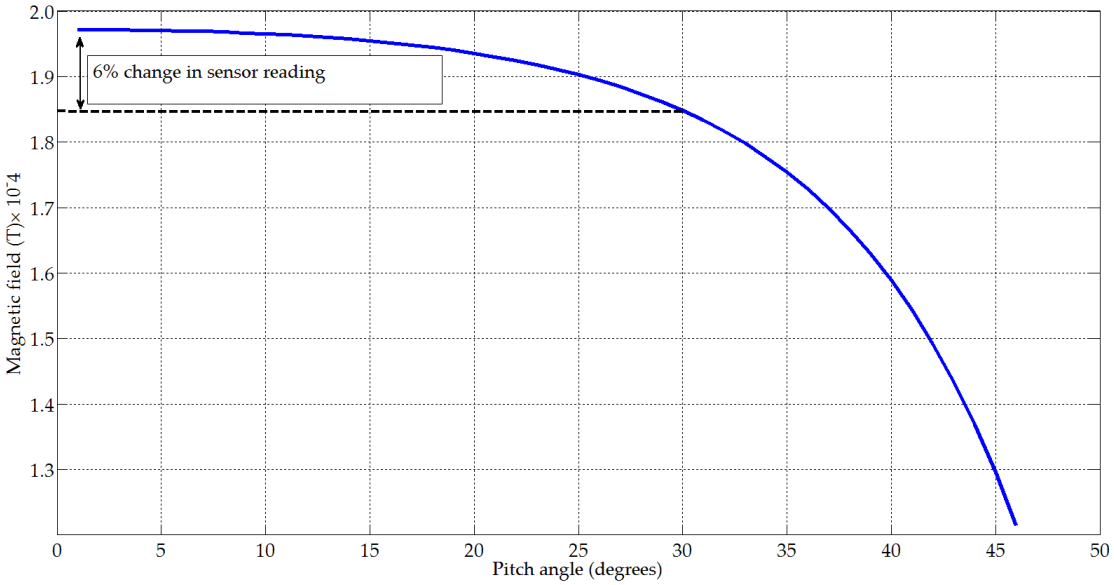

Figure 3-25: Magnetic field value at the location of *z* hall sensor change for a pitch axis rotation of the permanent magnet

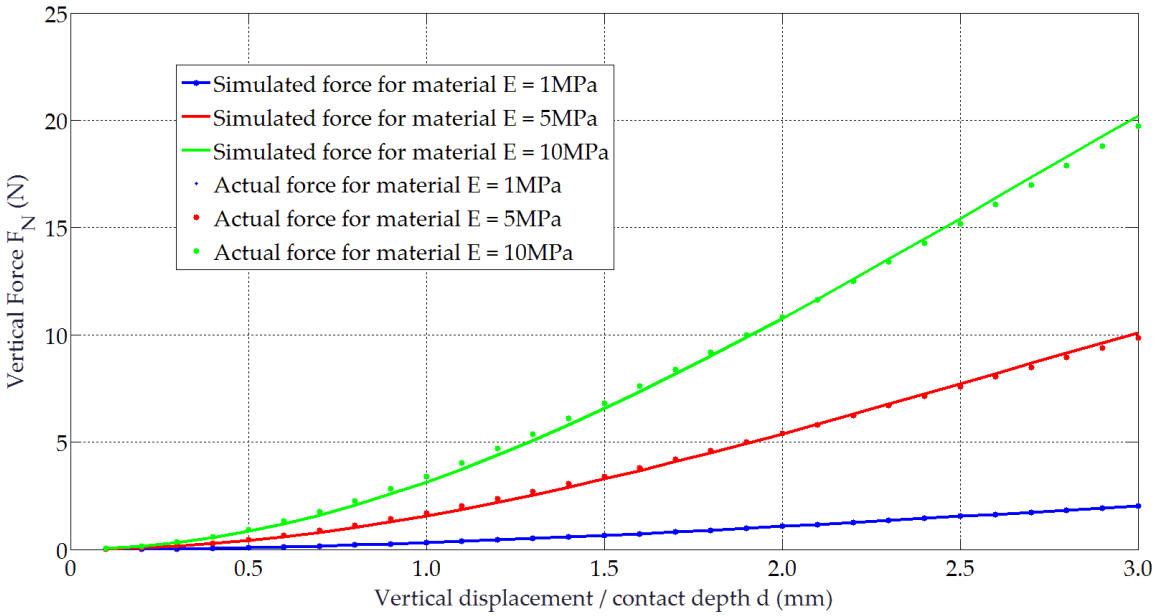

Figure 3-26: Normal force F_N vs. z directional displacement for materials with different stiffness

The sensitivity of the sensor depends on the stiffness of the soft material. As seen in **Figure 3-26**, by changing the material, the sensitivity of the sensor can be changed. For a Young's modulus of E = 1MPa, the maximum force that

can be measured with an error less than 5% is 3.0N, while for a modulus of 5MPa, it is approximately 9N. If the modulus is increased to 10MPa, the maximum force measurable increases to approximately 18N. Therefore, this sensor could be used to measure small and large forces just by changing the stiffness of the sensing element. It should be noted that even though Young's modulus of the rubber material behaves as a function of pre-compression and temperature, according to **Figure 3-27** and **Figure 3-28**, the material shows linear behavior up to a strain of 15%. Thus, the Young's modulus can be taken as a constant value for the calculations in equation (5) and (6) provided the deformation d is less than 15% of the strain. If the deformation of the soft element is larger than 15% of the strain, the soft material should be considered as a non-linear elastic material instead of a linear elastic material. The use of a nonlinear elastic model (hyper-elastic model) in the simulation will be considered in future as an improvement to the model. Furthermore, as the sensor will mostly be used in room temperature applications, the change in Young's modulus due to the temperature is small (see Stress strain curves for different temperatures in **Figure 3-27**), effects of temperature variations were ignored in this paper.

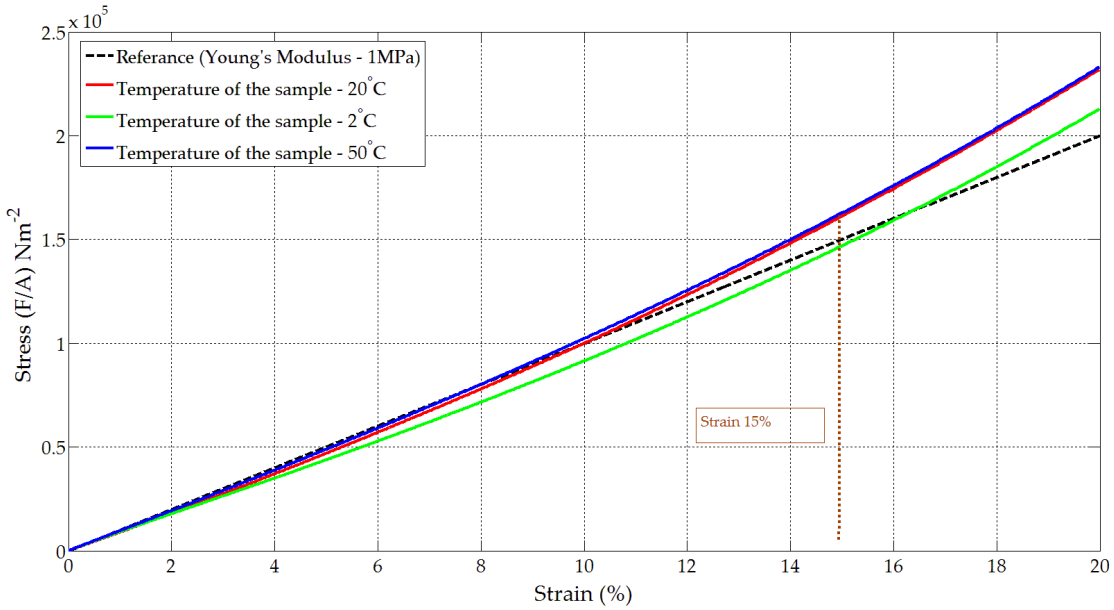

Figure 3-27: Stress strain curve of the silicon rubber material

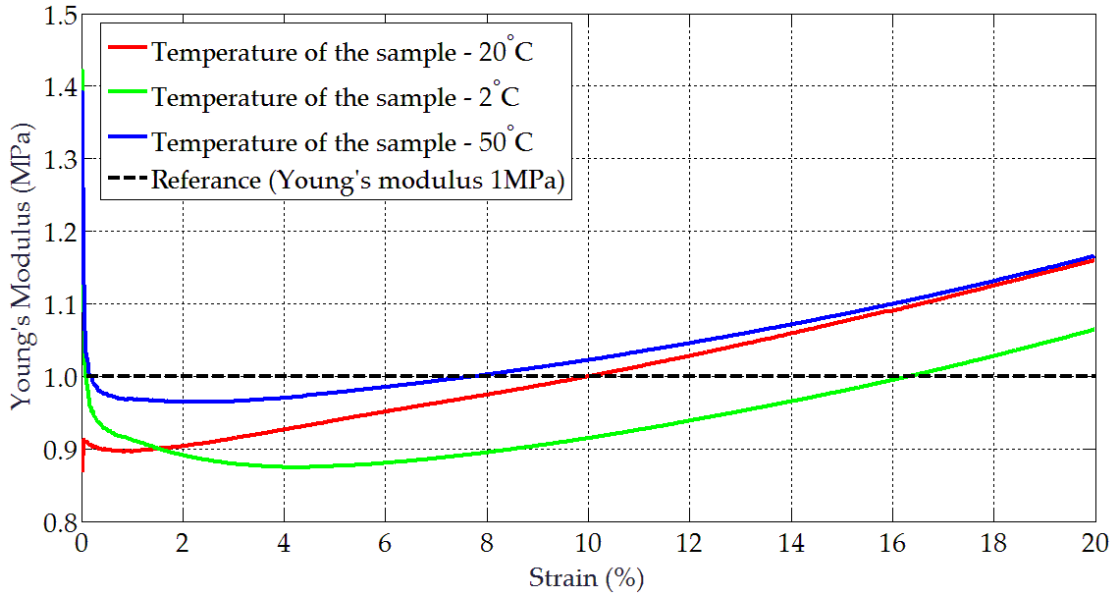

Figure 3-28: Change in the Young's Modulus with pre-stress (/pre compression)

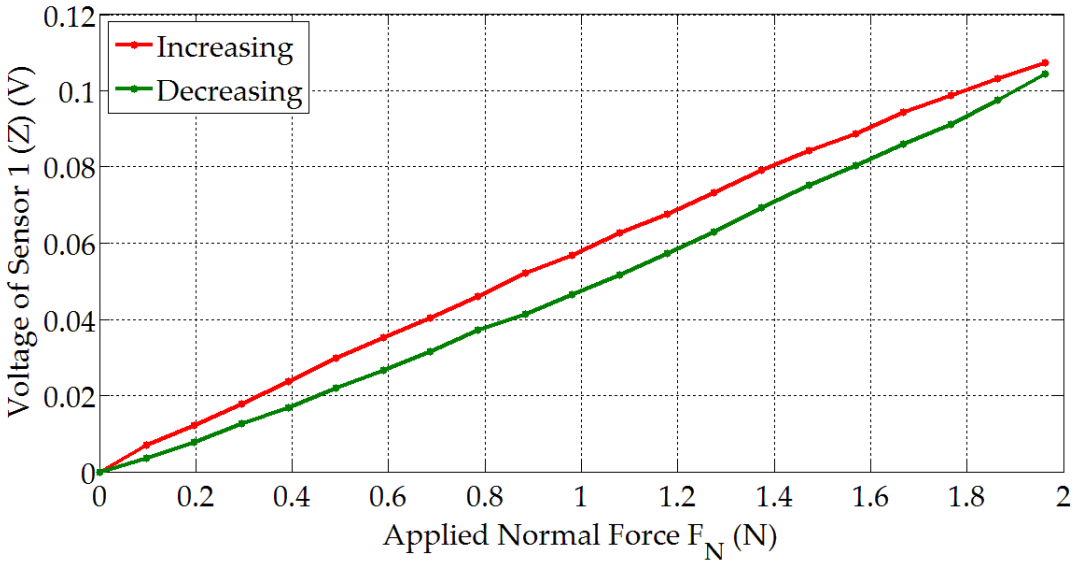

Figure 3-29: Hysteresis of the sensor in the normal direction (Z)

Figure 3-29 shows the maximum hysteresis of the sensor. The maximum hysteresis value is within 10% of the full scale value. The hysteresis of the sensor depends on the damping of the soft embodiment. In our calculations the soft material is assumed perfectly elastic having no damping. This assumption has made the calculations simple. The material selected showed minimum damping making the simulated and calculated values within acceptable range.

According to the Equation (5) and (6), the magnetic field of a permanent magnet is dependent on the distance of the point. Additionally, as per the equations, it is noted that the both components (B_R, B_Z) of the field calculation act significantly. To simplify the calculations, the orientation (yaw, pitch and roll) of the magnet is ignored. We believe that this assumption has led to most of the deviations in the magnetic flux density calculations (see deviation in **Figure 3-16**). Currently, the system does not include calculation of roll and pitch but if these components are added, the calculations will be more accurate. Additionally, the deviation in **Figure 3-16** can be caused because in the friction force F_μ calculation, the frictional force that caused by the sensor soft material sticking to the contact surface **[98]** is not included. Future improvements

include the frictional force F_μ having both components: coulomb friction and friction due to adhesion.

The concept of magnetic field measurement of a permanent magnet as the transduction principle has made the sensor robust. As the sensitive and fragile components (Hall sensors) are away from contacting with the external force, these components are safe from excessive loads. Additionally, as there are no electrical connections inside the soft embodiment, sensor has the ability to deform and come to its initial shape after the forces are removed. Finally, the modular behavior of the components of the sensor make it easy to change the sensitivity (by changing the stiffness of the soft embodiment), easy to repair, and due to the use of inexpensive components, disposable. Therefore this sensor provides an inexpensive solution for bio-medical applications as well as robotic applications in tactile sensing.

The tactile fingertip developed in section **3.9** was a hemispherical shape sensor which benefited from the simple calculation of the direction of the normal force for grasp planning. The softness of the sensor aided in the firm grasping of an object that was to be manipulated and the encompassing grasp was more stable than a grasping of a point contact by a ridged hemisphere.

The proposed sensor was cheap to construct with only a cylindrical magnet and three hall sensors for detecting the magnetic field. This cheap construction allows offsetting the sensors high vulnerability to wear and tear compared to ridged sensors. The material properties of the soft material have many advantages compeered to ridged constructions. The sensor system was highly customizable to facilitate larger spans of force measurement just only by changing the material properties of the soft overlay (Young's modulus of the material can be changed by the silicon rubber material, the mixing ratio etc...). And due to the solid construction of the sensor and the components, larger loads can be applied to the sensor without damaging the sensor.

The proposed force sensor is able to measure forces in the three axes. And due to the simple construction and robustness, it can be used in industrial applications.

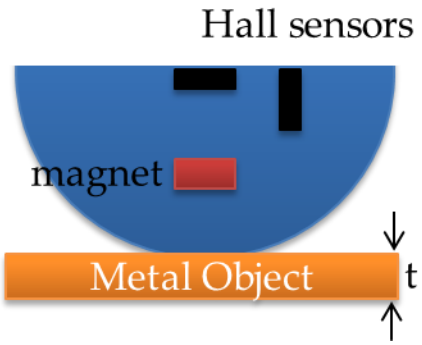

(a)

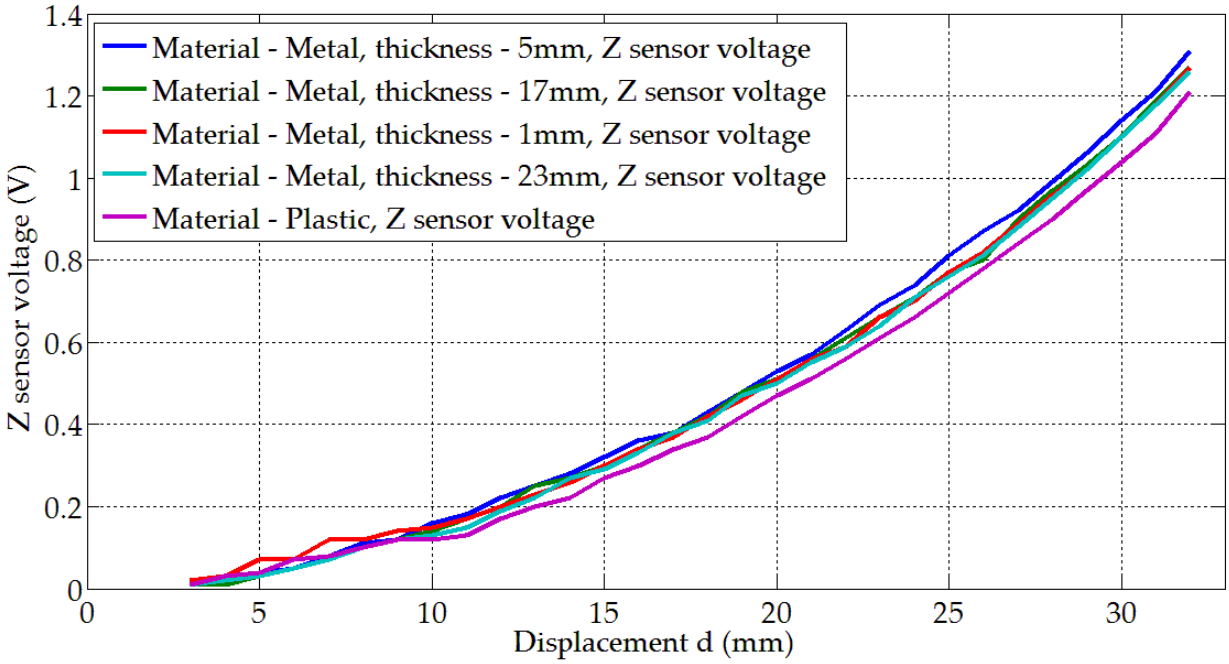

(b)

Figure 3-30: (a) hemispherical sensor was pushed onto ferromagnetic and non-ferromagnetic materials. (b) Sensor voltage difference for various materials and thickness

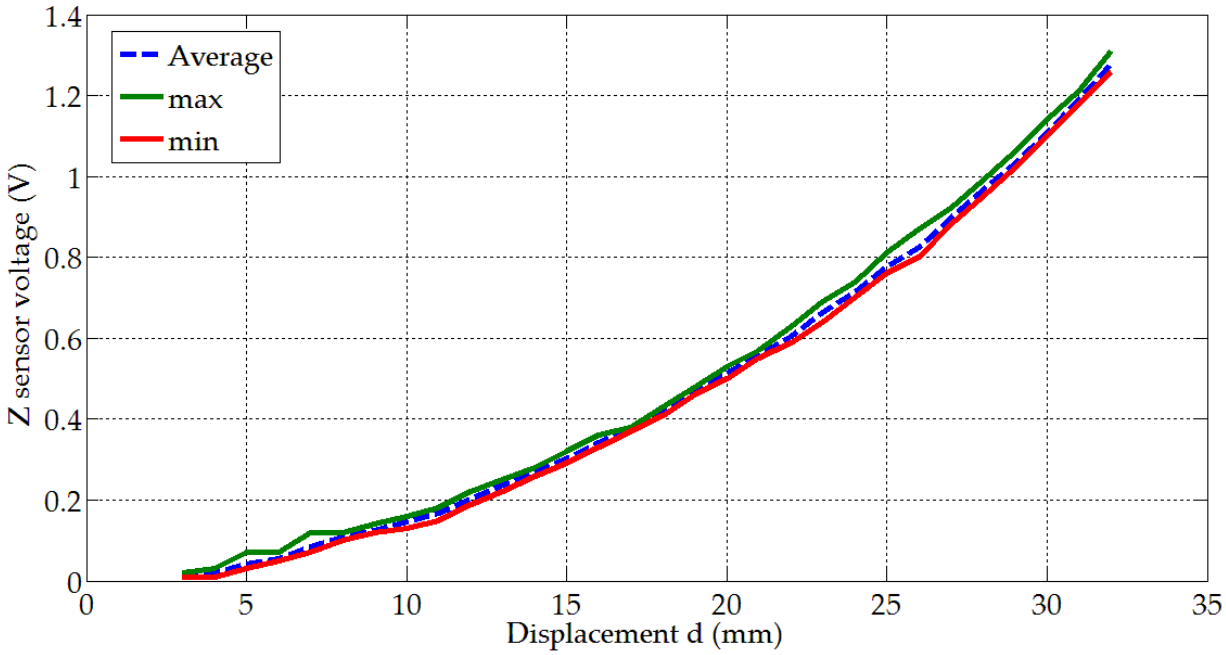

Figure 3-31: Sensor voltage deviations for a given contact depth for fero and non fero magnetic materials

In this sensor, one of the main shortcomings may have been the sensors magnetic field measurement being erroneous due to the fero-magnetic materials being close to the sensor. Nevertheless, experiments with multiple material types both fero-magnetic and nonfero-magnetic with varying thicknesses have shown that the sensor measurements did not change more than 5% of the actual value making evident that this sensor can be robust enough to be used in any situation where the material did not show magnetic properties (see **Figure 3-30**, and **Figure 3-31**).

The sensitivity of the sensor depends on the stiffness of the soft material. For a Young's modulus of $E = 1\,\text{MPa}$, the maximum force that can be measured with an error less than 5% was 23N. By increasing the stiffness of the soft material, the maximum measurable force too would increase. Therefore, this sensor could be used to measure small and large forces just by changing the stiffness of the sensing element. It should be noted that even though Young's modulus of the rubber material behaved as a function of pre-compression and

temperature, according to **Figure 3-27**, the material shows linear behavior up to a strain of 15%. Thus, the Young's modulus can be taken as a constant value for the calculations in equation provided the deformation d is less than 15% of the strain. If the deformation of the soft element was larger than 15% of the strain, the soft material should be considered as a non-linear elastic material instead of a linear elastic material. The use of a nonlinear elastic model (hyperelastic model) in the simulation will be considered in future as an improvement to the model. Furthermore, as the sensor will mostly be used in room temperature applications, the change in Young's modulus due to the temperature was small (see Stress strain curves for different temperatures in **Figure 3-28**).

Chapter 4

Development of a Tactile Fingertip Gripper and Manipulation Experiments Using the Gripper

One of the aims of this thesis was to develop a tactile sensing fingertip gripper to perform object manipulation tasks. The gripper should have the ability to perform dexterous object manipulations and environment exploration tasks similar to the functions of a human fingertip. This chapter introduces a two fingered gripper that was developed using the hemispherical fingertip developed in chapter 3. This gripper was used to hold an object which had a hole. The hole was inserted to a stationary peg. The tactile signals obtained by this sensor was recorded and analyzed. The two fingered gripper was used to measure moments applied to the object while inserting the peg to the hole. Because the single element fingertips could not measure three directional rotational moments applied to the object, a new tactile fingertip with multiple force sensor elements was presented. The sensors ability to measure three components of force and three components of moments which is applied to the manipulated object is reported.

4.1 Introduction

Grippers to a robot are as same as a tire to a car. It is with grippers that the robot interacts with the environment. If the robots to interact with humans in human friendly environments, such as homes and offices; the robot gripper should be able to hold and manipulate day to day objects used by humans. Thus an industrial gripper will not be sufficient as those grippers were meant for predefined types of objects whereas grippers of home robots should be adaptive to any type of object.

When designing the gripper system the number of fingers in the gripper matter. Humans have five fingers though most of the tasks done with five fingers could easily be carried out with just four. However, scientists have shown that at least two fingers are needed for the bare minimum of achieving two contact points for manipulation. Nevertheless, when it comes to picking up spherical objects, two point contact is not sufficient. Still, if the fingertips are soft, the fingertips would encompass the sphere and counteract the torques generated by the weight of the object. This softness will help two fingered gripper to easily pick up such objects. Thus, considering engineering complexity and necessary and sufficient conditions; a two fingered gripper having soft fingertips would suite most of the manipulation tasks.

The tactile fingertip introduced in chapter 3 has a soft hemispherical element that compresses when a force is applied to the circumference of the hemisphere. A neodymium permanent magnet was embedded inside the fingertip which displaced due to the applied force. The displacement of the magnet was calculated by measuring the change to the magnetic field at hall sensor locations. The force was proportional to the voltages of the hall sensors.

These force sensors were used as fingertips for the developed two fingered gripper. These hemispherical force sensors could measure the normal and tangential forces applied by gripping an object (see **Figure 4-1**(c)).

4.2 Two fingered tactile gripper

4.2.1 Gripper construction

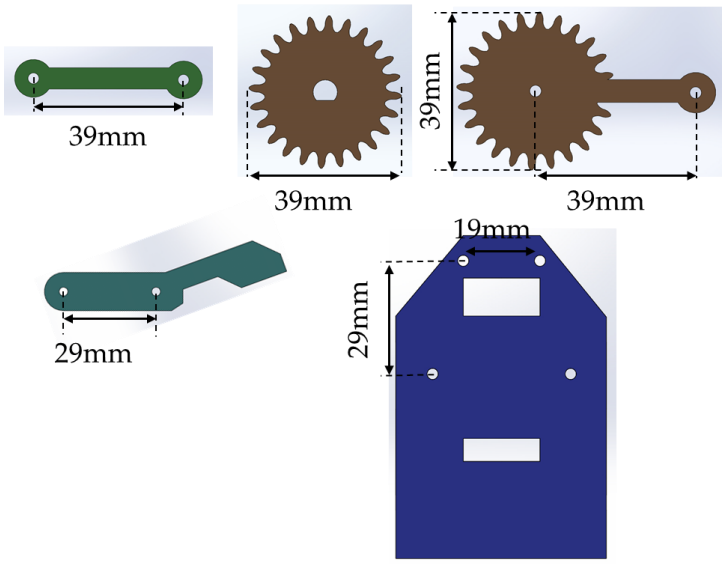

(a)

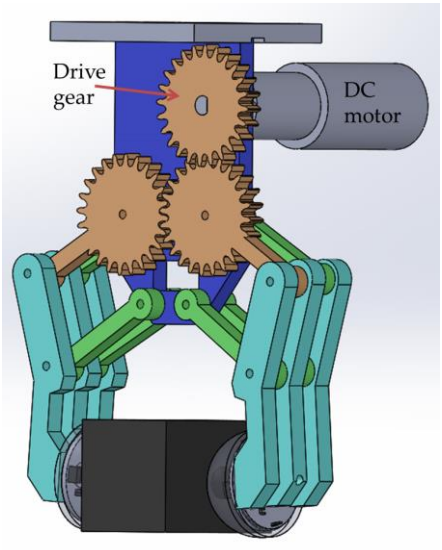

(b)

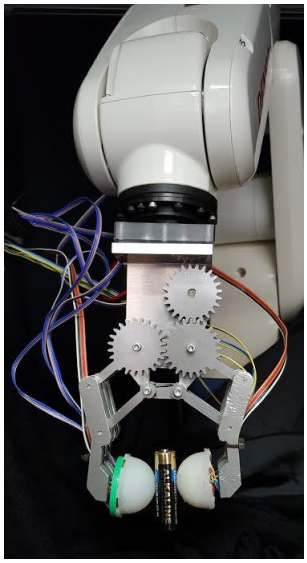

(c)

Figure 4-1: Two fingered gripper with soft force sensors as fingertips (a) main links and dimensions (b) Gripper 3D model and its components (c) gripper fixed to Denso robot arm for robot manipulation tasks

The two fingered gripper was constructed coping the parallel jaw gripper mechanism (see **Figure 4-1 (b)** and **(c)**). The jaws were moved by a rotational input generated by a driving gear fixed to a DC motor. The motor was driven by an Arduino motor shield and an Arduino Uno micro controller board. The inputs to the micro controller was from the computer which processed signals receved from the hall sensors that were fixed to the fingertips. The gripper was constructed by aluminium. The DC geared motor was a Faulhaber 47B-FU-107-KBED, and had a gear reduction of 14:1. It could exert a torque of 14N/cm. The motor had a magnetic encorder of 512 lines per revelution. For a rotation of 60^0 in the drive gear, the gripper could open the jaw fully and close. The mentioned hemispherical fingertips were fixed to the gripper. The signals needed for the open and closing of the gripper was processed after analyzing the signals obtained by the national instruments analog to digital converter. The gripper opening and closing was controlled by applying a predefined grip force and this force was measured using the force sensors.

4.3 Object manipulation

The developed gripper was fixed to a Denzo robot system and was used in an object manipulation task (**see Figure 4-2**). The gripper held an object between the two fingers as shown in the figure. The task of the robot was to insert a peg which was stationary on the base to a hole on the gripped object. Initially, the robot was controlled by preprogrammed motion and in the future,

we will try to control the robot with force feedback. The objective of this experiment was to identify the sensor signal obtained (see **Figure 4-5**) by the two soft fingertips while a manipulation is being carried out.

Figure 4-2: Gripper fixed to Denzo robot arm

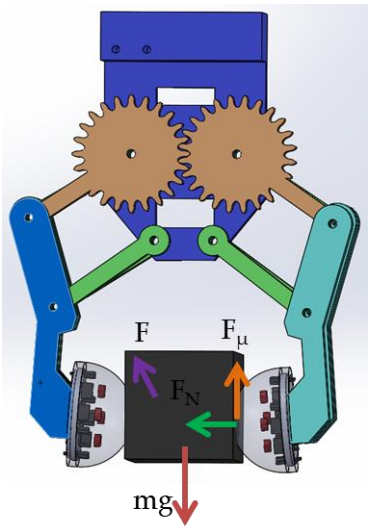

Figure 4-3: Force applied by the fingertips on a manipulated object. F_N is the grip force (normal force) while F_μ is the frictional force at the object sensor

contact surface. F is an external force applied on the object due to contact with a third object.

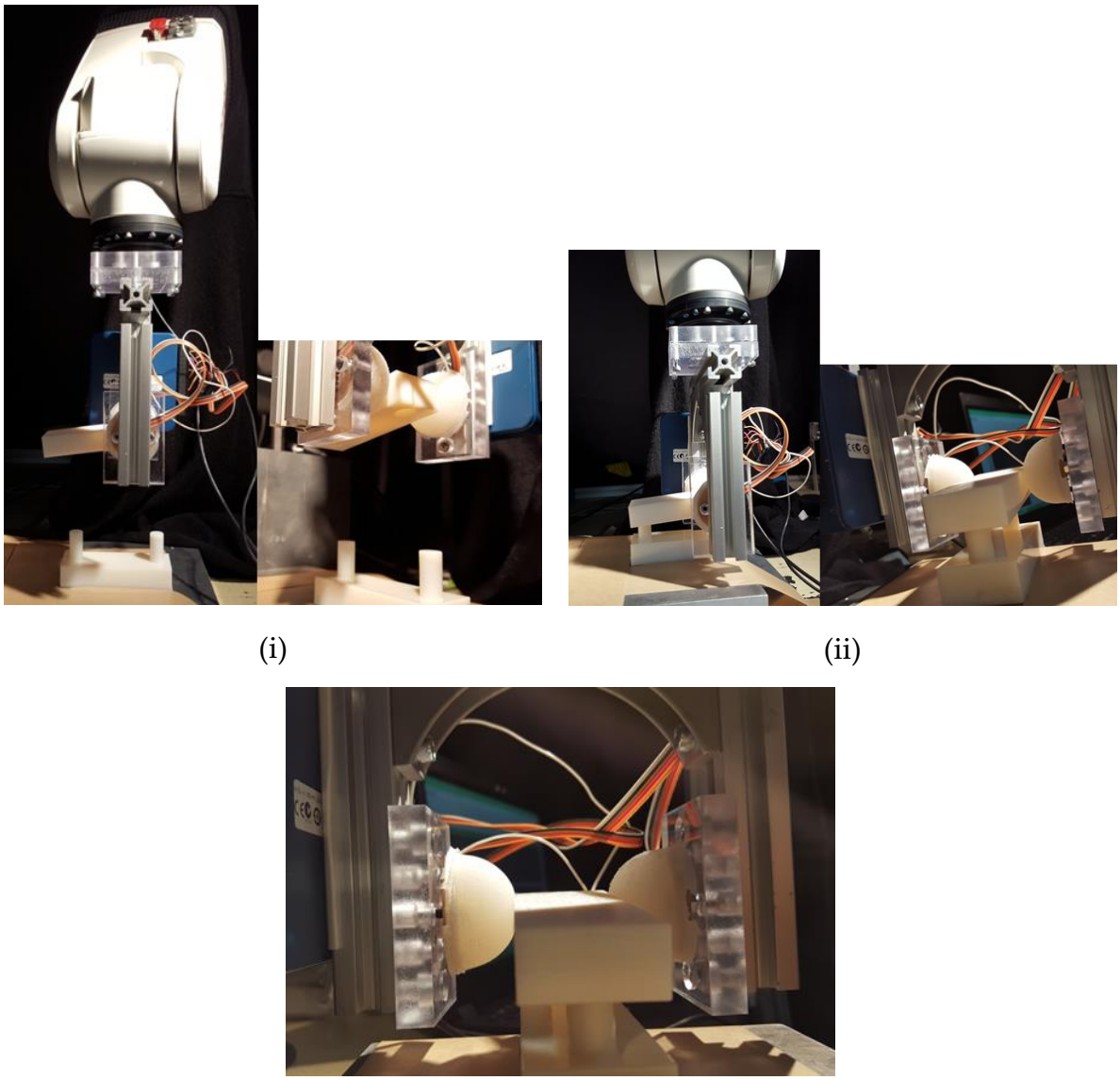

(i) (ii)

(iii)

Figure 4-4: Robotic manipulation. Peg in the hall experiments. (i) Object is griped by the gripper and moved close to the peg. (ii) Object brought close to the peg and aligned before insertion. (iii) Peg was inserted into the hole.

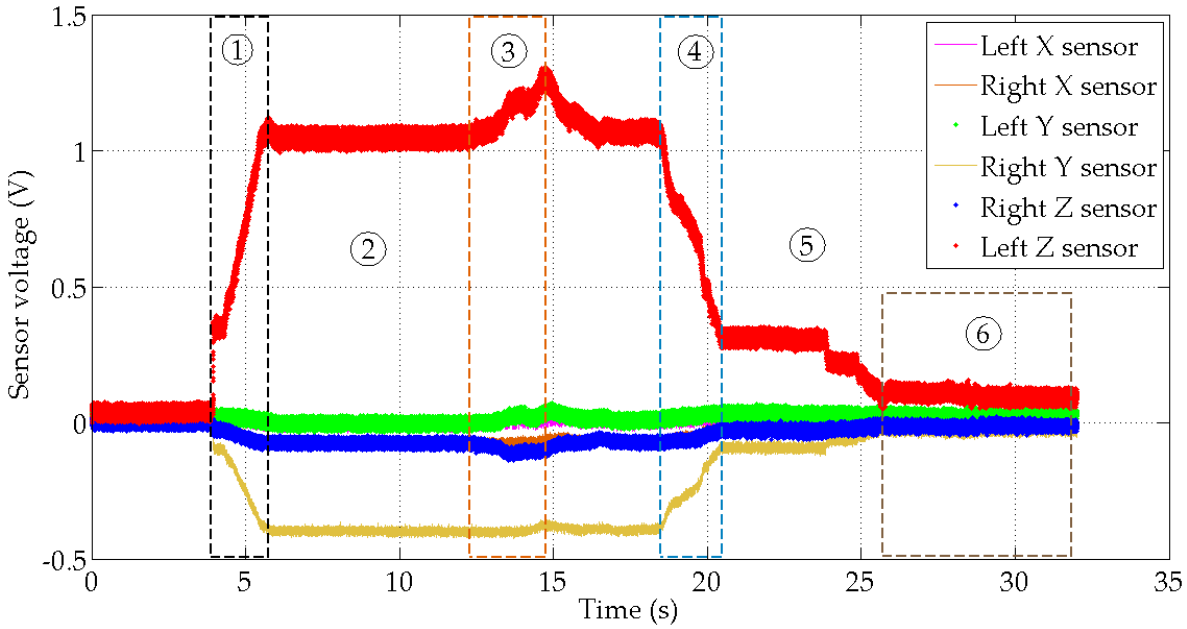

Figure 4-5: The sensor signals when the robot inserted the peg into the hole

According to **Figure 4-4** and **Figure 4-5**, the stages of the manipulation experiment could be separated in to the following.

1. The gripper tightened and when a reaction force was detected, grip force was gradually increased.
2. The hand moved to the required location to align with the peg
3. The hole was aligned with the peg (as the object was displaced by the misalignment of the peg and hole, grip forces varied. See **Figure 4-5**) at the section no.3 where the *z* directional forces increased and decreased after the peg was inserted to the hole, forces reduced gradually to the initial grip force.
4. the grip force was reduced gradually until the reaction force was zero. The force reduction was in two stages. As the object may be damaged by dropping the object if not properly seated, the rate of the removal of the grip force was smaller than the rate of the application of the grip force. The reduction was done in two stages. The force was reduces till the

force value relevant to the first detected reaction force. And then the force was reduced in a much slower rate.

5. Finally, the gripper loosened the object fully and moved away from the assembly.

By analyzing the sensor signals of all six sensors, the following observations were recorded.

1. the sensor had a settling time. This was due to the soft material having a damping effect.
2. There is significant damping in the sensors but it can be controlled by the selection of proper materials.
3. When the peg and the hole were misaligned, the interactions between the object and the peg produced moments around the two contact surfaces (see **Figure 4-6**). The imbalance caused the deviations in the sensor signals in both left and right with opposite reactions. This could be used in controlling the robot as a scheme to reduce unbalanced moments due to improper contact.

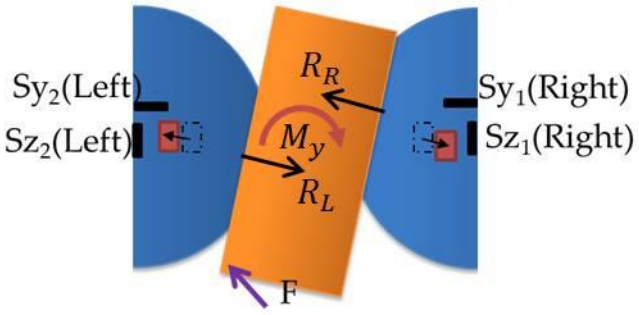

Figure 4-6: Moment produces due to the external force F and Reaction forces R_L and R_R

The proposed gripper used a parallel jaw type mechanism to close and open the fingers. The motion of the fingertip was circular. Thus, the deformation of the soft fingertips was not perpendicular to the sensor base. Therefore, the grip force did not distributed evenly. However, the force measured was acceptable for the controlling the gripper as grip force less than 20N, the vertical deformation was less than 2.5mm and that was small enough to assume that the deformation in the tangential direction was negligible due to the circular trajectory of the fingertip.

When analyzing the sensor data obtained from the peg in the hall experiment, we could identify that the initially applied grip force was varying when the peg was inserted to the hall. This happened because there was a change in the equilibrium of the object due to the generated moment from the external force *F* (see **Figure 4-6**). When the peg did not align correctly with the hole, the external force increased until the hole slide on to the peg and aligned itself correctly to be inserted. Then, when the hole and the peg aligned correctly, the peg went inside the hole and the external force reduced. This phenomenon is used by us humans when we want to assemble some components and when the two components are not aligned correctly; we move one component to a direction where we minimize the induced moment. This behavior is used in assembling transition fitting parts in assembly lines. Therefore, identifying moments applied on manipulated an object which occurs because of external forces is an important attribute of a tactile gripper system. However, the proposed sensor above could only detect forces applied in vertical and tangential directions. Therefore, a new fingertip sensor with multiple sensing elements was proposed.

4.4 Development of four element force gripper for moment measurement.

The fingertip design with multiple force sensor elements is shown in **Figure 4-7**. The fingertip was designed adhering to the same design concepts presented in chapter 3. However, the hemispherical fingertip consisted of four force sensor elements distributed along a Pitch Circle Diameter of 17mm compared to the initial fingertip design. This meant there were twelve hall sensor data to be processed for a single force sensor.

The force measurements of the four sensors were calculated similar to the method presented in chapter 3. The additional moments in three axes were calculated as follows.

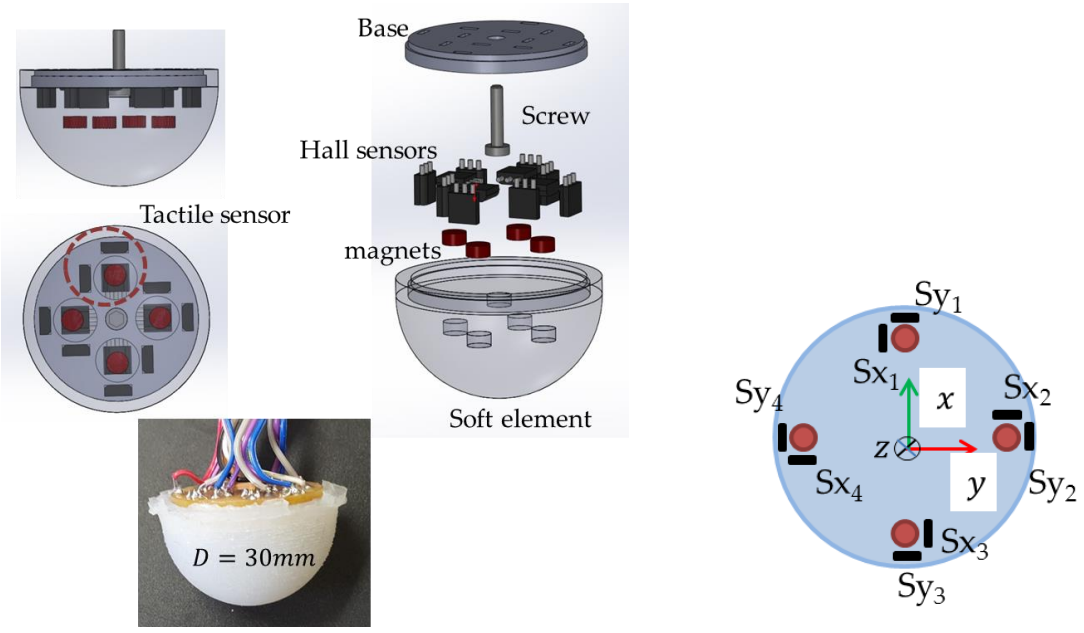

(a) (b)

Figure 4-7: Tactile fingertip with for sensor elements. (a) Components of the tactile fingertip. (b) Naming convention used to identify the hall sensors relevant to each force sensor elements

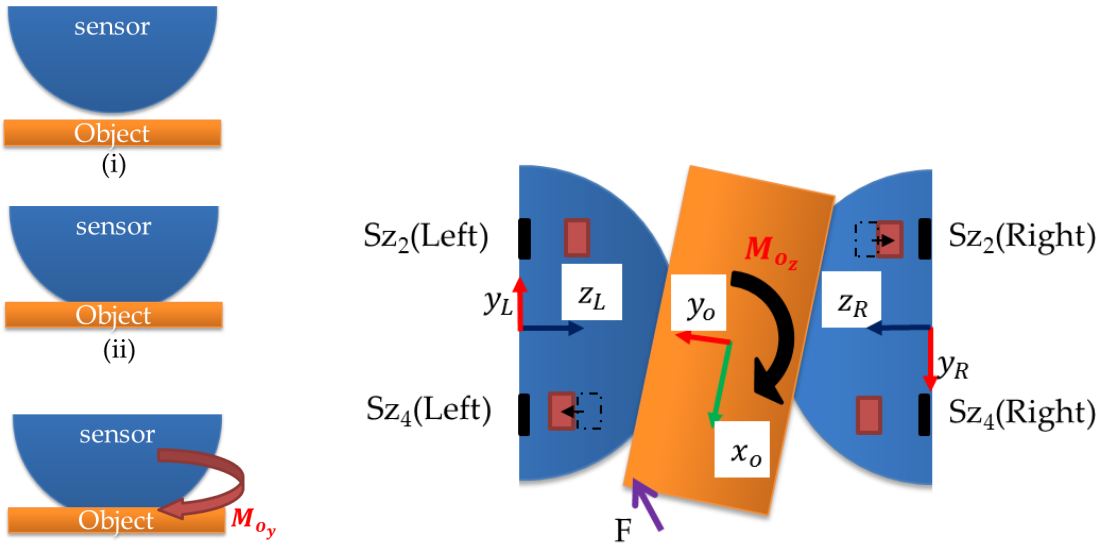

Figure 4-8: Moments generated on the manipulated object due to the external force

The moments generated around the three axes of the object coordinate system x_o, y_o, z_o are represented by M_{o_x}, M_{o_y}, and M_{o_z}. These moments are calculated from the following equations.

Moment M_{O_z} can be calculated from

$$M_{o_z} = K_{z1}\,[V_{z_4}(Left) - V_{z_2}(Right)] - K_{z2}\,[V_{z_2}(Left) - V_{z_4}(Right)] \qquad (11)$$

Moment M_{O_x} can be calculated from

$$M_{o_x} = K_{x1}\,[V_{z_1}(Right) - V_{z_3}(Left)] - K_{x2}\,[V_{z_1}(Right) - V_{z_3}(Left)] \qquad (12)$$

And Moment M_{O_y} can be calculated from

$$M_{o_y} = K_y \frac{\sum V_x}{4} \qquad (13)$$

where clockwise moment is positive while counterclockwise motion is considered be negative (see **Figure 4-9**). $V\_\_$ represents the voltage of each individual hall sensor, $K\_\_$ are constants which should be calculated experimentally.

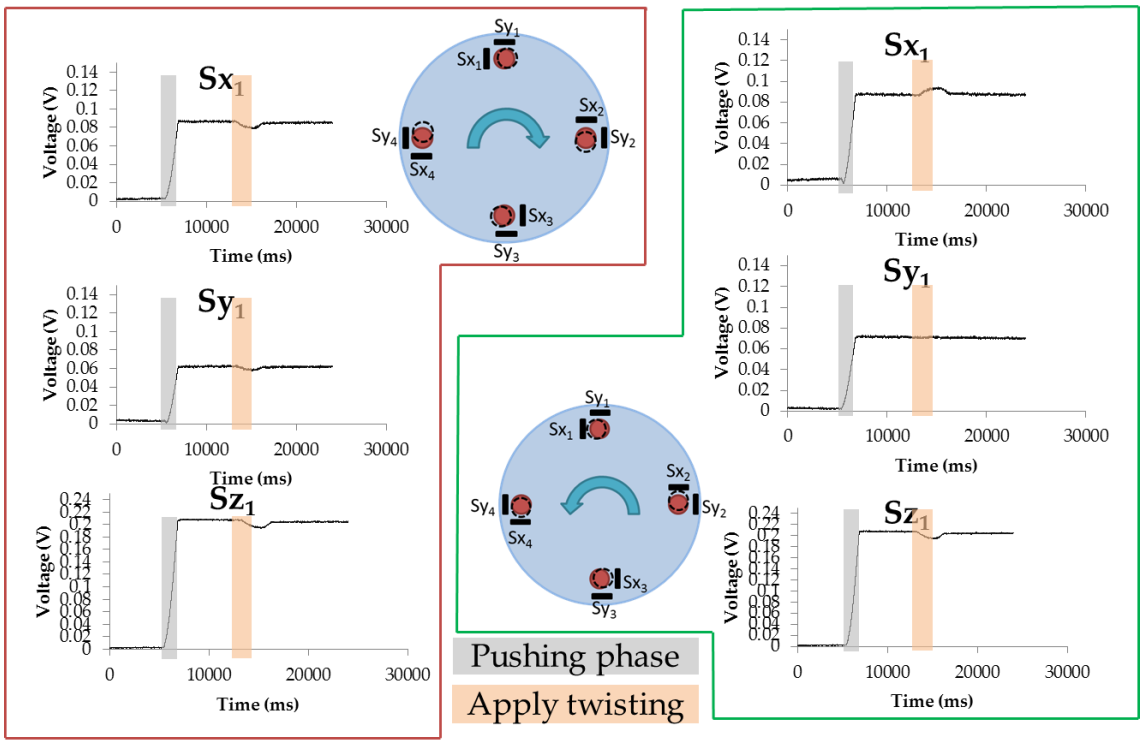

Figure 4-9: Sensor signals obtained for a clockwise and counterclockwise rotation

4.5 Discussion

In this chapter, we have proposed a two fingered parallel jaw gripper incorporating soft three axis force sensors. The forces sensor is a hemispherical shape sensor which is benefited from the simple calculation of the direction of the normal force for grasp planning. The softness of the sensor aids in the firm grasping of an object that is to be manipulated and the encompassing grasp was more stable than a grasping of a point contact by a ridged hemisphere. The

proposed sensor was cheap to construct. This cheap construction allows offsetting the sensors high ability to wear and tear compared to ridged sensors. The material properties of the soft material have many advantages compeered to ridged constructions. The sensor system is highly customizable to facilitate larger spans of force measurement just only by changing the material properties of the soft overlay. And due to the solid construction of the sensor and the components, larger loads can be applied to the sensor without damaging the sensor.

Chapter 5

Applications of the Soft Force Sensor: Material Classification

The developed sensor in chapter 3 had to be evaluated for its operation as a tactile sensor. A human could use his or her sense of touch to discriminate textures. This task is a complex operation where both tactile sensor data and intelligence needs to be used. Humans have the ability to discriminate textures within few hundred milliseconds just using few strokes by the fingertips. Thus, this chapter tries to identify the ability of this sensor coupled with Artificial Intelligence methods to identify 8 types of textures just by sliding on the texture few times.

5.1 Introduction

Though it may seem trivial, recognition and classification of materials, and texture is a compulsory ability of a robot system if it to work in an unstructured environment. An example would be a rescue robot navigating a corridor by feeling the wall and localizing itself by recognize a metal door or a glass window. This will be possible if the robot had the ability to distinguish walls, metals, and glass. If the robot had lost visibility, the most intuitive method to discriminate would be to touch and feel those different material and texture types. We humans too do such tasks every day. We turn on switches in the dark only by feeling the switch against the wall texture. Thus, it is natural to develop systems and methods to give same abilities to robots.

Humans mainly use fingertips to perceive materials and textures. The mechanoreceptors in fingertips detect tactile stimuli. However, biological tactile sensing system is complex comprising of different types of sensors per square centimeter detecting pressure, vibrations, stress and temperature stimuli [**24**], [**99**]. Each of these modalities coupled with vision, audition and prior experience help humans to identify or classify materials, and textures. In attempting to develop artificial systems with the same capabilities as the human tactile system, it is logical to mimic the human tactile system. But constriction of such a system with similar sensor density is currently not practical. Therefore, simple tactile sensors and methods have to be developed to achieve the same functions. Few tactile sensing fingertips were developed for texture classification and object manipulation by Wettels [**51**], Hosada [**100**], Oddo [**37**], and Chathuranga [**101**]. These sensors were covered with a soft overlay and contained different types of sensing elements, including strain gauges, polyvinylidene fluoride (PVDF), micro electromechanical (MEMS) force sensors, resistive type force sensors and accelerometers. These fingertips had the ability to detect forces and vibrations. Fingertip designed by Wettels [**99**] and Takamuku [**102**] also had temperature sensors. Tactile signals from these

fingertips were used either for material, texture classification tasks or object manipulation tasks or both.

Simultaneously with the sensor development, computational intelligence needed for material and texture recognition also had to be developed. Research in to biological tactile system and neural signal relevant to texture identification has found that humans differentiate textures by evaluating the roughness, hardness and stickiness of each sample [**103**]. This research explained that above quantities are represented by the physical quantities: vibratory power, compliance and friction. Earlier research by [**104**] explained that roughness which had element spacing greater than 1mm were identified by spatial variations in the sensors while roughness elements less than 1mm were identified by temporal variations of the tactile sensors. Additionally, Miyaoka [**105**] explained that roughness in fine surfaces is also influenced by amplitude information present in the surface unevenness. Therefore, it could be deduced that if the artificial tactile system had enough sensor density (according to [**104**] 1 sensor per $2mm^2$), textures which has roughness elements greater than 1mm can be identified by analyzing sensor data particular to spatial distribution. Also, if roughness elements are less than 1mm, the sensor's temporal data had to be analyzed. While above methods were used to classify textures, Lin [**99**] and Takamuku [**102**] used their developed fingers and thermal transients measurements to distinguish materials.

Above being a reason, many of the texture classification techniques had been centered on frequency analysis techniques. Fast Fourier transform (FFT) was one of the main techniques used in texture classification methods. Muhammad [**38**] converted tactile sensor signals into frequency domain data and separated the principle frequency and calculated the spatial frequency of the given texture or material. Another research used a piezo-electric microphone as a sensing element, with sound waves segment by FFT and a

supervised learning vector quantization technique to classify 18 materials [**106**]. Similarly, FFT was utilized to identify the first five major frequencies of a material, which were subsequently used in a classification algorithm called majority voting [**107**]. Similarly, spectral properties were again used to discriminate among five textiles by Oddo using k-nearest neighbour classifier [**18**]. Hu [**108**], Yoshioka [**109**], Song [**110**], Drimus [**111**] and Mukaibo [**112**] also utilised frequency spectrum data to discriminate textures. Although many researchers used temporal data and converted those to frequency data and used in classifiers, the main limitations of these method are its ability to identify only textures with periodic elements and the need of the palpation velocity to be constant and known. Furthermore, it only considered evaluating the roughness property of textures.

Apart from spectral properties being used in classifiers, other features such as sensor signal's mean, variance, skewness, and kurtosis etc. were employed by some texture classification algorithms. It is understood that these values can be used to represent properties of texture (roughness, compliance, and friction). Boissieu's method of classification was to use a force sensor covered with an elastic layer. It slid over 10 material samples and the samples were classified by two analytical methods: determining differences in Fourier coefficients and using the mean, variance, kurtosis, and spectral properties as features of a classifier neural network [**41**]. Similarly, Dallaire [**20**] and Giguere [**113**] used accelerometer sensor data and calculated mean, variance, skewness, kurtosis, fifth moment, sum of higher half of amplitude spectrum etc. as features for a supervised learning method. On the other hand, Kim [**39**] used a 4×4 MEMS tactile sensors signals as random Gaussian variables, with mean and variance calculated as features for classification. In another research, a dynamic friction model was utilized to calculate surface properties, such as static and kinetic frictional parameters, surface viscosity and texture, with these features subsequently used in several supervised learning algorithms, such as

Bayes classifiers, basis function networks and the k-NN method [**36**]. Fishel [**114**] calculated values proportional to traction, roughness, and fineness, and used those values in a discrimination algorithm called the Bayesian exploration. Chathuranga [**101**] used biomimetic tactile fingertip to discriminate eight textures using covariance signal of two nearby accelerometers embedded in the fingertip. These proposed methods in general had high classification accuracy for varieties of material and texture classes compared to the FFT based classification algorithms. This is because unlike frequency based classification, these classifications utilized all the properties of textures (roughness, compliance, friction) when generating features opposite of using roughness alone. However, apart from Chathuranga [**101**], all the methods used active touch with constant and known palpation velocity and normal force. These dependency of velocity and normal force is still an issue when these systems are to be incorporated into autonomous robots.

This chapter proposes a new algorithm to classify textures and materials based on three dimensional tactile data obtained by 3D soft tactile sensors. The features used in the algorithm are the Frobenius distance of the covariance matrix of the three dimensional tactile sensor data and the three means of the same set of data. Support Vector Machine (SVM) was used as the classifier on the selected class to choose the best class that fit with an unknown material or texture sample. The algorithm had an overall success of 89% of classifying 8 material and texture samples. The time taken for each classification was 0.28s making it a fast method to be used in a real time system. The advantages of this algorithm are its fast and simple computation, robustness of features to palpation velocity and normal force and high accuracy.

The following sections describe the experiments conducted, results obtained and the conclusions made from the findings. These results show that this classification method is robust and applicable to any system that could

detect tactile data in three dimensions. Additionally, this classification method was compared with previously proposed classification algorithms by Muhammad [**115**], and Boissieu [**41**].

5.2 Materials and methods

The tactile sensor is a 3d force sensor (see **Figure 3-1**) which was initially proposed in chapter 3 as a soft 3 axis force sensor. The sensor was fixed to a linear stage which could be moved in x and z directions in velocities up to 20mm/s. The sensor was connected to a computer and the movements of the sensor along a texture surface and the collection of sensor data were automated. A raw sensor data obtained for a texture (denim) when the sensor moved in a scanning trajectory is shown in **Figure 5-1**. It should be noted that even though this sensor data represent tactile information about a texture, straightforward information about the texture such as spatial period could not be correctly identified.

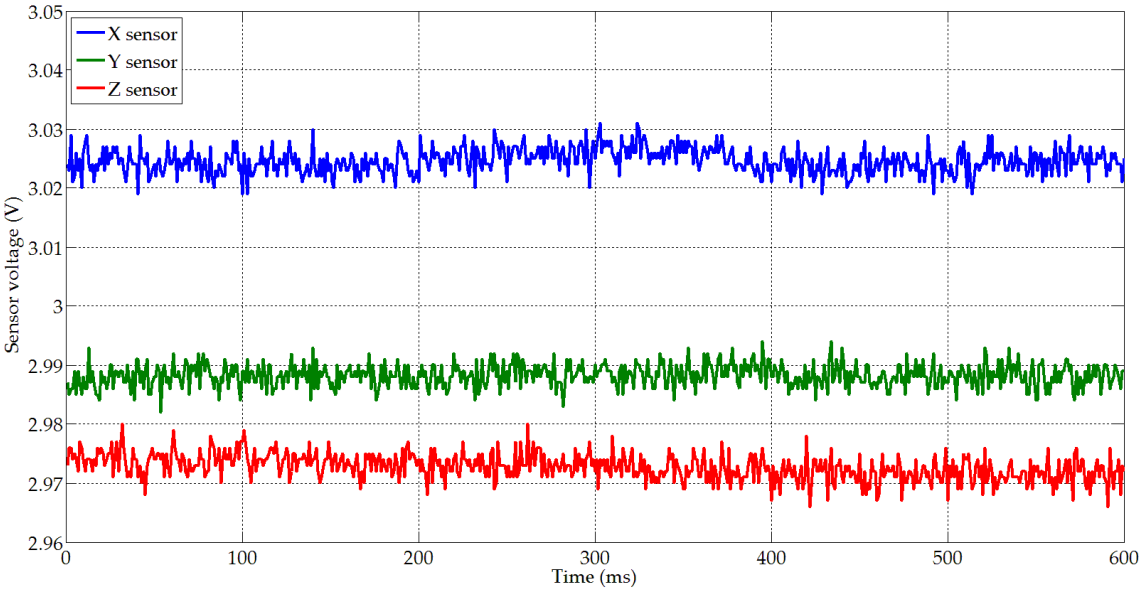

Figure 5-1: Raw sensor data obtained for an exploration on denim

5.3 Classification Strategy

5.3.1 Relationship between material texture and sensor signal

The soft element of the sensor deforms when normal and tangential forces are applied. The Normal force F_N was applied by the sensor being pressed onto the textured surface. The tangential force F_μ is applied when the sensor was slid along the textured surface when the frictional force is induced by the contact surfaces (see **Figure 5-2**).

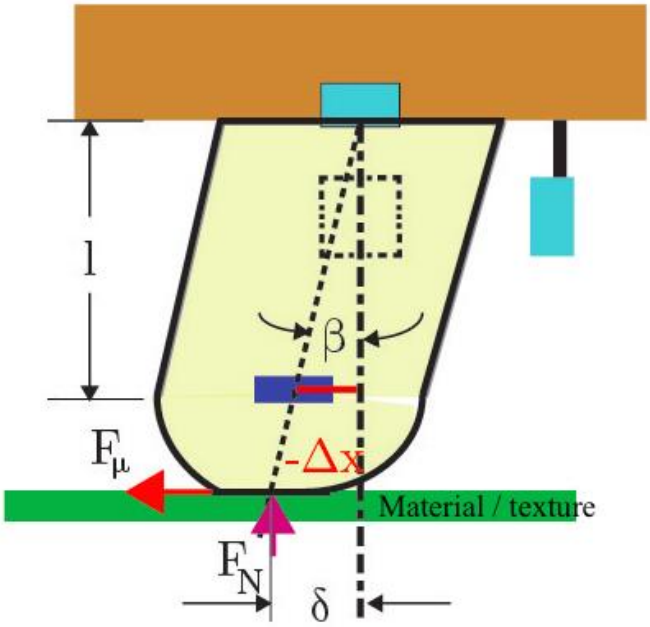

Figure 5-2: Schematic representation of the tactile sensor under exploration

It is known that the frictional force is consisted of two components [**98**]. The frictional force F_μ consists of frictional force due to the adhesive between the two surfaces $F_{\mu,adh}$, and the frictional force due to the deformation of the bodies in contact $F_{\mu,def}$.

$$F_\mu = F_{\mu,adh} + F_{\mu,\mathrm{def}} \qquad (13)$$

The adhesive frictional force is $F_{\mu,adh}$ proportional to the real contact area while deformational frictional force $F_{\mu,def}$ depends on the indentation of the

sliding element with the textured surface. Both contacts area and indentation depends on the normal force applied while in scanning. Therefore the general equation for dynamic and static friction $F_\mu = \mu F_N$ is held true. In our experiments, the frictional coefficient μ for each texture is considered same for the entire texture surface.

If the texture in the z direction is represented by a function $f(x)$ and the initial contact depth is d, normal force F_N can be written as:

$$F_N = K_s\big(d - f(x)\big) \qquad (14)$$

where K_s is the spring constant of the soft element. Additionally, if the soft element is in equilibrium, frictional force F_μ is offset by the bending force of the soft beam element. If the bending constant of the element is K_b, the bending formula can be written as

$$F_\mu = K_b \delta \qquad (15)$$

where δ is the tangential deformation of the soft beam. Now, substituting Equation (14) and Equation (15) in $F_\mu = \mu R$ we obtain

$$\delta = \frac{\mu K_b}{K_s}\big(d - f(x)\big) \qquad (16)$$

In this equation, all terms except $(d - f(x))$ are constant for a given exploration experiment. This indicates that the tangential displacement of the beam is a function of texture of the surface which is represent by $f(x)$. The function $d - f(x)$ is represented by the mean of the hall sensor signal.

The texture in y and z direction is represented by functions $g(x)$ and $f(x)$, and because of these textures, the Hall sensors in x, y and z directions

are stimulated. These signals are used in the feature construction of the classification algorithm.

5.3.2 Classification Features

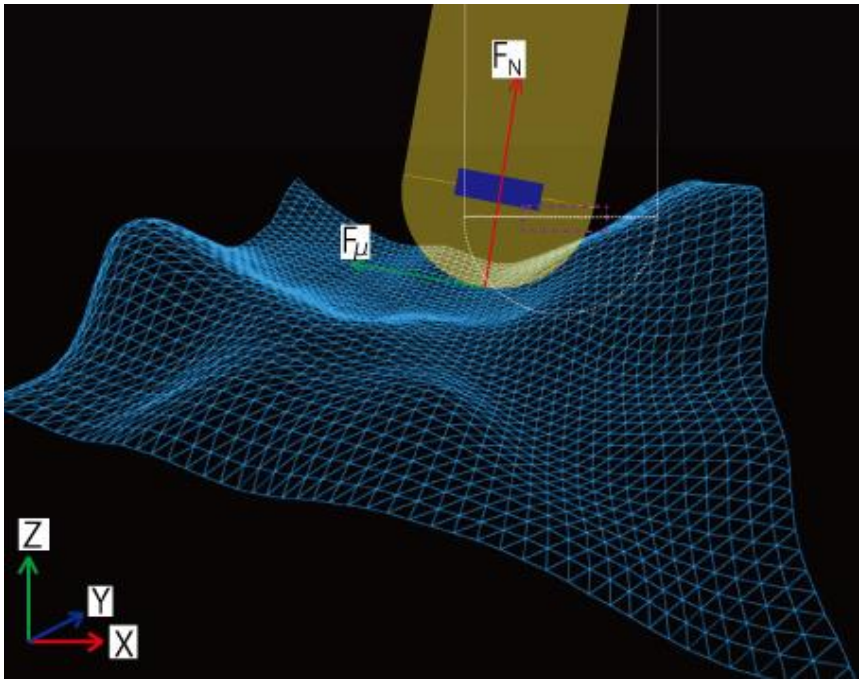

(a)

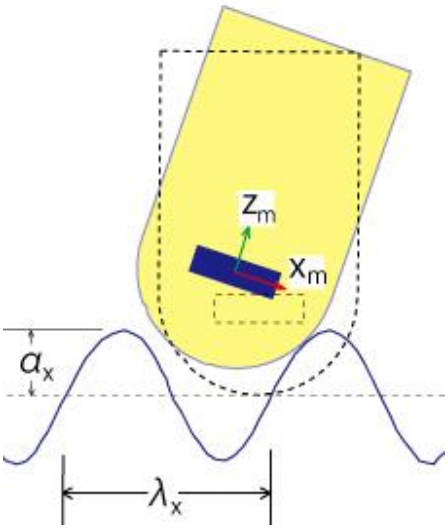

(b)

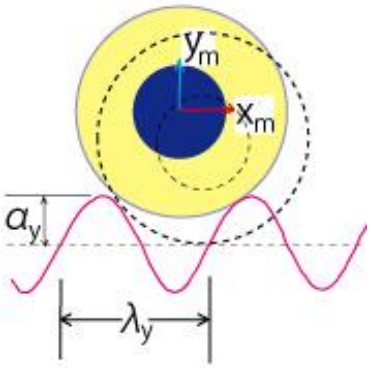

(c)

Figure 5-3: (a) Sensor moving on a textured surface (b) The textures is simulated as sinusoidal waves in vertical and horizontal planes

If a tactile sensor was used to explore the surface of a material by palpation, the soft silicon element of the sensor would deform in three directions x, y, z while the sensor is moving. These deformations are a function of the geometry of the sensor, the geometry of the surface (texture), the stiffness and damping of the sensor's soft material and the static and dynamic frictional coefficients of the material and the silicon sensor surface (**Figure 5-3**).

During each palpation test, the tactile sensor produces three sets of voltages, corresponding to x, y and z directions. This sensor signal V_s can be represented by three column vectors $\boldsymbol{X}, \boldsymbol{Y}, \boldsymbol{Z}$. Each of these vectors consists of voltage scalars x_i, y_i, and z_i.

$$\boldsymbol{V_s} = [\boldsymbol{X}\ \boldsymbol{Y}\ \boldsymbol{Z}]$$

$$\boldsymbol{X} = \begin{bmatrix} x_1 \\ \vdots \\ x_n \end{bmatrix}, \boldsymbol{Y} = \begin{bmatrix} y_1 \\ \vdots \\ y_n \end{bmatrix}, \boldsymbol{Z} = \begin{bmatrix} z_1 \\ \vdots \\ z_n \end{bmatrix}$$

Then, the covariance matrix $\boldsymbol{M_{Cov}}$ is written as:

$$\boldsymbol{M_{Cov}} = \begin{bmatrix} \sum \boldsymbol{XX} & \sum \boldsymbol{XY} & \sum \boldsymbol{XZ} \\ \sum \boldsymbol{YX} & \sum \boldsymbol{YY} & \sum \boldsymbol{YZ} \\ \sum \boldsymbol{ZX} & \sum \boldsymbol{ZY} & \sum \boldsymbol{ZZ} \end{bmatrix} \qquad (17)$$

where, for any column vector $\boldsymbol{A}$; $\boldsymbol{B}$ with same size:

$$\sum \boldsymbol{AB} = \sum_{i,j} (a_i - \bar{a})(b_i - \bar{b})$$

with $\bar{a}, \bar{b}$ being the means of the scalar values of vector $\boldsymbol{A}$, and $\boldsymbol{B}$.

The next step in feature generation was a simplification of the covariance matrix by calculating the Frobenius Norm of the matrix. The Frobenius Norm $\left|\left|D\right|\right|_F$ of the covariance matrix $\boldsymbol{M_{Cov}}$ can be calculated as

$$\left|\left|D\right|\right|_F = \sqrt{Trace((\boldsymbol{M}_{Cov})^T \boldsymbol{M}_{Cov})} \qquad (18)$$

The Frobenius Norm is therefore one of the classification features.

Apart from the Frobenius norm, incorporating the mean value $\boldsymbol{M}_{mean}$ of the sensors in three dimensions had increased classification accuracy.

$$\boldsymbol{M}_{mean} = [\,\bar{x}, \bar{y}, \bar{z}]$$

5.3.3 Classification Algorithm

Compared to regularized least squares (RLS) and regularized extreme learning machine (RELM), Support Vector Machine (SVM) has been reported to be a better binary classification, trading computational complexity with classification accuracy [**116**]. Therefore, we utilized SVM as the classifier, with a Gaussian Radial Basis Function kernel having a scaling factor σ of 1.0.

Algorithm 1 Proposed SVM based algorithm [**117**]

1: $\boldsymbol{C} \leftarrow$ material class set

2: $\boldsymbol{C_k} \leftarrow$material class set after k-th interation $\boldsymbol{C_k} \subset \boldsymbol{C}$, for the first iteration $k = 1, \boldsymbol{C_1} = \boldsymbol{C}$

3: $n_k \leftarrow$# of material classes in candidate set after k-th iteration

4: $m \leftarrow$# of permutations for selecting 2 materials from n_k

5: $\boldsymbol{for}\ k = 1,2,3\ \boldsymbol{do}$

6: $\quad\boldsymbol{for}\ i = 1,2, \ldots m\ \boldsymbol{do}$

7: $\quad\quad\boldsymbol{V_s} \leftarrow$ read tactile sensor data of unknown material

8: $\quad\quad$calculate $\boldsymbol{M_{Cov}}$, $||\boldsymbol{D}||$, and $\boldsymbol{M_{Mean}}$

9: $\quad\quad\boldsymbol{select}\ \boldsymbol{c_1} \leftarrow$ randomly select one class from $\boldsymbol{C_k}$

10: $\quad\quad\boldsymbol{select}\ \boldsymbol{c_2} \leftarrow$ select another class from $\boldsymbol{c_1} \neq \boldsymbol{c_2}$

11: $\quad\quad\boldsymbol{retrieve}\ \boldsymbol{M_{Cov}}, ||\boldsymbol{D}||_F$ and $\boldsymbol{M_{Mean}}$ of $\boldsymbol{c_1}, \boldsymbol{c_2}$ for training SVM

12: $\quad\quad\boldsymbol{train}\ SVM$

13: $\quad\quad\boldsymbol{classify}$ unknown material using SVM

14: $\quad\quad\boldsymbol{count}$ total count of classification results

15: $\quad\boldsymbol{end\ for}$

16: $\quad\boldsymbol{if}\ k < 3\ \boldsymbol{then}$

17: $\quad\boldsymbol{creat}\ \boldsymbol{C_{k+1}} \leftarrow$ 50% candidate matrix with maximum total count

18: ***else***

19: ***select class*** with maximum frequency as classification

20: ***end if***

21: ***end for***

As SVM is a binary classifier, we devised our material classification algorithm according to **Algorithm 1**. From the moment the tactile sensor started to collect tactile data in the exploration portion (AB section of **Figure 5-4**), it calculated the covariance matrix of the obtained signal and then the Frobenius distance of the matrix from the sensor data. Next, the algorithm chose Frobenius distance and mean of two material data sets from the training sample space and classified the Frobenius distance and mean of the unknown material using SVM. This was continued for all 28 combinations of pairs that could be made from the eight materials. The SVM outputs were recorded, and the highest 50% of the materials that had been selected as the possible unknown material were kept as candidate solution. Next, the same classification step was performed with the next set of tactile sensor data, but instead of training the SVM with all eight types of material, the training set was selected from the candidate solution set. After the palpation, the 50% of the remaining materials with the highest count was selected. In the final iteration, the candidate material with the highest frequency (probability) was selected.

5.3.4 Experiments

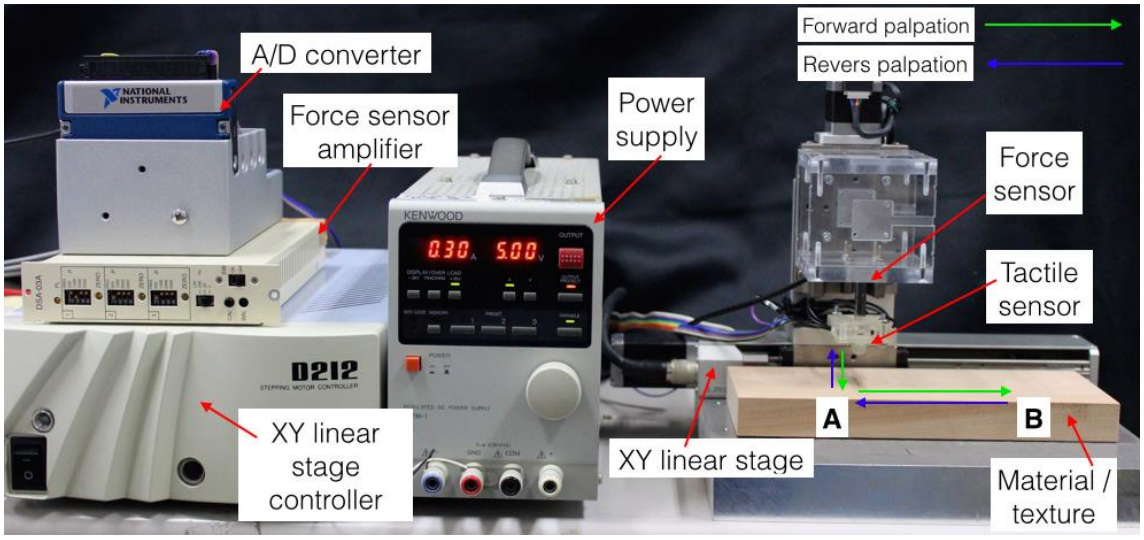

Figure 5-4: Experiment setup [**117**]

The experimental setup is shown in **Figure 5-4**. The system consists of a soft tactile sensor rigidly fixed to the vertical linear stage of the XY table (Suruga Seiki KXL06100-C2-F) via a Tech Gihan (USL 06-H5-50N-C) force sensor. Linear stages allow the tactile sensor to move in the x and z directions. The linear stages had a maximum speed of 50mm/s. The force sensor was a three axis force sensor. The force sensor signals were amplified and sent to a National Instruments NI9205 analog to digital converter.

The linear stages and the AD converters were connected to a computer and controlled by LabView™ software. The Data retrieval and the linear stage motion were synchronized. The AD converter had a sampling rate of 1kHz. The experimental data were collected and later stage processed using MatLab™ software. The computer used included an Intel Core I5-2400 3.10Ghz system with 16GB internal memory running Windows 7(64 bit).

5.3.5 Data collection

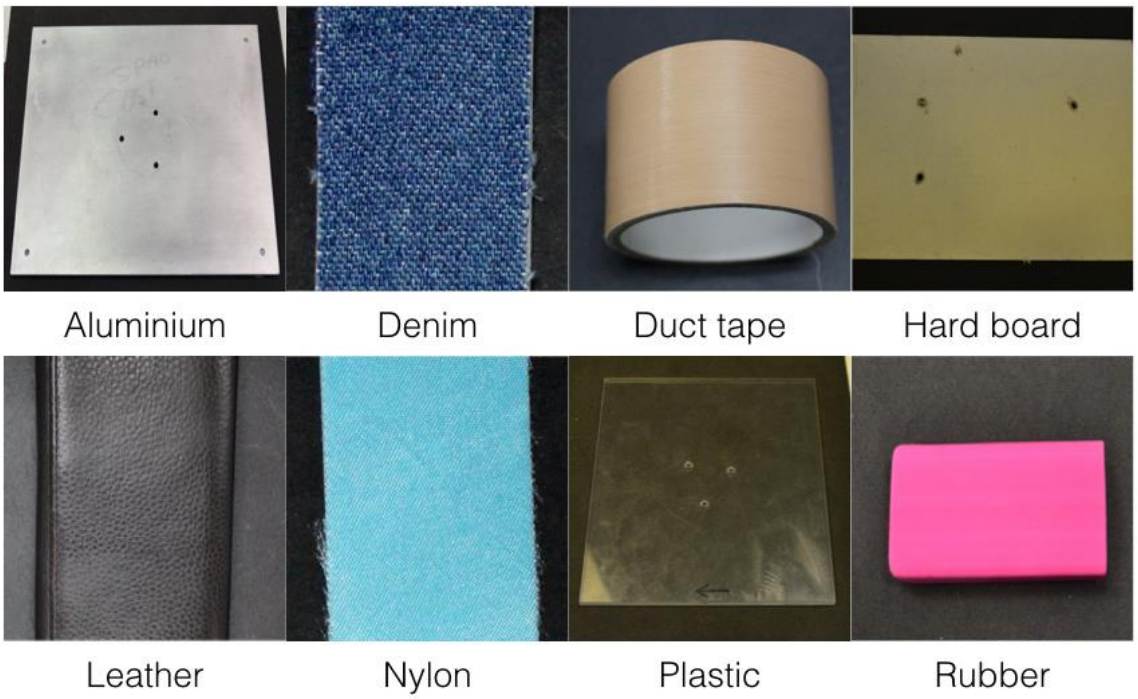

Figure 5-5: Eight textures and materials were used in the classification experiment [**117**]

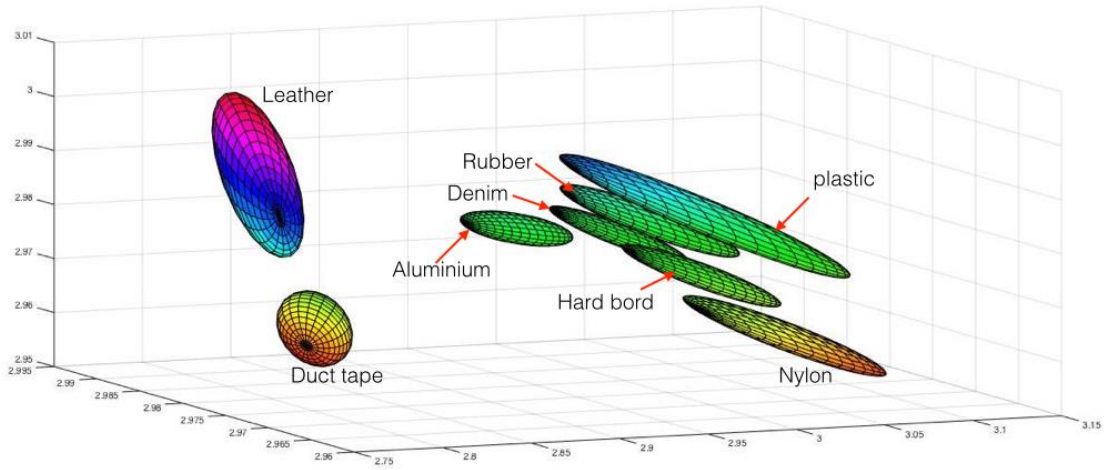

Figure 5-6: Gaussian ellipsoids of the data obtained for the eight materials and textures. The centers of the ellipsoids are the mean tactile sensor values in the x; y and z directions and the length of the semi-principal axis is the covariance values of the signal S

For the classification experiments, eight textured objects were selected (**Figure 5-5**) to validate the system and to show that it could be used to classify common materials and textures. These objects included samples with visible textures, such as fabrics, Duct tape and leather; and objects with invisible (micro-sized) texture, such as aluminum, hard board, and rubber. It included surfaces that were made artificially to have periodic textures. Few samples appeared to have no textures such as plastic, aluminum and glass.

These materials and textures were fixed to the base. The tactile sensor was moved on the material surface following the path shown in **Figure 5-4**. The contact depth of the soft tactile sensor was controlled by the motion of the z directional linear stage, and the palpation velocity was controlled by the x directional linear stage. Initially the z linear stage was lowered until the necessary vertical force was applied. Then the sensor was moved using the x stage. After the stage moved the programmed stroke length, it was returned to its initial position via the same route. The total motion was considered a single palpation motion of a finger performing an active exploration. The data from the force and tactile sensors were collected.

In these experiments, 120 sample data sets for each material class were recorded. From these samples, 100 randomly chosen data sets were used for training purposes and the remainder for testing and validation. Data were recorded from 30 locations on the material surface. The contact force was varied between 0.1-0.5N and the scanning velocity 10-20mm/s. For the classifier calculations, only the data relevant to the forward palpitation AB portion (**Figure 5-4**) were used.

5.3.6 Comparison of Existing and New Algorithms

To evaluate the performance of the above algorithm, it was compared with two other material classification algorithms.

1. the spatial period method [**38**], - identified as SPM and,
2. the neural network based classification method [**41**] – identified as NNCM.

5.3.6.1 Spatial period based classifier

The tactile sensor signal from the direction of the motion x was converted to the frequency domain using the FFT, with the tallest peak of the frequency distribution selected as the principal frequency, f_p, of the material or texture. By inputting f_p and palpation velocity V into the following equation, the spatial period λ was calculated. This λ was considered unique to each material.

$$\lambda = \frac{V}{f_p} \qquad (19)$$

The mean spatial period $\bar{\lambda}$ and variance σ_λ^2 were calculated for all the classes. For an unknown class, λ was calculated and the material or texture closest to the properties ($\bar{\lambda}$, σ_λ^2 of each class) was considered the candidate material or texture.

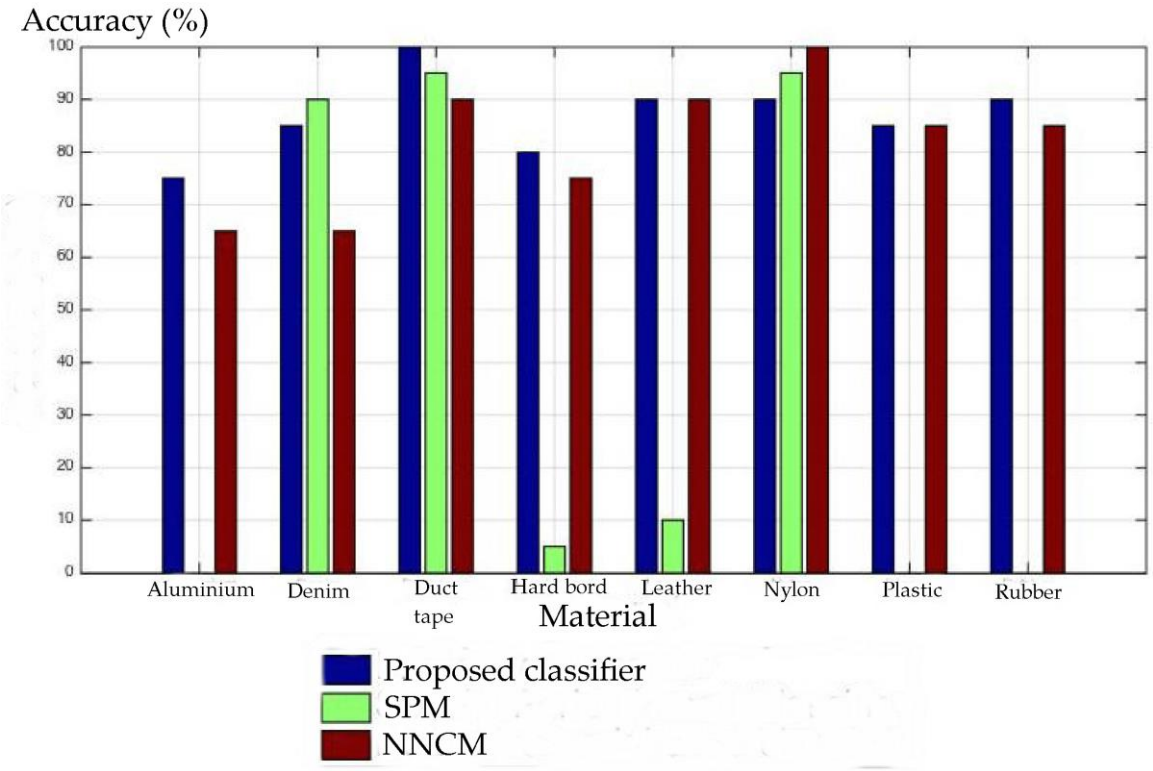

Figure 5-7: Parentage of each class being correctly classified by the three algorithms [**117**]

This algorithm (**Figure 5-7**) was 36% accurate in classifying materials. The average calculation time per classification was about 8μs.

5.3.6.2 Neural network based classifier

To use the neural network, the following features were calculated from the tactile data signal $\boldsymbol{V_s} = [\boldsymbol{X}, \boldsymbol{Y}, \boldsymbol{Z}]$

1. Frictional coefficient μ_U

$$\mu_U = \frac{\sqrt{x_i^2 + y_i^2}}{z_i} \qquad (20)$$

2. $\boldsymbol{X}$ signal variance σ_X^2

3. $\boldsymbol{X}$ signal directional kurtosis.

These features were input into a multi-layer perceptron (MLP) neural network and the neural network was trained with 900 samples. The algorithm was 81% accurate in classifying textures and materials (**Figure 5-7**). The average training and calculation time per test was about 0.88s.

5.4 Discussion

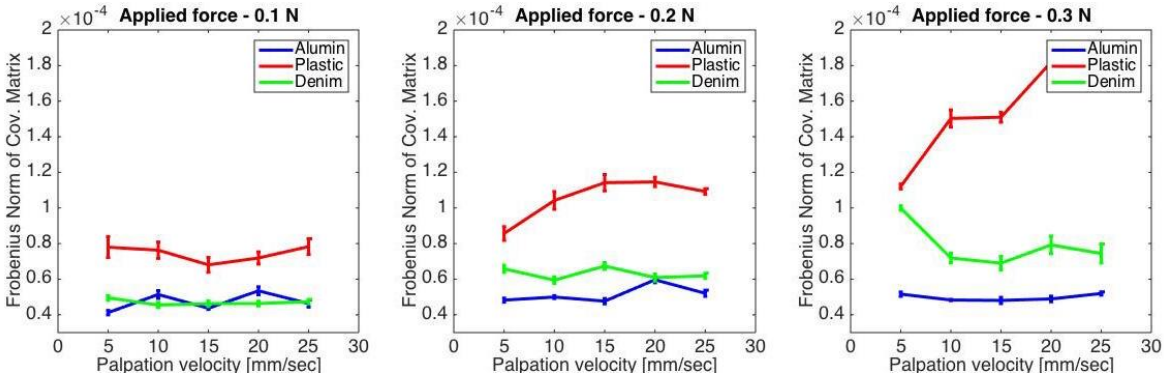

Figure 5-8: Robustness of features

Most of the features used for material classification in previous studies were based on the spacio-temporal changes in the sensing element. Therefore these features used were heavily influenced by:

1. palpation velocity
2. contact depth or the applied vertical force, and
3. orientation of the x and y directions of the sensor relative to the direction of palpation

Thus to understand the robustness of the proposed feature, the significance of the palpation velocity and the applied vertical force to the value of the proposed feature was evaluated.

5.4.1 Effect of scanning velocity:

In this experiment, three textures, aluminum, Denim and plastic; were explored using the vertical loads of 0.1 N, 0.2N and 0.3N and velocities of 5, 10, 15, 20

and 25 mm/s. The force sensor data and accelerometer data were recorded for each scan. Ten trials were conducted and the mean Frobenius norm and standard deviation of the norms were calculated, using equation (18) with tactile sensor data. **Figure 5-8** shows the results. For most trials, the Frobenius distance changed insignificantly for velocities of 10 mm/s, 15 mm/s, and 20 mm/s for a given material at all values of applied vertical force. Therefore, this classification feature could be used in a robot with varying exploration velocities, ranging from 10 to 20 mm/s. An n way analysis of Variances (n-ANOVA) study proved that the velocity was insignificant to the Frobenius norm within the given velocities. This robustness will be helpful for robot system to distinguish materials and objects moving relative to a hand and causing discrepancies in palpation velocity.

5.4.2 Effects of vertically applied force:

Figure 5-8 shows the change in Frobenius norm as the applied vertical force was changed from 0.1 N, 0.2N to 0.3 N. The lowest Frobenius distance was at the smallest applied force (0.1 N). In almost all cases, the Frobenius norm increased as the applied load increased. However, an ANOVA analysis showed that for lower vertical loads such as 0.1N and 0.2 N, the vertical loads were insignificant for variations in the Frobenius norm of each material. Therefore, to obtain greater accuracy with varying velocities, a smaller force such as 0.1N or 0.2N would be suitable for classification tasks.

The sensor used has a non-linear response to applied forces due to its inversely proportional relationship with the distance between the magnet and Hall sensor. This did not affect the proposed algorithm as only the variation of the sensor data between the three axes, x, y, and z was considered for feature generation. Consequently this algorithm can be utilized in any type of tactile sensing system that produces tactile data in three perpendicular directions.

The Frobenius norm of the covariance matrix and the mean values of the tactile data obtained from the three axes provide sufficient information to classify materials and textures. The eight material samples included those with textures that could be detected by a human observer and others without any textures detectable by humans. Nevertheless, the proposed system had the ability to detect subtle changes in the tactile sensor data due to differences in frictional coefficients. Thus, this proposed system has the capability to distinguish textures as well as different materials, further strengthening the robustness of the classification features.

The experiments performed to validate the classification features showed that the classification feature is non-responsive to changes in palpation velocity. Similarly, lower applied forces had no effect to the classification features resulting in a robust classification feature useful for robotic applications.

The proposed classification algorithm was executed within 280 μ s, making its application to a real time classification system possible. Calculations of Forbenious distance and mean, binary SVM did not consume resources, with an SVM execution time being 8μs. additionally the limited number of material classes contributed to the fast computation. Future research should include improvements in the algorithm and the effect on the algorithm of increasing the number of classes of material. The algorithms selected for comparison had fast computational ability, with each using a single palpation for computations. The results obtained from these comparative experiments are summarized in **Table 5-1**.

Table 5-1: Benchmark values of the three classification algorithms

Benchmark criterion	Proposed classifier	SPM	NNCM
Accuracy	89%	36%	81%
Number of features used	2	1	3
Time per classification	280μs	8μs	880μs
Effect of palpation velocity	minimum	high	high
Effect of contact force	minimum	high	high

Each algorithm classified materials with different accuracies. **Figure 5-7** shows that materials with spatial frequencies such as Denim, Duct tape and Nylon were classified correctly by the spatial period based algorithm while materials with invisible textures such as Aluminum, Plastic and rubber were misclassified. The other two methods had no visible relationship with type of materials texture and classification accuracy.

These observations indicate that the proposed new tactile sensor and the classification feature is a robust system, providing a simple yet powerful classification algorithm useful for robotic tactile systems.

Chapter 6

Concluding Remarks

6.1 Conclusions

Our objective of this thesis was to propose a tactile fingertip that was useful for robot application where the robot would perform the same object manipulation and exploration tasks as a human. In this respect we have first identified the necessary requirements for a robotic tactile sensor system. We conducted FEA simulations of human fingertip models and used anthropomorphic tactile fingertips developed by ourselves to come up with the requirements of a tactile system. We noted the necessary requirements for a robot tactile system. Then we realized that there was a lacking in a soft force sensor for developing such systems.

Thus, next logical step was to develop a soft tactile sensor capable of sensing force and vibration modalities. We developed a soft force sensor using a permanent magnet and three hall sensors. The sensor was simple in construction and could be used in developing fingertips. We conducted experiments extensively to characterize the sensor and we developed a mathematical model to correctly predict the deformations of the soft embodiment and to predict the magnetic field near hall sensors and then calculate the forces accurately using the mathematical models.

Next, we used the above developed sensor to develop a soft robotic finger. This finger was then fixed to a two fingered robot gripper. The gripper system was fixed to a robot arm and the total system performed object manipulation task by holding an object and inserting a peg to a hole. The

fingertip sensor data was analyzed and the information obtained by these sensors were explained and proved that the sensor system could be used in object manipulation tasks.

Finally to illustrate the ability of the proposed tactile sensor to be used in environmental exploration tasks like a human would perform material classification experiments were conducted using this tactile system. It was identified that the tactile systems and the classification algorithms were advanced enough to discriminate textures better than human. This concluded that the developed tactile sensor was extremely useful in developing anthropomorphic tactile sensor systems for robots.

6.2 Summary of contributions

The contribution of the thesis is as follows:

We presented the requirement of tactile sensors for robotic applications. Then we presented the requirements of such tactile sensors with reason. Then, we realized there were short comings in existing tactile systems and sensors. Thus, we proposed a new tactile sensor useful for tactile fingertip construction. We then used this fingertip to develop a gripper with tactile fingertips. We conducted experiments and showed with reason that the proposed sensor was suitable for developing tactile fingertips and these fingertips were capable of detecting tactile signals. By analyzing these signals, object manipulation and environment exploration tasks could be performed successfully.

6.3 Future work

6.3.1 Developing a tactile sensor array

The tactile fingertip proposed in this thesis was utilizing only a single fingertip. However, in order to have an effective fingertip, there should be multiple sensors (higher sensor density) in the fingertip. Nevertheless, incorporating multiple sensors to a fingertip still causes problems. The effect of one magnet would affect surrounding hall sensors making their information erroneous. These cross effects needs to be analyzed further. Analyzing these influences will provide design specification for miniaturizing the sensor to improve the sensor density.

6.3.2 Improvement of the tactile sensor

Currently, the tactile sensor can measure only forces. By including more hall sensors to the sensing unit would enable the prediction of the magnets orientation (roll, pitch). This would help to measure the deformations of the soft beam in other directions which would help to calculate the moments applied to the sensor.

References

[1] U. Reiser et al., "Care-O-bot 3 – Creating a product vision for service robot applications by integrating design and technology," in IEEE/RSJ International Conference on Intelligent Robots and Systems, 2009, pp. 1992-1997.

[2] da Vinci Surgery. (2016, February) da Vinci Surgery: Minimally Invasive Surgery. [Online]. http://www.davincisurgery.com/

[3] Advanced Osteotomy Tools. (2016, February) Advanced Osteotomy Tools-Products-CARLO. [Online]. http://www.aot-swiss.com/en/products

[4] Y.i Kuriyama, K. Yano, and M. Hamaguchi, "Trajectory Planning for Meal Assist Robot Considering Spilling Avoidance," in IEEE International Conference on Control Applicartions, 2008, pp. 1220-1225.

[5] Yoshiyuki Sankai, "HAL: Hybrid Assistive Limb Based on Cybernics," in Robotics Research. Berlin Heidelberg: Springer, 2010, pp. 25-34.

[6] ABB. (2016, February) ABB-Products-Robotics-YUMI. [Online]. http://new.abb.com/products/robotics/yumi

[7] Kawada Group. (2016, February) Nextage Industrial Robot. [Online]. http://nextage.kawada.jp/en/

[8] Deka research. (2016, February) Deka arm. [Online]. http://www.dekaresearch.com/deka_arm.shtml

[9] M.S. Johannes et al., "An Overview of the Developmental Process for the Modular Prosthetic Limb," The Johns Hopkins University Applied Physics Laboratory Technical Digest, vol. 30, pp. 207–216, 2011.

[10] J.L Collinger et al., "Collaborative Approach in the Development of High-Performance Brain–Computer Interfaces for a Neuroprosthetic Arm: Translation from Animal Models to Human Control," Clinical and Translational Science, vol. 7, no. 1, pp. 52-59, 2014.

[11] A. Bicchi, "Hand for dexterous manipulation and robust grasping: a difficult road towards simplicity," IEEE Transactions on Robotics and, vol. 16, no. 6, pp. 652-662, 2000.

[12] R.S. Johansson and J. R. Flanagan, "Coding and use of tactile signals from the fingertips in object manipulation tasks," Nature Reviews Neuroscience, vol. 10, no. 5, pp. 345-359, 2009.

[13] R.S. Dahiya and M. Valle, "Tactile sensing: definition and classification in: Tactile Sensing Technologies and System," Springer, pp. 13-17, 2013.

[14] C. Melchiorri, "Slip Detection and Control Using Tactile and Force Sensors," IEEE\ASME Transactions on Mechatronics, pp. 235-243, 2000.

[15] R.D. Howe, "Tactile sensing and control of robotic manipulation," Advance Robotics, pp. 245-261, 1994.

[16] M. Gentilucci, I. Toni, E. Daprati, and M. Gangitano, "Tactile input of the hand and the control ofreaching to grasp movements," Experimental Brain Research, pp. 130-137, 1997.

[17] G. Westling and R. S. Johansson, "Factors Influencing the Force Control During Precision Grip," Experimental Brain Research, pp. 277-284, 1984.

[18] C.M. Oddo, M Controzzi, L Beccai, C Cipriani, and M.C. Carrozza, "Roughness Encoding for Discrimination of Surfaces in Artificial Active-Touch," Robotics, IEEE Transactions on, vol. 27, no. 3, pp. 522-533, 2011.

[19] R.D.P. Wong, R. B. Hellman, and V. J. Santos, "Spacial asymmetry in tactile sensor skin deformation aids perception of edge orientation during haptic exploration," IEEE Transactions on Haptics, vol. 7, no. 2, pp. 191-202, 2014.

[20] P. Dallaire, P. Giguere, D. Emond, and B. Chaib-draa, "Autonomous tactile perseption: Acombined improved sensing and Bayesian nonparametric approach," Robotics and Autonomous Systems, vol. 62, pp. 422-435, 2014.

[21] N. Jamali and C. Sammut, "Material classification by tactile sensing using surface textures," in Robotics and Automation (ICRA), 2010 IEEE International Conference on, 2010, pp. 2336-2341.

[22] A. Khurshid, A. Ghafoor, and M. A. Malik, "Robotic Grasping and Fine Manipulation Using Soft Fingertip," in Advances in Mechatronics, Horacio Martinez-Alfaro, Ed., 2011, ch. 7.

[23] D.S. Chathuranga, V.A. Ho, and S. Hirai, "A bio-mimetic fingertip that detects force and vibration modalities and its application to surface identification," in 2012 IEEE International Conference on Robotics and Biomimetics, 2012, pp. 575-581.

[24] A.B. Vallbo and R.S. Johansson, "Properties of cutaneous mechanoreceptors in the human hand related to touch sensation," Human Neurobiol, pp. 3-14, 1984.

[25] R.S. Johansson and G. Westling, "Roles of glabrous skin receptors and sensorimotor in automatic control of precision grip when lifting rougher or more slippery objects," Experimental Brain Research, pp. 550-564, 1984.

[26] D.G. Caldwell, N. Tsagarakis, and A. Wardle, "Mechano-thermo and propriceptor feedback for integrated haptic feedback," in IEEE Conference on Robotics and Automation, 1997, pp. 2491-2496.

[27] F. Gonzalez-Crussi, The five senses.: Vintage Press/Random House, 1991.

[28] Z. Wang, D. S. Chathuranga, and S. Hirai, "Study on Fingertip Slippage using FE Model for Developing Human-Like Tactile Sensor," in International Conference on Real-time Computing and Robotics, 2015.

[29] G.J. Gerling, I.I. Rivest, D.R. Lesniak, J.R. Scanlon, and L. Wan, "Validating a population model of tactile mechanotransduction of slowly adapting type i afferents at levels of skin mechanics, single-unit response and psychophysics," IEEE Transactions on Haptics, vol. 7, pp. 216–228, 2014.

[30] D.S. Chathuranga, Z. Wang, and S. Hirai, "Challenges in Developing Soft Tactile Sensors for Robots that Detect Incipient Slip," in 7th International Conference on Information and Automation for Sustainability, 2014, pp. 1 - 7.

[31] P. Mittendorefer and G. Cheng, "Humanoid Multimodal Tactile-Sensing Modules," IEEE Transactions on Robotics, pp. 401-410, 2011.

[32] A. Schmitz et al., "Methods and Technologies for the Implementation of Large-Scal Robot Tactile Sensor," IEEE Transactions on Robotics, vol. 27, no. 3, pp. 389-400, 2011.

[33] S. Takenawa, "A Soft Three-Axis Tactile Sensor Based on Electromagnetic Induction," in IEEE International Conference on Mechatronics, 2009, pp. 1-6.

[34] Y. Ohmura, Y. Kuniyoshi, and A. Nagakubo, "Conformable and Scalable Tactile Sensor Skin for Curved Surfaces," in IEEE International Conference on robotics and Automation, 2006, pp. 1348 - 1353.

[35] H. Yousef, M. Boukallel, and K. Althoefer, "Tactile sensing for dexterous in-hand manipulation in robotics-A review," Sensors and Actuators, pp. 171-187, 2011.

[36] H. Liu, X. Son, J. Bimbo, L. Seneviratne, and K. Althoefer, "Surface Material Recognition through Haptic Exploration using an Intelligent Contact Sensing Finger," in IEEE International Conference on Intelligent Robots and Systems, 2012, pp. 52-57.

[37] C.M. Oddo, M. Controzzi, L. Beccai, C. Ciprian, and M.C. Carrozza, "Roughness Encording for Discrmination of Surface in Artificial Active-Touch," IEEE Transactions on Robotics, pp. 522-533, 2011.

[38] H.B. Muhammad et al., "A capacitive tactile sensor array for surface textur discrimination," Microelectronic Engineerin, pp. 1811-1813, 2011.

[39] S.H. Kim, J. Engel, C. Liu, and D.L. Jones, "Texture classification using a polymer-based MEMS tactile sensor," Journal of Micromechanics and Microengineering, pp. 912-920, 2005.

[40] V. A. Ho, D. V. Dao, S. Sugiyama, and S. Hirai, "Development and Analysis of a Sliding Tactile Soft Fingertip Embedded With a Microforce/Moment Sensor," Robotics, IEEE Transactions on, vol. 27, no. 3, pp. 411-424, 2011.

[41] F. Boissieu, C. Goden, C. Serviere, and D. Baudois, "Tactile Texture Recognition with a 3-Axial Force MEMS integrated Artificial Finger," in Proceedings of Robotics: Science and Systems, 2009.

[42] N. Jamali and C. Sammut, "Majority Voting" Material Classification by Tactile Sensing Using Surface Texture," IEEE Transactions on Robotics, pp. 508-521, 2011.

[43] P.A. Schmidt, E. Mael, and R.F. Wurtz, "A sensor for dynamic tactile information with applications in human-robot interaction and object exploration," in Robotics and Autonomous Systems, 2006, pp. 1005-1014.

[44] X. Ding, K. Kuribayashi, and T. Hashida, "Development of a New Type Tactile

Sensor Using Micro Electromagnetic Coil for Human Robot," in IEEE International Symposium on Micromechatronics and Human Science, 2000, pp. 181-187.

[45] Y. Tanaka, M. Tanaka, and S. Chonan, "Development of a sensor system for collecting tactile information," Microsystem Technologies, pp. 1005-1013, 2007.

[46] T. Liu, Y. Inoue, and K. Shibata, "A Small and Low-Cost 3-D Tactile Sensor for a Wearable Force Plate," IEEE Sensors Journal, pp. 1103-1110, 2009.

[47] M. Tanaka, J.L. Leveque, H. Tagami, K. Kikuchi, and S. Chonan, "The "Haptic Finger" - a new device for monitoring skin condition.," Skin Research and Technology, pp. 131-136, 2003.

[48] S. Takamuku, T. Iwase, and K. Hosoda, "Robust material discrimination by a soft anthropomorphic finger with tactile and thermal sense," in IEEE/RSJ International Conference on Intelligent Robots and Systems, 2008, pp. 3977 - 3982.

[49] K. Hosoda, Y. Tada, and M. Asada, "Anthropomorphic robotic soft fingertip with randomly distributed receptors," Robotics and Autonomous Systems, pp. 104-109, 2006.

[50] S. Shirafuji and K. Hosoda, "Detection and prevention of slip using sensors with different properties embedded in elastic artificial skin on the basis of previous experience," Robotics and Autonomous Systems, 2012.

[51] N. Wettels, V.J. Santos, R.S. Johansson, and G.E. Leob, "Biomimetic Tactile Sensor Array," Advance Robotics, pp. 829-849, 2008.

[52] N. Wettels and G.E. Loeb, "Haptic Feature Extraction from a Biomimetic Tactile Sensor: Force, Contact Location and Curvature," in IEEE International Conference on Robotics and Biomimetics, 2011, pp. 2471-2478.

[53] J.A. Fishel and G.E. Loeb, "Bayesian exploration for intelligent identification of textures," Frontiers in Neurorobotics, pp. 1-20, 2012.

[54] D. Dornfeld and C. Handy, "Slip Detection Using Acoustic Emission Signal Analysis," in IEEE International Conference on Robotics and Automation, 1987, pp. 1868-1875.

[55] M.R. Tremblay and M. R. Cutkosky, "Estimate Friction Using Insipient Slip Sensing During Manipulation Task," in IEEE International Conference on Robotics and Automation, 1993, pp. 429-434.

[56] J.S. Son, E.A. Monteverde, and R.D. Howe, "A Tactile Sensor for Localizing Transient Events in Manipulation," , 1994, pp. 471-476.

[57] D. Gajin et al., "Grasping Force Control of Multi-fingered Robot Hand based on Slip Detection Using Tactile Sensors," in IEEE International Conference on Robotics and Automation, 2008, pp. 2605-2610.

[58] E.G.M. Holweg et al., "Slip Detection by Tactile Sensors: Algorithms and Experimental Results," , 1996, pp. 3234-3239.

[59] D.S. Chathuranga, Z. Wang, and S. Hirai, "An Anthropomorphic Tactile Sensor System with its Applications in Dexterous Manipulations," in IEEE International Conference on Cyber Technology in Automation, Control and Intelligent Systems, 2015, pp. 1085-1090.

[60] R. S. Dahiya, G. Metta, M. Valla, and G. Sandini, "Tactile Sensing - From Humans to Humanoids," IEEE Transactions on Robotics, pp. 1-20, 2010.

[61] D.S. Chathuranga, Z. Wang, A. Mitani, and S. Hirai, "A biomimetic soft fingertip applicable to haptic feedback systems for texture identification," in IEEE International Symposium onHaptic Audio Visual Environments and Games

(HAVE), 2013, pp. 29-33.

[62] M.R. Tremblay, W. J. Packard, and M. R. Cutkosky, "Utilizing sensed incipient slip signals for grasp force control," in Japan-USA Symposium on Flexible Automation, 1992.

[63] M. Lee, "Tactile sensing: new directions, new challenges," The International Journal of Robotics Research, vol. 19, no. 7, pp. 636-643, 2000.

[64] S. Khan, S. Tinku, L. Lorenzell, and R. D. Dahiya, "Flexible tactile sensor using screen-printed p(VDF-TrFE) and MWCNT/PDMS composites," IEEE sensors Journal, vol. 15, no. 6, pp. 3146-3155, 2015.

[65] D.S. Chathuranga, V. A. Ho, and S. Hirai, "Investigation of a biomimetic fingertip's ability to discriminate fabrics based on surface textures," in IEEE/ASME International Conference on Advance Intelligent Mechatronics, 2013, pp. 1667-1674.

[66] V. A. Ho et al., "Development of a Low-Profile Sensor Using Electro-conductive Yarns in Recognition of Slippage," in IEEE Int. Conf. on Intelligent Robots and Systems, 2011, pp. 1946-1953.

[67] D.S. Chathuranga, Z.Wang, Y.Noh, T. Nanayakkara, and S. Hirai, "Magnetic and Mechanical Modelling of a Soft Three-Axis Force Sensor," IEEE Sensors Journal, 2016.

[68] K.N. Tarchanidis and J. N. Lygouras, "Data Glove With a Force Sensor," IEEE Transactions on Instrumentation and Measurements, vol. 52, no. 3, pp. 984-989, 2003.

[69] V.A. Ho et al., "Development of a Low-Profile Sensor Using Electroconductive Yarns in Recognition of Slippage," in IEEE International Conference on Intelligent

Robots and Systems, 2011, pp. 1946-1953.

[70] J. Missinne et al., "Two axis optoelectronic tactile shear stress sensor," Sensors and Actuators A: Physical, vol. 186, pp. 63-68, 2012.

[71] K. Kim et al., "Polymer-based flexible tactile sensor up to 32 × 32 arrays integrated with interconnection terminals," Sensors Actuat. A, Phys., vol. 156, pp. 284-291, 2011.

[72] Y.W.R. Amarasinghe, A. L. Kulasekera, and T. G. P. Priyadarshana, "Quantum Tunneling Composite (QTC) Based Tactile Sensor Array For Dynamic Pressure Distribution Measurement," in 7th International Conference on Sensing Technology, 2013, pp. 1-4.

[73] D.M. Vogt, Y. L. Park, and R. J. Wood, "Design and Characterization of a Soft Multi-Axis Force Sensor Using Embedded Microfluidic Channels," IEEE sensors Journal, vol. 13, no. 10, pp. 4056-4064, 2013.

[74] Y. Noh et al., "A Three-Axial Body Force Sensor for Flexible Manipulators," in IEEE/ASME International Conference on Robotics and Automation, 2014, pp. 6388-6393.

[75] M.I. Tiwanaa, A. Shashankb, S. J. Redmondb, and N. H. Lovell, "Characterization of a capacitive tactile shear sensor for application in robotic and upper limb prostheses," Sensors and Actuators A: Physical, vol. 165, no. 2, pp. 164–172, 2011.

[76] T. Zhang et al., "Fingertip Three-Axis Tactile Sensor for Multifingered Grasping," IEEE Transactions on Mechatronics, vol. 20, no. 4, pp. 1875-1885, 2015.

[77] J. Missinne, A. Monte, Y. Tijtgat, N. Rossey, and G. V. Steenberge, "Miniature Multiaxial Optoelectronic Shear Stress Sensing System Based on a Segmented Photodiode," IEEE sensors Journal, vol. 15, no. 8, pp. 4286-4291, 2015.

[78] J.B. Chossat, Y. L. Park, R. J. Wood, and V. Duchaine, "A Soft Strain Sensor Based on Ionic and Metal Liquids," IEEE Sensors Journal, vol. 13, no. 9, pp. 55-60, 2013.

[79] C. Ledermann, S. Wirges, D. Oertel, M. Mende, and H. Woern, "Tactile sensor on a magnetic basis using novel 3D hall sensor - first prototypes and results," in IEEE 17th International conference on intelligent engineering systems, 2013, pp. 55-60.

[80] K. Kim, S. Zhang, J. Tian, P. Han, and X. Jiang, "Face-shear mode ultrasonic tactile sensor array," in IEEE International Ultrasonics Symposium, 2012, pp. 1059-1062.

[81] J.J. Clark, "A magnetic field based compliance matching sensor for high resolution, high compliance tactile sensing," in Proc. IEEE ICRA, 1988, pp. 772-777.

[82] W.C. Nowlin, "Experimental results on Bayesian algorithms for interpreting compliant tactile sensing data," in Proc. IEEE ICRA, 378-383, p. 1991.

[83] E. Torres-Jara, I. Vasilescu, and R. Coral, "A soft touch: Compliant tactile sensors for sensitive manipulation," Massachusetts Inst. Technol., Cambridge, Tech. Rep. MITCSAIL-TR-2006-014, 2006.

[84] L. Jamone, L. Natale, G. Metta, and G. Sandini, "Highly sensitive soft tactile sensor for an anthropomorphic robot hand," IEEE sensors Journal, vol. 15, no. 8, pp. 4226-4233, 2015.

[85] L. Jamone, F. Nori, G. Metta, and G. Sandini, "James: A humanoid robot acting over an unstructured world," in Proc. 6th IEEE-RAS Int. Conf. Humanoid Robots, 2006, pp. 143-150.

[86] S. Youssefian, N. Rahbar, and E. Torres-Jara, "Contact behavior of soft spherical tactile sensor," IEEE sensors Journal, vol. 14, no. 5, pp. 1435-1442, 2014.

[87] Q. Liang, D. Zhang, Y. Ge, and Q. Song, "A novel miniature four-dimensional force/torque sensor with overload protection mechanism," IEEE Sensors Journal, vol. 9, no. 12, pp. 1741-1747, 2009.

[88] P. Polygerinos, L. D. Senevirathne, R. Razavi, T. Schaeffter, and K. Althoefer, "Triaxial catheter-tip force sensor for MRI- guided cardiac procedures," IEEE/ASME Transactions on Mechatronics, vol. 18, no. 1, pp. 386-396, 2013.

[89] I. Kao and F. Yang, "Stiffness and contact mechanics for soft fingers in grasping and manipulation," IEEE Transactions on Robotics and Automation, vol. 20, no. 1, pp. 132-135, 2004.

[90] T. Maeder, V. Fahrny, S. Stauss, G. Corradini, and P. Ryser, "Design and characterisation of low-cost thick-film piezoresistive force sensors for the 100 mN to 100 N range," in XXIX International Conference of IMAPS Poland Chapter, 2005.

[91] Y.L. Park, K. Chau, R. J. Black, and M. R. Cutkosky, "Force Sensing Robot Fingers using Embedded Fiber Bragg Grating Sensors and Shape Deposition Manufacturing," in IEEE International Conference on Robotics and Automation, 2007, pp. 1510-1516.

[92] Y. Zhang, A. W. Allen, J. Yi, and T. Liu, "Understanding Tire/Road Stick-Slip Interactions with Embedded Rubber Force Sensors," in IEEE International conference on Advanced Intelligent Mechatronics, 2012, pp. 550-555.

[93] J.D. Jackson, Classical Electrodynamics, 3rd ed.: Wiley, 1998.

[94] A.N Mladenovic and S.R. Aleksic, "Magnetic field calculation of a permanent magnet," in 51st Internationales Wissenschaftliches Kolloquium, 2006, pp. 3-9.

[95] J. Back et al., "Control a contact sensing finger for surface haptic exploration," in

Robotics and Automation (ICRA), 2014 IEEE International Conference on, 2014, pp. 2736-2741.

[96] H. Yussof, J. Wada, and M. Ohka, "Object handeling task based on active tactile and slippage sensation in a multi-fingered humanoid robot arm," in IEEE International Conference on Robotics and Automation, 2009, pp. 502-507.

[97] B. Winstone, G. Griffiths, C. Melhuish, T. Pipe, and J. Rossiter, "TACTIP- Tactile fingertip device, challenged in reduction of size to ready for robot hand integration," in IEEE International Conference on Robotics and Biomimetics, 2012, pp. 160-166.

[98] J.V. Kuilenburg, M. A. Masen, and E. van der Heide, "The role of the skin microrelief in the contact behaviour of human skin: Contact between the human finger and regular surface texture," Tribology International, vol. 65, pp. 81-90, 2013.

[99] C.H. Lin, T. W. Erickson, J. A. Fishel, N. Wettels, and G. E. Loeb, "ignal Processing and Fabrication of a Biomimetic Tactile Sensor Array with Thermal, Force and Microvibration Modalities," in IEEE International Conference on Robotics and Biomimetics, 2009, pp. 129-134.

[100] K. Hosoda, "Robot Finger Design for Developmental Tactile Interaction," Embodied Artificial Intelligence, vol. 3139, pp. 219-230, 2004.

[101] K.V.D.S. Chathuranga, V. A. Ho, and S. Hirai, "A bio-mimetic fingertip that detects force and vibration modalities and its application to surface identification," in IEEE Int. Conf, on Robotics and Biomimetics, 2012, pp. 575-581.

[102] S. Takamuku, T. Iwase, and K.Hosoda, "Robust material discrimination by a soft anthropomorphic finger with tactile and thermal sense," in IEEE international

Conference on Robotics and Automation, 2008, pp. 3977-3982.

[103] T. Yoshioka, S. J. Bensmaia, J. C. Craig, and S. S. Hsiao, "Texture perception through direct and indirect touch: An analysis of perceptual space for tactile texture in two modes of exploration," Somatosensory and Motor Research, vol. 24, pp. 53-73, 2007.

[104] T. Yosioka, B. Gibb, A. K. Dorsch, S. S. Hsiao, and K. O. Johnson, "eural Coding Mechanisms Underlying Perceived Roughness of Finely Textured Surfaces," The Journal of Neuroscience, vol. 21, no. 17, pp. 6905-6916, 2001.

[105] T. Miyaoka, T. Mano, and M. Ohka, "Mechanisms of fine-surface-texture discrimination in human tactile sensation," Journal of Acoustic Society of America, vol. 105, no. 4, pp. 2485-2492, 1998.

[106] W.W.M. Cuevas, J. Guerrero, and S. M. Gutierrez, "A First Approach to Tactile Texture Recognition," in IEEE International Conference on Systems Man and Cybernetics, 1998, pp. 4246-4250.

[107] N. Jamali and C. Sammut, "Majority voting: material classification by tactile sensing using surface texture," IEEE Transactions in Robotics, vol. 27, no. 3, pp. 508-521, 2011.

[108] H. Hu et al., "A finger-shaped tactile sensor for fabric surfaces evaluation by 2-dimensional active sliding touch," Sensors (Basel), vol. 14, no. 3, pp. 4899-4913, 2014.

[109] T. Yoshioka and J. Zhou, "Factors Involved in Tactile Texture Perception through Probes," Advanced Robotics, vol. 23, no. 6, pp. 747-766, 2009.

[110] A. Song, Y. Han, H. Hu, and J. Li, "A Novel Texture Sensor for Fabric Texture Measurement and Classification," Transactions on Instrumentation and

Measurement, vol. 63, no. 7, 2014.

[111] A. Drimus, M. B. Petersen, and A. Bilberg, "Object texture recognition by dynamic tactile sensing using active exploration," in IEEE International Symposium on Robot and Human Interactive Communication, 2012, pp. 277-283.

[112] Y. Mukaibo, H. Shirado, M. Konyo, and T. Maeno, "Development of a Texture Sensor Emulating the Tissue Structure and Perceptual Mechanism of Human Fingers," in IEEE International Conference on Robotics and Automation, 2005, pp. 2565 - 2570.

[113] P. Giguere and G. Dudek, "A Simple Tactile Probe for Surface Identification by Mobile Robots," IEEE Transactions on Robotics, vol. 27, no. 3, pp. 534-544, 2011.

[114] J.A. Fishel and G. E. Loeb, "Bayesian exploration for intelligent identification of textures," Frontiers in Neurorobotics, pp. 1-20, 2012.

[115] H.B. Muhammad et al., "A Capacitive tactile sensor array for surface texture discrimination," Microelectronic Engineering, vol. 88, no. 8, pp. 1811-1813, 2011.

[116] S. Decherchi, P. Gastaldo, R.S. Dahiya, M. Valle, and R. Zunino, "Tactile-Data Classification of Contact Materials Using Computational Intelligence," IEEE Transactions on Robotics, vol. 27, no. 3, pp. 635-639, 2011.

[117] D.S. Chathuranga, Z.Wang, Y.Noh, T.Nanayakkara, and S.Hirai, "Robust Real time Material Classification Algorithm Using Soft Three Axis Tactile Sensor: Evaluation of the Algorithm," in IEEE/RSJ International Conference on Intelligent Robots and Systems, 2015, pp. 2093-2098.